

Fabrication of Superhydrophobic-Superoleophilic Membranes for Oil-Water Separation Applications

By

©S. Abbas Rasouli

A thesis submitted to the School of Graduate Studies in partial fulfilment
of the requirements for the degree of

Master of Engineering (M.Eng.)

Faculty of Engineering and Applied Science
Memorial University of Newfoundland

February 2021

St. John's, Newfoundland and Labrador
Canada

ABSTRACT

The increasing volume of industrial oily wastewater and recent oil spill incidents have negatively affected the ecosystem and human health. Accordingly, it has been a worldwide challenge to separate the water or oil from such oily wastewater effectively. Recently, owing to the low efficiency of conventional techniques, a great interest has been paid in using membranes with engineered wettability especially superhydrophobic-superoleophilic (SHSO) ones, for oil-water separation applications.

In this research, the SHSO mesh is fabricated to examine the effectiveness of membrane surface modification for oil-water separation purposes. After cleaning and activating the stainless-steel mesh by piranha solution, two different silanes with short- and long-alkyl functional chains (Dynasylan[®] Sivo 408 and Dynasylan[®] F8261, respectively) are used to modify the mesh surface via a dip-coating technique. Functionalized silica micro and nanoparticles with different ratios are tried to evaluate their potential as morphology modifiers. The superhydrophobic and superoleophilic membranes are then characterized by the contact angle, sliding angle, scanning electron microscopy (SEM), energy dispersive X-ray (EDX), Fourier transform infrared spectroscopy (FTIR), Transmission Electron Microscopy (TEM), and X-ray Powder Diffraction (XRD) techniques. Utilization of Dynasylan[®] F8261 as a coating solution leads to a higher water contact angle (WCA) due to having a longer alkyl functional chain, compared to Dynasylan[®] Sivo 408. Moreover, the combination of micro (25%) and nano (75%) particles results in the highest WCA (165.8°), followed by the scenario of only nanoparticles with a WCA of 163.8°. The coating solution with only nanoparticles is thus proposed as the optimal case, since the microparticles tend to settle, making the solution non-homogeneous based on the SEM results. Analysis of

characterization tests confirms that the as-prepared mesh exhibits SHSO properties. The stability analysis is also conducted by submerging the SHSO membranes into solutions of NaCl (1M), H₂SO₄ (0.1M), and NaOH (0.1M). Except for the NaOH solution, this mesh maintains its SHSO properties in the solutions of NaCl and H₂SO₄ over one-month stability assessment. The results of static oil-water separation show a higher separation efficiency for hexane (99%) than canola oil (97%), owing to the lower viscosity of hexane.

The dynamic oil-water separation tests are also performed using coated mesh tubes in a cross-flow gravity-based separator. The oil-water mixture is pumped into the tube side for 70 minutes. The oil-water mixture level is adjusted to avoid the breakthrough of the water phase into the SHSO membrane. The effluents of oil and water from the system are directed to the secondary separators to analyze the oil and water separation efficiency. Different oil concentrations (10, 30, and 50 vol%) and total flow rates (5, 10, and 15 mL/min) are examined to evaluate the performance of the SHSO mesh in separating oil from the oil-water mixture. The maximum oil separation efficiency of 97% is obtained from a scenario with 10 vol% oil and 5 mL/min total flow rate. Conversely, the minimum oil separation efficiency (86%) occurs for the case with a 15 mL/min total flow rate and 50 vol% oil. The water separation efficiency is not affected by changing oil-water mixture characteristics, as it reached the maximum level (100%) shortly. The flower-like silica nano-roughness on the SHSO mesh tube by decreasing the pore size from around 80 to 45 μm effectively prohibits the water phase from entering the mesh pores up to 3 cm H₂O column. By increasing the oil permeate flow rates from 0.5 to 7.5 ml/min, the oil permeation flux increases from 314 to 790 (L/m².h). By the time, the production rate of oil and water shows a linear behaviour indicating that the SHSO coated mesh does not experience the fouling phenomenon.

Both separated phases are very clear. Therefore, the proposed methodology can have practical applications in oil removal from oily wastewater and oil spill incidents.

ACKNOWLEDGEMENTS

I would like to express my sincere gratitude and appreciation to all those who gave me their support, assistance and necessary advice to complete my research work and write this thesis. First and foremost, I express my sincere gratitude and thanks to my supervisor, Dr. Sohrab Zendehboudi, for his support, helpful guidance, and encouragement throughout the entire research work. His detailed and constructive comments, patience, and understanding helped me towards the successful completion of thesis work. I would like to thank my co-supervisor, Dr. Xili Duan, for his continued support, technical meetings, and guidance towards my thesis completion. I would also like to thank Dr. Nima Rezaei, Assistant Professor at the School of Engineering Science, Lappeenranta University of Technology, Finland. His spectacular insights and visions have always inspired me throughout this research. He always supported me and guided me on exact paths to achieve my goal and complete my research tasks.

Special thanks are extended to Memorial University for providing excellent resources for conducting this research program; the School of Graduate Studies (SGS), Memorial University, Suncor, Innovate NL, and the Natural Sciences and Engineering Research Council of Canada (NSERC) for their financial supports.

I also want to express my heartfelt appreciation to Dr. Yahui Zhang, Dr. Yan Zahng, and Dr. Faisal Khan, who shared their limited lab spaces to complete my research experiments.

Most importantly, none of this would have been possible without the love and patience of my family. My beloved wife, Hamideh, and my immediate family have been a constant source of love, concern, support, and strength all these years.

Table of Contents

ABSTRACT	i
ACKNOWLEDGEMENTS	iv
List of Figures	viii
List of Tables	xii
1. CHAPTER ONE	1
Introduction and Overview	1
1.1. Motivation.....	2
1.2. Experimental Phases	5
1.3. Thesis Structure	6
2. CHAPTER TWO	11
Literature Review (Superhydrophobic and Superoleophilic Membranes for Oil-Water Separation Application: A Comprehensive Review)	11
Abstract	12
2.1. Introduction.....	12
2.2. Oil Contamination and Separation Technologies	16
2.2.1. The source of oil contaminations and their potential hazards.....	16
2.2.2. Oil-water separation technologies.....	18
2.2.3. Hydrophilic and hydrophobic membranes.....	20
2.3. Surface Wetting Phenomena.....	23
2.3.1. Wetting states.....	23
2.3.2. Wetting states at molecular level	25
2.3.3. Superhydrophobic and superoleophilic wettability state	28
2.4. Surface Wetting Modification Methods.....	30
2.4.1. Conventional methods	30
2.4.2. Innovative methods.....	33
2.5. Fabrication of Superhydrophobic and Superoleophilic Membranes	39
2.5.1. Pretreatment	40
2.5.2. Modifying surface morphology	42
2.5.3. Surface chemistry modification	43

2.6.	Superhydrophobic and Superoleophilic Membranes for Oil-Water Separation	46
2.6.1.	Mesh-based superhydrophobic and superoleophilic membranes	47
2.6.2.	Superhydrophobic and superoleophilic porous membranes	60
2.6.3.	Superhydrophobic and superoleophilic films	72
2.7.	Challenges and Future Perspective of Superhydrophobic and Superoleophilic Membranes for Oil-Water Separation.....	75
2.8.	Conclusions.....	76
3.	CHAPTER THREE	115
	Design, Fabrication, and Characterization of a Facile Superhydrophobic and Superoleophilic Mesh-Based Membrane for Selective Oil-Water Separation	115
	Abstract.....	116
3.1.	Introduction.....	116
3.2.	Materials and Methods.....	120
3.2.1.	Materials	120
3.2.2.	Fabricating SHSO mesh.....	121
3.2.3.	Characterizing SHSO mesh	124
3.3.	Results and Discussions	127
3.3.1.	Mesh wettability analysis.....	127
3.3.2.	Surface characterization analysis	130
3.3.3.	Mesh chemical stability analysis	136
3.3.4.	Oil-water separation test	139
3.4.	Conclusions.....	140
4.	CHAPTER FOUR.....	152
	Selective and Continues Oil Removal from Oil-Water Mixture, Using Tubular Superhydrophobic and Superoleophilic Membrane	152
	Abstract.....	153
4.1.	Introduction.....	154
4.2.	Experimental Methods	157
4.2.1.	Chemicals used	157
4.2.2.	Fabrication process of SHSO mesh tube	157
4.2.3.	Characterization methods of the SHSO mesh tube.....	158
4.2.4.	Separation test set up, procedure, and assessment.....	159
4.3.	Results and Discussion	162

4.3.1. Morphological evaluation of the SHSO stainless-steel mesh	162
4.3.2. Dynamic oil-water separation tests	164
4.4. Conclusions	177
5. CHAPTER FIVE	187
Summary and Recommendations for Future Work.....	187
5.1. Literature Review (Chapter 2)	188
5.2. Fabrication and Characterization of SHSO Membranes (Chapter 3)	189
5.3. Oil-water Separation Tests (Chapter 4)	191
5.4. Recommendations for Future Work.....	192

List of Figures

Figure 2.1. The schematic of the separation process in membranes [159] 20

Figure 2.2. Three different contact conditions between surfaces and liquids based on (a) Young’s state, (b) Wenzel state, and (c) Cassie-Baxter state. The corresponding equations based on these three theoretical approaches help measure the contact angle between the oil droplet and solid surface 23

Figure 2.3 A comparison of the effect of final surface coating in the LbL modification of a glass surface, using binder PDDA, SiO₂ NPs, and FLs, such as silane, fluorosilane, and fluorosurfactant: (a) chemical representation of the layers and (b) contact angle of water and hexadecane on different surfaces [186]..... 27

Figure 2.4. Illustration of membrane types for oil-water separation based on wettability: (a) oleophilic and hydrophobic; (b) oleophobic and hydrophilic; (c) oleophilic and hydrophilic; and (d) oleophobic and hydrophobic. 28

Figure 2.5. Plasma irradiation technique using inorganic gas (Ar) for generating a superhydrophobic surface with WCA of 167°[192]. 34

Figure 2.6. Fabrication of superhydrophobic surface using ion beam irradiation technique [193]. 35

Figure 2.7. Application of femtosecond laser to fabricate superhydrophobic polycarbonate (PC) surface [18]. 36

Figure 2.8. A typical process to fabricate superhydrophobic and superoleophilic surfaces. 40

Figure 2.9. A schematic of activation of oxygen based functional groups. 41

Figure 2.10. Effect of pretreatment method on contact angle of water on Au coated film: (a) no pretreatment, (b) 10 min UV irradiation, (c) 20 min UV irradiation, (d) piranha solution, (e) oxygen plasma, and (f) air plasma [219]. 42

Figure 2.11. Different methods of surface morphology change with application to oil-water separation. Top-down methods: (a) femtosecond laser irradiation on the platinum surface [223], (b) oxygen and bromite plasma etching and reactive ion synthesis [224], (c) SS HF acid etched [225], and (d) lotus-like papillary structure using soft lithography of polydimethylsioxane (PDMS)

[226]. Bottom-up methods: (e) template technique to create PDMS cone array [227], (f) raspberry-like colloidal system of PAA-functionalized PS core with silica NPs [228], (g) PS in tetrahydrofuran (THF)/dimethylformamide (DMF) solvent through electrospun [229], and (h) hydrothermal approach for creating ZnO nanorods [230]. 44

Figure 2.12. Classification of superhydrophobic and superoleophilic membranes with application to oil-water separation..... 47

Figure 2.13. Impact of carbon fiber thickness (membrane thickness) and multi-wall CNTs roughness on: (a) separation efficiency and (b) membrane flux, for a superhydrophobic and superoleophilic membrane [264]. 67

Figure 3.1. Schematics of the experimental procedures for (a) stainless steel mesh cleaning, (b) mesh activation, (c) coating solution preparation, and (d) mesh coating. 122

Figure 3.2. Mechanism of bonding between silane (Dynasylan® R8261) and activated stainless steel mesh (modified after Mostafaei et al. [53]). In this figure different steps are given: (a) hydrolysis, (b) condensation, (c) adsorption through hydrogen bonding, and (d) covalent bonding (or, grafting)..... 124

Figure 3.3. Oil-water separation experimental set up using SHSO mesh tube: (a) schematic picture, and (b) actual set up. Oil is shown in brown and water is shown in light blue color. 126

Figure 3.4. Static WCA on coated stainless steel mesh in the presence of air at ambient condition. The wt% of the NPs and MPs in the solid are given in the x-axis. The contact angle results are averaged for three replicates. 129

Figure 3.5. Snapshot of the water droplet starting to slide on an SHSO mesh (coated with F12) by increasing the inclination angle. The sliding starts in the frame (b). 129

Figure 3. 6. Transmission electron microscopy (TEM) pictures from solids used in the coating solution: (a) NPs (Aerosil® R812), (b) MPs (SIPERNAT® D13), and (c) mixture of NPs+MPs. 130

Figure 3.7. Scan electron microscopy of four SHSO mesh samples at 1,000X magnification: (a) silanized (F7), (b) F8 coating with 100% MPs, (c) F11 coating with 75% NPs and 25% MPs, and

(d) F12 coating with 100% NPs. The long-chain silane is used in all coatings. The nominal size of the mesh opening is 75 μm .	132
Figure 3.8. A schematic of the flower-like roughness features of the SHSO mesh (coated with F12). The dashed yellow circles are approximately fitted to the mesh opening, and the white circles are fitted to the pore opening, corresponding to the breakthrough condition for the non-wetting phase. The numbers in the figure show diameter in μm .	133
Figure 3.9. Overlay of XRD patterns for the clean mesh (blue), silanized mesh (red), and mesh coated with F12 (black); γ and α are austenite and martensite steel phases, respectively.	134
Figure 3.10. EDX analysis of the SHSO mesh coating (F12).	135
Figure 3.11. FTIR spectra of the SHSO mesh (coated with F12) in wavelength range 400 to 4000 cm^{-1} .	136
Figure 3.12. Chemical stability analysis through WCA measurements. The SHSO mesh samples are aged at room temperature in H_2SO_4 (0.1 M, shown in blue), NaOH (0.1 M, shown in red), and brine (1 M, shown in black) solutions over four weeks. The markers indicate the average of contact angle values for five replicates.	137
Figure 3.13. Scanning electron microscopy pictures (at 500X magnification) of the SHSO mesh exposed to: (a) 1.0 M H_2SO_4 , and (b) 1.0 M NaOH for one week.	138
Figure 4.1. Schematic of dynamic oil-water separation setup	161
Figure 4.2. SEM images with magnification of 100X and the shape of water droplet on the mesh (a) cleaned and (b) SHSO coated mesh.	163
Figure 4.3. SEM and TEM images of the SHSO mesh; (a) SHSO mesh with 500X magnification and (b) with 5,000X magnification. (c) The TEM image of functionalized silica NPs as roughness on the surface of mesh with 30,000X magnification.	164
Figure 4.4. Oil (a) and water (b) collection vs time in dynamic oil-water separation test for oil-water mixtures under different flow rates and concentrations (% vol oil)	166
Figure 4.5. The oil permeates flux vs time in dynamic oil-water separation for different oil concentrations and total flow rate of the oil-water mixture.	168

Figure 4.6. The height of oil around SHSO mesh tube vs time in dynamic oil-water separation for different O:W concentrations and total flow rate of the oil-water mixture. 169

Figure 4.7. Dynamic oil-water separation set up (a) and the height of oil around mesh tube at (b) qt= 5 mL/min, 10 vol% oil, (c) qt= 5 mL/min, 30 vol% oil, (d) qt= 5 mL/min, 50 vol% oil, (e) qt= 10 mL/min, 10 vol% oil, (f) qt= 10 mL/min, 30 vol% oil, (g) qt= 10 mL/min, 50 vol% oil, (h) qt= 15 mL/min, 10 vol% oil, (i) qt= 15 mL/min, 30 vol% oil, (j) qt= 15 mL/min, 50 vol% oil..... 170

Figure 4.8. Separation efficiency tests for oil (a, b, c) and water (d, e, f) vs time at different oil concentrations under constant total flow rate (qt)..... 174

Figure 4.9. Separation efficiency tests for oil (a, b, c) and water (d, e, f) vs time at different total flow rates (qt) under constant oil concentration. 175

List of Tables

Table 2.1. Conventional methods for separation of oil from oily wastewaters.	22
Table 2.2. Advantages and disadvantages of different methods for the fabrication of superhydrophobic and superoleophilic membranes.....	37
Table 2.3. A summary of available pathways for wettability alteration to superhydrophobic and superoleophilic with implication of oil-water separation.	45
Table 2.4. Superhydrophobic and superoleophilic mesh-based membranes for oil-water separation.	56
Table 2.5. Superhydrophobic and superoleophilic porous membranes for oil-water separation..	69
Table 2.6. Superhydrophobic and superoleophilic surfaces for oil-water separation application (Film)	74
Table 3.1. Coating formulations with different silanes and solid particles.	123
Table 4.1. The rate of oil and water collection for different scenarios of oil-water mixture.....	167

1. CHAPTER ONE

Introduction and Overview

1.1. Motivation

Oily wastewater treatment is becoming a serious environmental concern with rapid population growth and industrial developments. During processing in various industries, such as petrochemicals [1], metal [2], food [3], mining [4], leather [5], and textile [6], a large amount of oily wastewater is produced daily. Also, oil production and transportation facilities face the risk of oil spill incidents that cause serious impact on the environment and human health [7]. The resultant oil-water systems should be appropriately treated before being discharged into the water bodies.

To date, various methods, such as gravity separation, centrifugation, air flotation, electric field, coagulation, and adsorption have been employed to separate oil from water mixtures. These methods have some drawbacks such as low selectivity, fairly expensive, operator-based, and time-consuming procedures; they might also produce secondary pollutants [8]. Membrane filtration, a known separation technology, has been extensively applied for oil-water separation purposes [9] due to its durability, simplicity, and economic features [10]. Functionalized membranes with superhydrophobic-superoleophilic (SHSO) wettability have gained tremendous attention for oil-water separation applications. With a high affinity towards the oil phase, they are able to completely repel the water phase [11]. For a given oil-water mixture, the separation efficiency is strongly dependent on the wetting state and surface roughness. The surface roughness improves the oil separation efficiency; but it also reduces the maximum permeation flux by decreasing pore size.

SHSO membranes are commonly fabricated after surface cleaning and activation, creating hierarchical structures on the membrane surface, and modifying surface chemistry with low surface energy materials [8]. A variety of physical techniques (e.g., sandblasting, abrasion, and ultrasonication) [12], chemicals (acetone, ethanol, and deionized water), and a combination of

these methods are used for surface cleaning purposes [13]. For the surface activation step, various techniques are employed, such as plasma (air or oxygen), acid/oxidizers (i.e., $\text{H}_2\text{SO}_4/\text{H}_2\text{O}_2$, $\text{H}_2\text{SO}_4/\text{H}_2\text{CrO}_4$, and $\text{H}_2\text{SO}_4/\text{CrO}_3$), ultraviolet (UV)/ozone, and corona treatments [14]. Based on the literature, there are different methods such as chemical vapor deposition (CVD) [15], sol-gel [16], acid erosion [17], laser [18], electrochemical [19, 20], rough polymer film [21], and crystal growth to generate the surface roughness [22]. The surface chemistry can be also modified by the use of various materials, including silanes [23, 24], thiols [25, 26], and stearic acid [27, 28].

Although SHSO surfaces are becoming more common, selection of a simple, inexpensive, and efficient fabrication method with long-term mechanical and chemical stability is still challenging. Accordingly, metallic mesh-based membranes (i.e., stainless-steel and copper-based) are employed to fabricate SHSO membranes due to their mechanical strength and lower pressure drop [29]. Apart from the base material, a micro- and nano-scale roughness can improve the mechanical stability of the membrane [30]. Hence, complex hierarchical roughness can be created through lithography templating, casting, laser, and 3D printers on the membrane surface. However, these futuristic approaches are still time-consuming and expensive in large-surface applications. More investigations are required to address these aspects. Dip-coating into a colloidal solution can be a fast and reliable approach that modifies both surface free energy and surface geometrical structure simultaneously while constructing complex hierarchical roughness [31].

Recently, we prepared a comprehensive review of theoretical and practical approaches for the fabrication and characterization of SHSO surfaces. SHSO membranes were first introduced by Fang et al. in 2004 [32], through spray-coating PTFE particles onto the surface of SS mesh to achieve a WCA of 156° . Yang et al. [33], employed the same method, spray-coated SS mesh by epoxy/attapulgitite (44.4 wt%) and obtained a WCA of 160° with 98% oil-water separation

efficiency. Xiang et al. [20] grafted n-dodecyl mercaptan by polydopamine onto the different substrates (i.e., SS, Ni, Cu, Fe) through an electrodeposition method. Their popcorn-like micro-nano hierarchical structures showed a WCA of 162° and separation efficiency of 98%. Using a mixture of phenol formaldehyde and $\text{Mg}(\text{OH})_2$ nanoparticles in stearic acid, Cao et al. [34], achieved a WCA of 151° and separation efficiency of 94%. Most of the SHSO membranes studies have been focused on the static oil-water separation [11, 13, 17, 20, 33-48]. To the best of our knowledge, there are only a few studies to evaluate continuous/dynamic oil-water separation efficiency using the super wetting surfaces. For instance, Dunderdale et al. [49], continuously separated oil and water by designing an apparatus with two antagonistic stainless-steel meshes, including poly sodium methacrylate (as a superoleophobic mesh) and poly stearyl methacrylate (as a superhydrophobic mesh). A high separation efficiency of $99\text{-}100\% \pm 0.4\%$ mol/mol was achieved for a mixture with 50 vol% n-hexadecane in water. Ezazi et al. [50] investigated the continuous separation of stabilized oil-in-water emulsion using Fe- TiO_2 spray-coated SS meshes. They obtained a separation efficiency of over 97% and flux recovery of about 99% upon implementing a continuous separation process.

As described, many studies have evaluated the SHSO membrane performance for oil-water separation applications, but this research field still requires more experimental works on reducing the cost/time of fabrication process, determining the SHSO mesh stability in various harsh conditions, adjusting with more industrial applications, and further understanding of the separation mechanism. To accomplish the current knowledge gap in this area, we propose a novel and inexpensive method for fabrication of SHSO stainless steel mesh for an effective and dynamic oil water separation.

1.2. Experimental Phases

At the first phase of this research work, the fabrication of a SHSO membrane through dip-coating is investigated where the influence of the solid particle with different ratios (MPs:NPs) on the wettability of the SHSO mesh membrane is studied in the presence of organo-alkylsilanes with short- and long alkyl-chain sizes. Moreover, the stability and separation efficiency of the fabricated membrane are studied. In the second phase of this project, dynamic/continuous oil-water separation tests are performed at different concentrations (10, 30, and 50 vol% oil) and total flow rates (5, 10, and 15 mL/min) over a period of 70 minutes. In this phase, important aspects such as the cumulative volumes of oil and water, the separation efficiency of oil and water, the oil permeation flux, pore opening, and the height of oil around the mesh tube are investigated based on a proper design of experiment approach.

The main contributions/phases of this research project are given below:

- The impacts of long- and short-chain silane, as well as the different ratios of nano-to microparticles on membrane wettability, are evaluated through WCA tests. The long-chain alkyl silane features a better hydrophobicity at all levels of the solid compositions. With both silanes, the maximum contact angle for water is obtained when the solid part of the coating solutions contains 75% nanoparticles and 25% microparticles.
- The contact angle hysteresis is calculated for the SHSO membrane.
- The stability of as-fabricated SHSO mesh is evaluated while exposing the mesh to the solutions of 0.1 M NaOH, 1 M H₂SO₄, 1 M NaCl over four weeks.
- Surface morphology, the dominant surface elements, coating structure, surface functional groups, and NPs morphology are detected using characterization tests such as SEM, EDX, XRD, FTIR, and TEM, respectively.

- Static oil-water separation analysis is performed for canola oil and hexane in water separately using the as-fabricated SHSO mesh.
- The performance of the as-fabricated SHSO mesh tube in a dynamic/continuous cross-flow separation setup is investigated over a 70-minutes time period by changing oil concentration and total flow rate.
- The oil permeation flux, the height of oil around the mesh tube, and oil and water production rates are investigated over the separation process.

1.3. Thesis Structure

This thesis consists of a series of manuscripts accepted or under review for publication, as listed below:

Chapter Two has been submitted to the Journal of Materials and Design. The manuscript provides a systematic literature review on the fabrication and characterization of the SHSO surfaces used in the oil-water separation processes. It further highlights the pros and cons of the fabrication and characterization techniques, current status and prospects of SHSO membranes, and potential future research directions.

Chapter Three has been published in the Chemical Engineering Science Journal. Using a facile one-step dip-coating technique, the effects of length of alkylsilane (short and long) as well as ratio of nano- to micro- particles (0, 25, 50, 75, and 100 wt%) on the wettability state of SHSO stainless-steel mesh are investigated. Sivo 408 and Dynasylan[®] F8261 are employed as the short- and long-chain silanes, respectively. Furthermore, Aerosil[®] R812 and SIPERNAT[®] D13 are utilized as the nano and microparticles, respectively. The fabricated SHSO mesh is characterized through measurements of WCA and sliding angle, SEM, XRD, EDX, FTIR, chemical stability analysis, and static oil-water separation efficiency tests.

Chapter Four will be submitted to the Applied Materials and Interfaces Journal soon. A part of the experiments (dynamic oil-water separation tests) was conducted during the COVID-19 lockdown using a simplified experimental setup in my home office. As a new approach, we employ the SHSO stainless-steel mesh tube coated with the best coating solution based on our previous research (100% NPs and long-chain silane). In this research phase, we investigate the impacts of oil concentration (10, 30, and 50 vol%) and total flow rate of the oil-water mixture (5, 10, and 15 mL/min) on the oil and water separation efficiency, and oil permeation flux of SHSO membrane, through dynamic tests.

Chapter five summarizes a brief of each chapter (description and conclusions) and recommendations for future work.

References

1. Pendashteh, A.R., et al., *Membrane foulants characterization in a membrane bioreactor (MBR) treating hypersaline oily wastewater*. Chemical Engineering Journal, 2011. 168(1): p. 140-150.
2. Rubio, J., M.L. Souza, and R.W. Smith, *Overview of flotation as a wastewater treatment technique*. Minerals Engineering, 2002. 15(3): p. 139-155.
3. Zhong, J., X. Sun, and C. Wang, *Treatment of oily wastewater produced from refinery processes using flocculation and ceramic membrane filtration*. Separation and Purification Technology, 2003. 32(1): p. 93-98.
4. Gupta, R.K., et al., *Oil/water separation techniques: a review of recent progresses and future directions*. Journal of Materials Chemistry A, 2017. 5(31): p. 16025-16058.
5. Doble, M. and A.K. Kruthiventi, *CHAPTER 9 - Industrial Examples*, in *Green Chemistry and Engineering*, M. Doble and A.K. Kruthiventi, Editors. 2007, Academic Press: Burlington. p. 245-296.
6. Cheryan, M. and N. Rajagopalan, *Membrane processing of oily streams. Wastewater treatment and waste reduction*. Journal of Membrane Science, 1998. 151(1): p. 13-28.
7. Li, Q., C. Kang, and C. Zhang, *Waste water produced from an oilfield and continuous treatment with an oil-degrading bacterium*. Process Biochemistry, 2005. 40(2): p. 873-877.
8. Liu, D., et al., *Selective separation of oil and water with special wettability mesh membranes*. RSC Advances, 2017. 7(21): p. 12908-12915.
9. Unno, H., H. Saka, and T. Akehata, *OIL SEPARATION FROM OIL-WATER MIXTURE BY A POROUS POLY(TETRAFLUOROETHYLENE) (PTFE) MEMBRANE*. Journal of Chemical Engineering of Japan, 1986. 19(4): p. 281-286.
10. Saththasivam, J., K. Loganathan, and S. Sarp, *An overview of oil-water separation using gas flotation systems*. Chemosphere, 2016. 144: p. 671-680.

11. Zhang, Y., et al., *Facile fabrication of zinc oxide coated superhydrophobic and superoleophilic meshes for efficient oil/water separation*. RSC Advances, 2018. 8(61): p. 35150-35156.
12. Ebnesajjad, S., *Material Surface Preparation Techniques*, in *Handbook of Adhesives and Surface Preparation*. 2011, Elsevier. p. 49-81.
13. Li, H., et al., *Two-dimensional ZnO nanoflakes coated mesh for the separation of water and oil*. Materials Research Bulletin, 2013. 48(1): p. 25-29.
14. Li, L., et al., *Roles of silanes and silicones in forming superhydrophobic and superoleophobic materials*. Journal of Materials Chemistry A, 2016. 4(36): p. 13677-13725.
15. Wen, N., et al., *An alternative fabrication of underoil superhydrophobic or underwater superoleophobic stainless steel meshes for oil-water separation: Originating from one-step vapor deposition of polydimethylsiloxane*. Separation and Purification Technology, 2018. 204: p. 116-126.
16. Zhang, X., et al., *A one-pot sol-gel process to prepare a superhydrophobic and environment-resistant thin film from ORMOSIL nanoparticles*. RSC Advances, 2014. 4(19): p. 9838-9841.
17. Wang, Q., et al., *Stable highly hydrophobic and oleophilic meshes for oil-water separation*. Vol. 253. 2007. 9054-9060.
18. Bhagat, S.D. and M.C. Gupta, *Superhydrophobic microtextured polycarbonate surfaces*. Surface and Coatings Technology, 2015. 270: p. 117-122.
19. Xu, Z., et al., *Fabrication of superhydrophobic nano-aluminum films on stainless steel meshes by electrophoretic deposition for oil-water separation*. Applied Surface Science, 2018. 427: p. 253-261.
20. Xiang, M., et al., *Fabrication of a novel superhydrophobic and superoleophilic surface by one-step electrodeposition method for continuous oil/water separation*. Applied Surface Science, 2018. 434: p. 1015-1020.
21. Darmanin, T., M. Nicolas, and F. Guittard, *Electrodeposited polymer films with both superhydrophobicity and superoleophilicity*. Physical Chemistry Chemical Physics, 2008. 10(29): p. 4322-4326.
22. Wu, J., et al., *A hierarchical mesh film with superhydrophobic and superoleophilic properties for oil and water separation*. Journal of Chemical Technology & Biotechnology, 2012. 87(3): p. 427-430.
23. Zhang, X., et al., *Bioinspired Multifunctional Foam with Self-Cleaning and Oil/Water Separation*. Advanced Functional Materials, 2013. 23(22): p. 2881-2886.
24. Liu, H., et al., *Robust translucent superhydrophobic PDMS/PMMA film by facile one-step spray for self-cleaning and efficient emulsion separation*. Chemical Engineering Journal, 2017. 330: p. 26-35.
25. Ma, W., et al., *Durable superhydrophobic and superoleophilic electrospun nanofibrous membrane for oil-water emulsion separation*. Journal of Colloid and Interface Science, 2018. 532: p. 12-23.
26. Jian, S., et al., *Design and fabrication of superhydrophobic/superoleophilic Ni₃S₂-nanorods/Ni-mesh for oil-water separation*. Surface and Coatings Technology, 2018. 337: p. 370-378.

27. Yue, X., et al., *In situ one-step fabrication of durable superhydrophobic-superoleophilic cellulose/LDH membrane with hierarchical structure for efficiency oil/water separation*. Chemical Engineering Journal, 2017. 328: p. 117-123.
28. Yang, C., et al., *A stable eco-friendly superhydrophobic/superoleophilic copper mesh fabricated by one-step immersion for efficient oil/water separation*. Surface and Coatings Technology, 2019. 359: p. 108-116.
29. Wang, H., et al., *Review: Porous Metal Filters and Membranes for Oil–Water Separation*. Nanoscale Research Letters, 2018. 13(1): p. 284.
30. Yuzhang, Z., et al., *Recent progress in developing advanced membranes for emulsified oil/water separation*. NPG Asia Materials, 2014. 6(5): p. e101.
31. Kaur, H., V.K. Bulasara, and R.K. Gupta, *Influence of pH and temperature of dip-coating solution on the properties of cellulose acetate-ceramic composite membrane for ultrafiltration*. Carbohydrate Polymers, 2018. 195: p. 613-621.
32. Feng, L., et al., *A Super-Hydrophobic and Super-Oleophilic Coating Mesh Film for the Separation of Oil and Water*. Angewandte Chemie International Edition, 2004. 43(15): p. 2012-2014.
33. Yang, J., et al., *Durable superhydrophobic/superoleophilic epoxy/attapulgitic nanocomposite coatings for oil/water separation*. Surface and Coatings Technology, 2015. 272: p. 285-290.
34. Cao, W.-T., et al., *Facile preparation of robust and superhydrophobic materials for self-cleaning and oil/water separation*. Colloids and Surfaces A: Physicochemical and Engineering Aspects, 2017. 529: p. 18-25.
35. Feng, L., et al., *A Super-Hydrophobic and Super-Oleophilic Coating Mesh Film for the Separation of Oil and Water*. Angewandte Chemie, 2004. 116(15): p. 2046-2048.
36. Lee, C. and S. Baik, *Vertically-aligned carbon nano-tube membrane filters with superhydrophobicity and superoleophilicity*. Carbon, 2010. 48(8): p. 2192-2197.
37. Wang, C.-F., et al., *Ultraviolet-Durable Superhydrophobic Zinc Oxide-Coated Mesh Films for Surface and Underwater–Oil Capture and Transportation*. Langmuir, 2012. 28(26): p. 10015-10019.
38. Wang, S., M. Li, and Q. Lu, *Filter Paper with Selective Absorption and Separation of Liquids that Differ in Surface Tension*. ACS Applied Materials & Interfaces, 2010. 2(3): p. 677-683.
39. Yang, H., et al., *Facile preparation of super-hydrophobic and super-oleophilic silica film on stainless steel mesh via sol–gel process*. Applied Surface Science, 2010. 256(13): p. 4095-4102.
40. Hsieh, C.-T., et al., *Hierarchical oil–water separation membrane using carbon fabrics decorated with carbon nanotubes*. Vol. 286. 2016. 148-154.
41. Yang, H., et al., *Functional silica film on stainless steel mesh with tunable wettability*. Surface and Coatings Technology, 2011. 205(23): p. 5387-5393.
42. Liu, Y., et al., *Bioinspired structured superhydrophobic and superoleophilic stainless steel mesh for efficient oil-water separation*. Colloids and Surfaces A: Physicochemical and Engineering Aspects, 2016. 500: p. 54-63.
43. Matin, A., et al., *Superhydrophobic and superoleophilic surfaces prepared by spray-coating of facile synthesized Cerium(IV) oxide nanoparticles for efficient oil/water separation*. Applied Surface Science, 2018. 462: p. 95-104.

44. Baig, U., et al., *Facile fabrication of superhydrophobic, superoleophilic photocatalytic membrane for efficient oil-water separation and removal of hazardous organic pollutants*. Journal of Cleaner Production, 2019. 208: p. 904-915.
45. Li, J., et al., *A diatomite coated mesh with switchable wettability for on-demand oil/water separation and methylene blue adsorption*. Separation and Purification Technology, 2017. 174: p. 275-281.
46. Xiao, C., et al., *Ultrastable coaxial cable-like superhydrophobic mesh with self-adaption effect: facile synthesis and oil/water separation application*. Journal of Materials Chemistry A, 2016. 4(21): p. 8080-8090.
47. Matin, A., et al., *Facile fabrication of superhydrophobic/superoleophilic microporous membranes by spray-coating ytterbium oxide particles for efficient oil-water separation*. Journal of Membrane Science, 2018. 548: p. 390-397.
48. Du, Z., et al., *Facile Preparation of Ag-Coated Superhydrophobic/Superoleophilic Mesh for Efficient Oil/Water Separation with Excellent Corrosion Resistance*. Langmuir, 2018. 34(23): p. 6922-6929.
49. Dunderdale, G.J., et al., *Continuous, High-Speed, and Efficient Oil/Water Separation using Meshes with Antagonistic Wetting Properties*. ACS applied materials & interfaces, 2015. 7(34): p. 18915-18919.
50. Ezazi, M., et al., *Selective Wettability Membrane for Continuous Oil–Water Separation and In Situ Visible Light-Driven Photocatalytic Purification of Water*. Global challenges, 2020. 4(10): p. 2000009-n/a.

2. CHAPTER TWO

**Literature Review (Superhydrophobic and Superoleophilic Membranes for
Oil-Water Separation Application: A Comprehensive Review)**

Abstract

Superhydrophobic and superoleophilic (SHSO) membranes have gained remarkable attention, particularly in oil-water separation applications. This paper provides a comprehensive review on SHSO membranes, available fabrication and characterization methods, the pros and cons of these techniques, current status and future prospect of SHSO surfaces, and potential future research directions. Here, the metallic mesh-based membranes exhibited higher mechanical strength, lower pressure drop, and higher permeability compared to porous membranes. Using facile methods (based on colloidal assembly) and applying a rough polymer film are found to be cheaper alternatives in creating surface roughness, which is required to achieve the SHSO conditions. To adjust the surface energy for such wetness conditions, a majority of the studies in the literature use stearic acid, and different silanes and thiols. Techniques such as scanning electron microscopy (SEM), X-ray powder diffraction (XRD), Fourier transform infrared spectroscopy (FTIR), X-ray photoelectron spectroscopy (XPS), atomic force microscopy (AFM), and permeation tests are also used to quantify the membrane performance; while limited studies have performed short-term stability analysis, using contact angle measurements. One of the aspects that is overlooked in the literature is the influence of fouling on the performance of the SHSO membranes that can be covered in future research.

Keywords: Superhydrophobic; Superoleophilic; Membrane; Fabrication methods; Characterization techniques; Oil-water separation

2.1. Introduction

Oil-water separation becomes important in applications such the treatment of oily wastewater and oil spill removal. A considerable volume of industrial oily wastewater is produced in textile [6],

food [3], leather [5], metal processing [2], oil and gas [1], and mining [4] industries. The oil spill can occur in oil exploration and production [7], refining [51], and transportation [52] phases in the oil industry, imposing severe environmental and economic impacts [53-55]. Despite the global awareness about the adverse environmental and health effects of the oil spills incidents, they only account for less than 10% of the oil entering the oceans [56]. A critical review of different oil-water separation technologies is available in the literature [4]. Various methods such as gravity settling [10, 56, 57], centrifugation [58], gas flotation [59], electric field [60], coagulation [61], membrane filtrations [9], and electrochemical [62] technologies are commonly used for oil-water separation. However, low selectivity, long separation time [10, 56, 57], high energy input [58, 63], large land requirement [27], and the production of secondary pollutants [64, 65] are among the drawbacks of the conventional oil-water separation strategies.

Membrane filtration with special wetting condition has found tremendous attention in the last 10 years. Surfaces with extreme wetting (e.g., superhydrophilic/superoleophilic) or extreme non-wetting conditions (e.g., superhydrophobic/superoleophobic) have been fabricated and used in various industrial sectors dealing with oil-water separation. A simultaneously superhydrophobic and superoleophilic (mesh-based) membrane was first introduced in 2004 by Feng et al. [32]. In 2010, the catastrophic *Deepwater Horizon* oil spill occurred in the Gulf of Mexico where 100 million barrels of oil were leaked from a faulty valve [66]. Less than 10% of the water surface oil contamination was recovered by mechanical methods [67]. Such a low recovery efficiency revitalized research on superhydrophobic and superoleophilic membranes and sorbents, as selective tools to effectively capture the oil by rejecting water [68].

Feng et al. [32] used a stainless steel (SS) mesh as a base material, and spray coated the clean mesh with a suspension of polytetrafluoroethylene (PTFE, 30 wt%), polyvinyl acetate (PVAC, 10% as

an adhesive), polyvinyl alcohol (PVA, 8% as a dispersant), water (50% as a diluent), and sodium dodecylbenzenesulfonate (SDBS), 2% as a surfactant). The coated mesh was cured at 350°C. They noticed a water contact angle (WCA) of 156.2°, an OCA of zero for diesel oil, and a sliding angle of 4°. The general procedure of fabricating superhydrophobic and superoleophilic membranes includes three main steps of 1) surface preparation involving cleaning and activation, 2) surface roughness modification, and 3) surface chemistry modification. In addition to abrasion and sandblasting as physical methods for removal of loose materials [12], successive cycles of chemical cleaning (with and without ultrasonication) are applied through using deionized water, acetone, and ethanol to eliminate the contaminations [13]. To prepare the surface for superhydrophobic and superoleophilic coating, surface activation methods such as acid/oxidizers (e.g., H₂SO₄/H₂O₂, H₂SO₄/H₂CrO₄, and H₂SO₄/CrO₃), plasma (air or oxygen), ultraviolet (UV)/ozone, and corona treatments have been used in previous research and engineering works [14, 69]. The micro- and nano- surface roughness types are required for the superhydrophobic and superoleophilic wetting condition. These hierarchical micro- and nano-roughness schemes are created by top-down methods such as lithography, etching, laser ablation, annealing, and sandblasting [70-78], and/or bottom-up methods such as layer-by-layer (LbL) assembly, hydrothermal, anodizing, electrodeposition, colloidal assembly, rough polymer films, templating, casting and replication, and 3D printing [71, 72, 74-76, 79, 80]. To attain proper surface energy for superhydrophobic and superoleophilic wettability condition, organic, inorganic, and organic-inorganic composite chemicals are employed to reduce the surface energy [72, 75]. Among the inorganic chemicals, silanes are the most widely used chemical solutions to lower the surface energy of superhydrophobic and superoleophilic membranes [17, 23, 24, 41, 81-92], while in the

category of organic coatings, stearic acid [11, 13, 27, 28, 34, 42, 48, 88, 93-95], and a variety of thiols [20, 25, 26, 47, 96-101] appear to be dominant chemicals.

Superhydrophobic and superoleophilic functionalized SS [11, 13, 17, 20, 22, 33-37, 41-43, 46-48, 102, 103] and copper (Cu) [28, 83, 84, 96-100, 104-108] mesh-based membranes have found more attention by researchers and engineers, because of their mechanical strengths, and lower pressure drop (compared to the porous membranes). The mesh pore opening and thickness control the flow rate of permeate for a given oil. For example, Shi et al. [109] used a single wall carbon nanotube (CNT) film with a thickness of 30–120 nm and obtained up to three orders of magnitude higher permeate flux (up to 100,000 L/(m².h.bar)), compared to conventional filters. With the recent advancements in 2D materials such as graphene, they are expected to play a key role in fabrication of ultra-thin filters with application to oil-water separation. Creating the hierarchical micro-and nano-roughness is an important step in achieving the super wetting or super non-wetting conditions. Although specific hierarchical micro- nano roughness structures are created in the literature using lithography, femtosecond laser ablation, templating, casting, and 3D printing [110-116], there are still cost and scaling limitations to be overcome, implying more research and engineering activities are needed to address these aspects. Methods on the basis of electrochemistry and crystal growth are also used to create superhydrophobic and superoleophilic surfaces with hierarchical micro-nano structures such as spikes [117], flake [13], flower-like [22], coral [108], and pillars [117]; they can be effective alternatives to construct complex roughness patterns. The facile approaches such as colloidal assembly or applying a rough polymer film [20, 21, 24, 33, 35, 38, 43, 47, 81, 83-86, 89, 90, 93, 103, 104, 118-124] include reduced number of process steps; they also appear to be as effective as the complex methods for creating hierarchical superhydrophobic and superoleophilic surfaces.

We organize the structure of this review paper in eight Sections. Following the introduction, a general background on oil contamination states and available oil-water separation technologies is given in Section 2. In Section 3, the theoretical foundation of different wetting states is provided. Section 4 reviews different methods for modifying surface morphology and chemistry. Section 5 briefly describes existing experimental methodologies to fabricate superhydrophobic and superoleophilic surfaces. In Section 6, we present three forms of superhydrophobic and superoleophilic surfaces that are used in oil-water separation, including film, mesh-based membranes, and porous membranes. Section 7 provides a brief discussion on current challenges and future perspectives of the superhydrophobic and superoleophilic membranes employed in oil-water separation operations. Finally, in Section 8, concluding remarks are listed.

2.2. Oil Contamination and Separation Technologies

2.2.1. The source of oil contaminations and their potential hazards

Although unexpected oil spills gain more attention (due to their short- and long-term intensive impacts on the environment), they only account for about 10% of the oil entering the ocean. A majority of the pollutants come from natural seeps, motor oil leakage, run-off oil from paved urban areas, and untreated industrial oily wastewater systems [56]. In terms of size, the oil contaminations can be categorized to free oil ($\geq 150 \mu\text{m}$), dispersed oil (20 to $150 \mu\text{m}$), emulsified oil ($\leq 20 \mu\text{m}$), and dissolved oil ($\leq 5 \mu\text{m}$). Free oil can be easily removed by gravity settling and floatation compared to other types of dispersed or emulsified oils [125, 126].

The primary sources of the industrial oily wastewater are food, metal processing (where cooling is required [126]), mining, textile, oil and gas, and chemical industries [4, 127]. In general, the concentration of oil in industrial oily wastewater systems varies from 10 ppm to 200,000 ppm [125, 128]. The development/design of effluent treatment systems to meet the regulations of

discharging oily wastewater is, therefore, imperative [128]. Governmental agencies have established quantitative (e.g., mg/L) and qualitative (no visible sheen in wastewater) measures for the intensity of oil contaminations in water [129]. These standards, however, may differ from one country to another. For example, the United States Environmental Protection Agency limits the daily discharge of oily wastewater up to 42 mg/L for oil and gas industries [130], while this limit is 10 mg/L in China [27].

The oily wastewater can cause odor annoyance, pipeline corrosion, and interference with the proper sewage treatment process, prompting potential health risks by utilizing dissolved oxygen of water [64, 131]. Bio-assay data demonstrate that oily wastewater brings acute and chronic toxicity to aquatic invertebrates [132-134]. For example, long-term exposure of both embryo and larvae at an oil concentration of 0.06 mg/L led to a significantly higher mortality rate due to a greater surface area-to-volume ratio [135]. Moreover, exposure of shrimp larvae to an Arctic crude oil of 0.015 mg/L and 0.06 mg/L resulted in a higher mortality and developmental time with increased oil concentration [136].

The hazardous materials found in industrial oily wastewater can affect human health, as well. Detrimental dermatologic and pulmonary effects are reported among the oil industry workers due to exposure to the barium that is used in drilling fluids [137, 138]. Furthermore, prolonged exposure to gasoline and its additives can cause cancer and central nervous system toxicity [137]. Due to the hazardous and toxic by-products in the oil and gas industry, the produced water treatment should be considered before discharging the oil contaminations into surface waters [138]. These wastewater sources can also include heavy metals and chemicals used in hydraulic fracturing [139, 140]. The Environmental Protection Agency has identified over 1000 chemicals in hydraulically fractured wells [141, 142]. Most of these carcinogenic compounds have potential

to act as endocrine disrupting chemicals [143, 144], which can interfere with hormonal activities [139, 145].

2.2.2. Oil-water separation technologies

In this section, we summarize numerous techniques used for oil-water separation, including gravity settling, centrifugation, gas flotation [10, 146], coagulation (and electrocoagulation) [147-151], adsorption, and membrane filtration [127]. Physical, chemical and biological methods of oil-water separation are the main treatment categories in various industrial and municipal sectors [152]. The chemical methods usually have higher operating costs, demand skilled operators, and require reliable process monitoring and control [6, 27].

Gas flotation methods, such as sparging or dissolved gas floatation (pressure-swing mode), can be employed to buoy the oil contamination droplets in a continuum of water. In the gas floatation systems, the gas bubbles (either injected or exsolved) adhere to the dispersed oil droplets to make agglomerates that can float. Researchers have also suggested use of surfactant to increase the removal efficiency of the oil droplets from water in a gas floatation system. In a sparging system, air is usually used in gas sparging due to its abundance. The gas floatation technique is more efficient for oil concentrations < 1000 mg/L [10]. The centrifugation increases the driving force to separate oil from oil-water mixture, which is especially beneficial when the oil and water have similar density values; however, the centrifugation is energy-intensive [58, 63]. Coagulation is a technology with high adaptability that has been widely used for treating oily wastewaters. This method can also be used for emulsified oil or dissolved oil, where colloids and suspended solids aggregate to form bigger flocs; the precipitated flocs can be removed from the system through sedimentation [153]. Despite the success of coagulation approach, the choice of coagulant and its concentration depend on the composition of wastewater; this treatment technique is expensive and

also produces secondary pollution that can harm aquatic species [64, 65]. Electrocoagulation is suggested to improve the separation driving force through coagulation process. The electric field increases the rate of coalescence and accelerates the agglomeration of smaller droplets that move towards the electrodes; these larger agglomerates can be separated easier under gravity forces [154]. Adsorption is another method that is used for oil-water separation, featuring low cost, high efficiency, and small space requirement [130]. Conventional absorbers including wool [155], zeolites [156], and activated carbon [157] may have some disadvantages (e.g., low selectivity, low absorption capacity, and difficulty in recycling) in the oil-water separation process [158]. Factors such as pH, temperature, suspended oil, concentration of heavy metal, organic chemical, organic-metal complex, and salinity influence the performance of adsorbents [130].

Filtration is an important strategy for oil-water separation that can separate oil from water based on size and capillarity. Membranes are semi-permeable surfaces that can be natural, synthetic, neutral, and charged that are suitable for separation of suspended solids, macromolecules, multivalent ions, and dissolved and ionic materials, respectively. Their thickness varies from several hundred micrometers to less than 10 nm. Pressure, temperature, and concentration gradients between the feed and permeate are usually the main factors for transferring phases through the membrane [159]. Over the past decade, membrane filtration has become an essential separation technique because of lower energy consumption and lower potentials of producing secondary pollutants. Based on the size of membrane opening, they are classified into microfiltration (MF), nanofiltration, ultrafiltration (UF), and reverse osmosis (RO). Membranes can also be useful to remove stable emulsified oils from water. Typically, the concentration of oil in wastewater is in the range 0.1 to 1%; using MF or UF, an oil separation efficiency of 40 to 70%

is usually obtained [6]. Natural oils and fats impose permeate flux impairment, and increase fouling risk [6]. Figure 2.1 illustrates the process of separation in membranes.

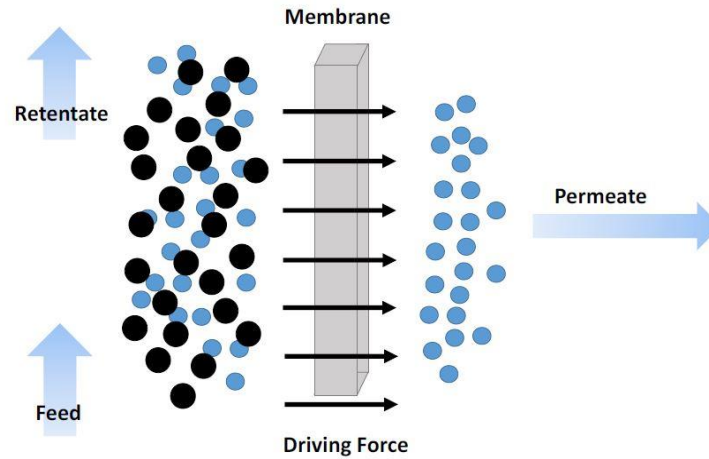


Figure 2.1. The schematic of the separation process in membranes [159]

The oil-water separation methods that were briefly discussed in this section can be used as stand-alone or hybrid with other techniques. A summary of the advantages and disadvantages of different technologies used for oil-water separation is given in Table 2.1. Limitations, such as low separation efficiency, generation of secondary pollutants, and presence of oil droplets with various sizes have motivated researchers to develop different effective methods. In recent years, advanced filtration technology with functionalized membranes has gained considerable attention for efficient water purification [125].

2.2.3. Hydrophilic and hydrophobic membranes

Generally, when it comes to using membranes for oil-water separation, two common surface wettability can be listed, either hydrophilic or hydrophobic membranes. The hydrophilic feature is known as the “water-loving” property, encouraging surface wettability. Water droplets can be spread on the surface and adsorb into the pores of hydrophilic membranes. On the contrary, water-hating characteristics can be found in hydrophobic (water repellent) membranes. Due to low surface energy of these membranes, spherical water droplets are created on the surface of

hydrophobic membranes [160]. Accordingly, the objective in hydrophobic membranes is to trap the oil droplets from an oil-water emulsion, but hydrophilic membranes are utilized to pass through water droplets for water purification purposes [161]. Compared to hydrophilic membranes, the hydrophobic ones exhibit lower flux rate and higher thermal stability (i.e., approximately 460°C is needed for the decomposition of hydrophobic membranes). However, hydrophilic membranes are favorable for gravity-driven separation processes, by passing oil-water mixtures through a hydrophilic membrane, oil droplets form a layer cake on the surface of the membrane, which eventually blocks membrane pores. Therefore, fouling as a primary challenge in the filtration technology should be considered particularly in hydrophilic membranes [160].

Table 2.1. Conventional methods for separation of oil from oily wastewaters.

Treatment	Advantages	Disadvantages	Driving force(s)	Screen Criteria/Remarks	Ref.
Gravity Settling	<ul style="list-style-type: none"> - Separation of bulk oils - Low energy consumption - Economical 	<ul style="list-style-type: none"> - Not efficient for high-density oil 	<ul style="list-style-type: none"> - Density difference 	<ul style="list-style-type: none"> - In American petroleum institute (API) tanks: oil droplets > 150 μm - In plates: oil droplets > 50 μm 	[10, 56, 57]
Centrifugation	<ul style="list-style-type: none"> - Efficient for free and dispersed oil - Fast separation 	<ul style="list-style-type: none"> - Produces low-quality oil - High energy demand - Fouling - Time-consuming - Expensive maintenance - Space limitations 	<ul style="list-style-type: none"> - Relative centrifugal force 	<ul style="list-style-type: none"> - Suitable for separating oil droplets with a size of 1 to 15 μm and oil contamination concentration of 20 to 30 mg/L 	[10, 56, 162, 163]
Gas Flotation	<ul style="list-style-type: none"> - Effective separation - Energy efficient - Simple operation 	<ul style="list-style-type: none"> - Requires large air volume - Slow separation 	<ul style="list-style-type: none"> - Solubility (in dissolved air floatation) - Density difference 	<ul style="list-style-type: none"> - More efficient with a smaller gas bubble, saltier wastewater, and oil droplet > 20 μm 	[10, 56]
Electrocoagulation	<ul style="list-style-type: none"> - Effective separation - Economical - Simple operation 	<ul style="list-style-type: none"> - Initial high expenditure - Anode passivation - High energy consumption 	<ul style="list-style-type: none"> - Voltage 	<ul style="list-style-type: none"> - Efficient up to 40 V and 1 cm distance between the electrodes - Energy consumption reduced to half, using voltage pulsation mode 	[126, 164]
Coagulation	<ul style="list-style-type: none"> - Good separation - Flexibility to be combined with floatation for higher separation efficiency 	<ul style="list-style-type: none"> - High operating costs - Skilled operator dependent - Secondary pollution problem - Composition dependent 	<ul style="list-style-type: none"> - Density difference 	<ul style="list-style-type: none"> - More efficient with oil droplets ≥ 50 mg/L 	[27, 149, 150, 165, 166]
Membrane Filtrations	<ul style="list-style-type: none"> - Fast separation - Pressure dependent 	<ul style="list-style-type: none"> - Fouling - High energy demand - High operating costs 	<ul style="list-style-type: none"> - Size 	<ul style="list-style-type: none"> - Polymeric membranes can be degraded under high temperatures >50°C 	[10, 56, 125, 164]
Electrochemical	<ul style="list-style-type: none"> - Controlled coating thickness 	<ul style="list-style-type: none"> - Deterioration of electrodes 	<ul style="list-style-type: none"> - Oxidation-reduction reactivity - Voltage 		[167]
Adsorption	<ul style="list-style-type: none"> - Low chemicals consumption - High removal of oil and chemical oxygen demand - Low cost and low-energy consumption process - Natural sorbents are environmentally friendly 	<ul style="list-style-type: none"> - Low hydrophobicity - High water uptake - Low efficiency - High retention time - Secondary pollutant in regeneration stage 	<ul style="list-style-type: none"> - Intermolecular and chemical forces (Coulombic, Debye, Keesom, ion-ion, ion-dipole, covalent, and hydrogen bond) 	<ul style="list-style-type: none"> - Not recommended for oil concentrations >50 mg/L - Not suitable for emulsified oil 	[10]

2.3. Surface Wetting Phenomena

2.3.1. Wetting states

The surface wetting characteristic is critical in oil-water separation application. The state-of-wetting is commonly characterized by contact angle of liquid on the solid surface in the presence of another fluid (e.g., gas). The equilibrium contact angle was derived from thermodynamics framework, which relates the contact angle to the interfacial tension according to Young's equation [168]:

$$\cos\theta_Y = \frac{\gamma_{SG} - \gamma_{LS}}{\gamma_{LG}} \quad (2.1)$$

where θ_Y refers to the equilibrium static contact angle of the liquid in the presence of a solid and gas, as depicted in Figure 2.2 (a); and γ_{SG} , γ_{LS} , and γ_{LG} stand for the solid-gas, liquid-solid and liquid-gas interfacial tension, respectively.

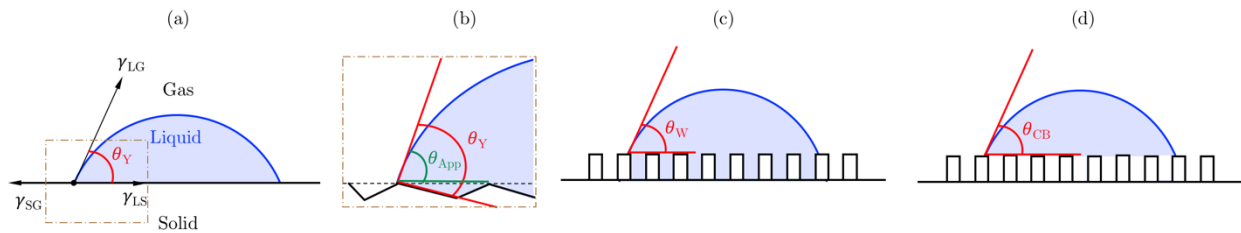


Figure 2.2. Three different contact conditions between surfaces and liquids based on (a) Young's state, (b) Wenzel state, and (c) Cassie-Baxter state. The corresponding equations based on these three theoretical approaches help measure the contact angle between the oil droplet and solid surface

Wenzel accounted for the effect of surface roughness on contact angle [169]. Let r be the ratio of the actual rough surface area to that of the horizontal projected (smooth) area. The apparent contact angle, which is measured (see Figure 2.2 (b)), can be correlated to the actual equilibrium contact angle through Wenzel's model [169]:

$$\cos\theta_{App} = r\cos\theta_Y \quad (2.2)$$

In Equation (2.2), θ_{App} represents the apparent contact angle and r denotes the surface roughness parameter. The extreme wetting and non-wetting states are shown in panels (c) and (d) of Figure 2.2, respectively; Figure 2.2 (c) illustrates the Wenzel state, while Figure 2.2 (d) shows the Cassie-Baxter state [170]. In Equation (2.2), the apparent contact angle can be replaced from the Wenzel model (e.g., $\cos\theta_W = r\cos\theta_Y$). In the Cassie-Baxter state, pockets of gas (e.g., air) are trapped below the liquid surface interface; these trapped air pockets do not allow the rough solid surface to be wetted by the liquid. The contact angle on the basis of the Cassie-Baxter model (θ_{CB}) is correlated to equilibrium contact angle from Young's model through the following correlation:

$$\cos\theta_{CB} = f_1\cos\theta_Y - f_2 \quad (2.3)$$

where f_1 and f_2 are the areas of the solid and gas under the liquid drop per unit projected area below the drop, respectively. According to Milne and Amirfazli [171], the simplified form of the Cassie-Baxter model that is conventionally used in the literature is only valid for a limiting case where the pillar top surfaces (exposed to the liquid drop) are flat. This means that in general, $f_1 + f_2 \geq 1$ [171]. The surface roughness of lotus leaves provides Cassie-Baxter non-wetting state to water droplets where only about 2-3% of the water droplet becomes wetted by the leaves.

With regard to water droplets, this extreme non-wetting state is known as lotus effect, super non-wetting or superhydrophobicity. It has been theoretically shown that both the Wenzel and Cassie-Baxter models are valid when the size of liquid droplet is much larger than the size of surface roughness (or heterogeneities) [172]. Kim et al. concluded that regardless of the wetting state, the contact angle at local minimum is correctly estimated from the theory when the size of the liquid drop is 40 times (or more than) the characteristics length of roughness [173]. Intermediate wetting state (so-called Marmur state, mixed state, and penetrating state) is also possible where the air

pockets in the rough pore spaces below the liquid drop are partially wetted by the liquid. Moreover, the co-existing of the Wenzel-Cassie states and the transition from one state to another are possible, suggesting that the measured contact angle may be a meta stable condition, which can be perturbed (e.g., through vibration) towards an equilibrium stable condition [174].

For a water droplet on a solid surface, in the presence of air, the contact angle of 90° is the threshold for wetting (hydrophilic) and non-wetting (hydrophobic) states. Surfaces with a static WCA greater than 90° are hydrophobic and those with a static $WCA < 90^\circ$ are hydrophilic. In general, two criteria are required for a surface to be hydrophobic: 1) high contact angle and 2) low rolling angle [175]. The term *superhydrophobic* is used for extreme non-wetting surfaces (regarding water droplet). In contrast, *superhydrophilicity* (static $WCA < 10^\circ$) refers to a state in which the surface is wetted extremely with water. Likewise, oleophilic and superoleophilic states are used for a solid surface wetted by oil (organic) phase; oleophobic and superoleophobic terms are used for solid surfaces not wetted by oil. Initially, *superhydrophobicity* was used in 1996 by Onda et al. [176]; it is since accepted as a common (popular) term among the scientific community [177]. The superhydrophobic surfaces are generally known with a static $WCA > 150^\circ$ as well as a small rolling angle ($< 10^\circ$) and contact angle hysteresis [178]. A critical review of the hydrophobic surfaces was written by Li et al. [72]. The terminology *superhydrophilicity* was first used in 2000 by Fujishima et al. [179]. This extreme wetting condition is characterized by a static $WCA < 10^\circ$ [180].

2.3.2. Wetting states at molecular level

At molecular level, the functional groups control the wettability of the surface. For instance, $-\text{OH}$, $-\text{COO}^-$, $-\text{COOH}$, $-\text{NH}_2$, $-\text{NH}_3^+$, $-\text{OSO}_3^-$, and $-\text{OSO}_3\text{H}$ can form hydrogen bonding with water molecules and exhibit hydrophilic features, while fluorocarbon, hydrocarbon or silicone-based polymers decrease the surface energy, promoting hydrophobicity [181]. An excellent review of the

hydrophobic surfaces was conducted by Drelich et al. [182]. From a molecular perspective, the most hydrophilic surface is obtained when the exposed functional group is capable of forming hydrogen bonding, such as $-\text{OH}$, $-\text{COOH}$, and $-\text{POOH}$; however, without surface roughness, a zero contact angle of water is not observed on these surfaces [182]. Similarly, the ionizable functional groups also provide hydrophilicity. They will dissociate to form highly hydrated ions, such as carboxylate, sulfonate, and alkyl ammonium ions [183]. For these functional groups, the wettability will be significantly affected by the pH; the surface will become more wetted, in general, if the functional groups are more ionized [184]. Thus, for the acidic and basic moieties, the surface will become wetted at higher and lower pH values, respectively. It should be noted that pH has no effect on the wetness characteristic when the functional group is not ionizable [184]. Furthermore, molecules with aliphatic (linear) chains have better hydrophobicity than branched or aromatic molecules, owing to the steric effect of the neighboring branches and aromatic ring that reduces the hydrophobic interactions with the water molecules [185]. Generally, surfaces tend to become more hydrophobic, and temperature also magnifies the hydrophobicity [185]. Oils typically are non-polar that may only contain a few polar groups and feature a low dielectric constant. As a result, they may not interact through van der Waals or hydrogen bonding to wet the surfaces with polar functional groups [185]. On the other hand, the hydrophobic surfaces have less interaction with water as a result of non-polar functional groups (e.g., F) at the surface [185]. In general, the hydrophobicity is affected by the length and shape of the functional groups [185]; by increasing the length of an alkyl chain, the surface would be more hydrophobic.

Brown and Bhushan [186] used LbL surface modification and achieved all four states of the wetting (e.g., superhydrophobic-superoleophilic, superhydrophobic-superoleophobic, superhydrophilic-superoleophilic, and superhydrophilic-superoleophobic), as depicted in Figure

2.3. In their study, the glass surface was used as the building block onto which polydiallyldimethyl ammonium chloride (PDDA) was deposited as a binder, a layer of 7 nm SiO₂ linked between the nanoparticles (NPs) and the functional layer (FL). Without any FLs, the surface with binder and NPs exhibited superhydrophilic and superoleophilic for which the contact angles of water and hexadecane were both zero [186]. Using methyltrichloro silane as the FL, the surface exhibited superhydrophobic and superoleophilic where the contact angle of water was 161°, while that of hexadecane was zero. By using 1H, 1H, 2H, and 2H-perfluorosilane in the FL, the surface becomes superhydrophobic and superoleophobic where the contact angles of water and hexadecane were 163° and 157°, respectively. Finally, utilizing an amphoteric fluorosurfactant in the FL (DuPont™ Capstone™ FS-50), the surface showed superhydrophilic and superoleophobic properties characterized with a contact angle of <5° for water and a contact angle of 157° for hexadecane.

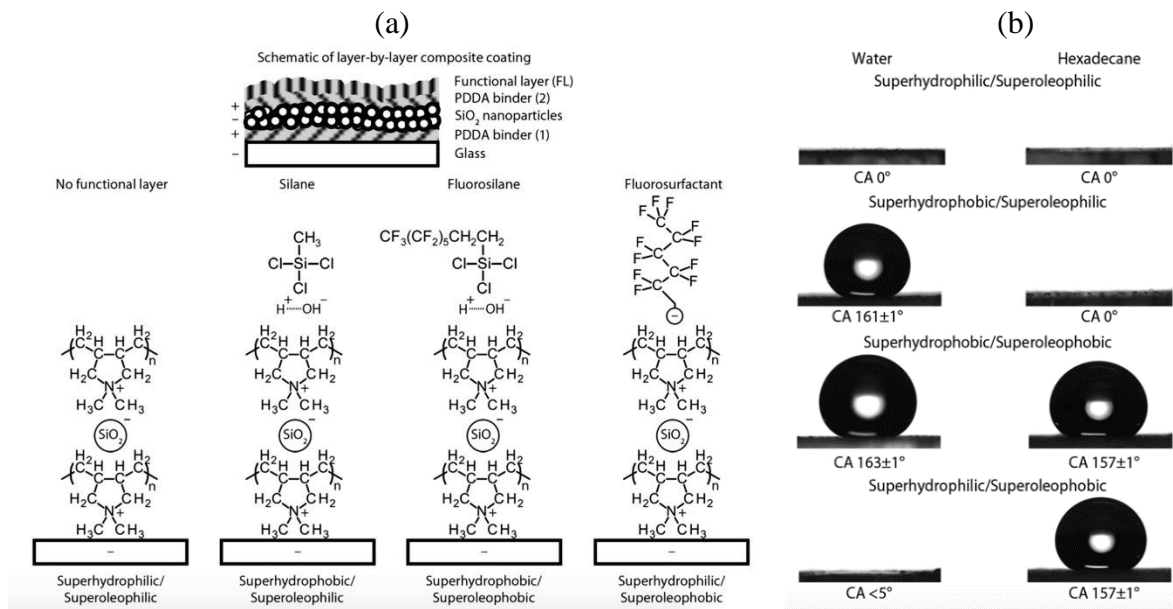


Figure 2.4 A comparison of the effect of final surface coating in the LbL modification of a glass surface, using binder PDDA, SiO₂ NPs, and FLs, such as silane, fluorosilane, and fluorosurfactant: (a) chemical representation of the layers and (b) contact angle of water and hexadecane on different surfaces [186].

Similar to the wettability states presented in , the combined affinities of a surface for water and oil allow for four different types of membranes, based on wettability. These membrane types are demonstrated in Figure 2.5. The first category is oleophilic and hydrophilic (simultaneously), as displayed in Figure 2.5(a). This type of membranes permeates both water and oil, and is not common in oil-water separation application but can be used to separate solids. The second category is hydrophilic and oleophilic, as shown in Figure 2.5(b). This type of membranes was introduced in 2004 by Feng et al. [187]; they have since found great applications in oil-water separation for oil removal. The third category is oleophobic and hydrophobic (see Figure 2.5 (c)); these membranes are also not common in oil-water separation, but they can be potentially employed to separate the gas phase. The oleophobic and hydrophilic membranes are the last category. These membranes have been conventionally used in oil-water separation to separate oil by removing water from an oil-water mixture.

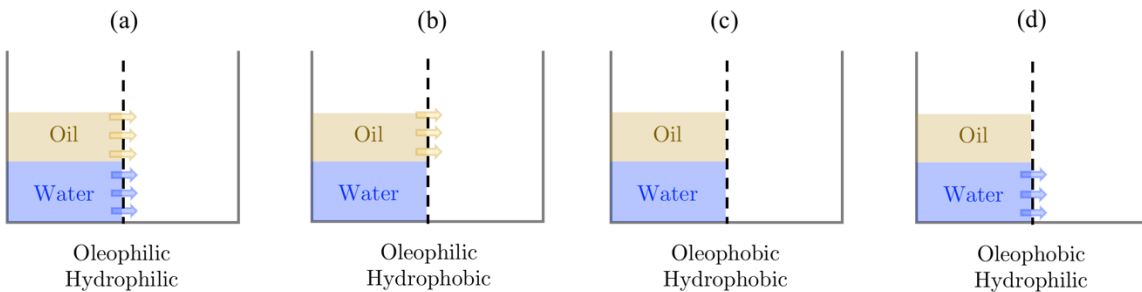


Figure 2.5. Illustration of membrane types for oil-water separation based on wettability: (a) oleophilic and hydrophobic; (b) oleophobic and hydrophilic; (c) oleophilic and hydrophobic; and (d) oleophobic and hydrophobic.

2.3.3. Superhydrophobic and superoleophilic wettability state

The WCA and OCA on membrane surface are important characteristics for oil-water separation applications [188]. The membrane wetting is governed by surface geometry (morphology) and surface free energy [74]. The effect of surface free energy of the interacting phases on the contact angle is given by the Young's equation [168]. The condition for superhydrophobicity is commonly

identified with WCA $>150^\circ$ and small contact angle hysteresis. The first superhydrophobic surface was fabricated in 1996 using fractals and alkyl ketene dimer for which WCA= 174° was achieved [176]. This superhydrophobic condition cannot be achieved solely by the modification of the surface chemistry. In fact, for obtaining WCA $>120^\circ$, hierarchical micro- and nano-surface roughness is required [189]. The role of surface roughness is assessed via the liquid contact angle on a flat substrate (θ_Y). Wenzel's equation [169] predicts that the wetting is enhanced by the surface roughness when $\theta_Y < 90^\circ$ (hydrophilic conditions); the water wettability is lowered by the roughness when $\theta_Y > 90^\circ$ (hydrophobic conditions).

The Cassie-Baxter wetting condition can result in the superhydrophobicity when air is trapped in the micro- and nano-channels, causing the extreme non-wetting condition. Due to the difference between the surface tension of water-air ($\gamma_{WA}=72$ mN/m) and that of the oil-air (usually $\gamma_{OA}<35$ mN/m), it is possible to control the wettability of a surface according to Young's equation [168]. Hydrophilicity and oleophilicity refer to the conditions in which the surface energy of a substrate is higher than both oil and water phases. Hence, wetting the substrate by either oil or water is unavoidable. Conversely, a substrate with surface energy less than oil and water demonstrates hydrophobicity-oleophilicity properties. Because of this surface energy contrast for water and oil (usually $\gamma_{OA}=20\text{--}30$ mN/m), most hydrophilic surfaces are also oleophilic [70, 190]. Most of the low surface energy materials that are usually hydrophobic still show a greater surface energy than oil (>35 mN/m); these surfaces tend to be oleophilic ($\theta_{OA}<5^\circ$) [71, 191]. To meet the superhydrophobic and superoleophilic condition, the surface energy of the final coating should be in the range 30 mN/m $< \gamma < 72$ mN/m [190].

2.4. Surface Wetting Modification Methods

Different methods have been used to alter the wettability towards superhydrophobic and superoleophilic. In this section, some known techniques for construction of superhydrophobic and superoleophilic membranes as well as their pros and cons are briefly discussed; these methods include dip coating [1-4], spin coating [5-8], spray coating [9-11], LbL [12, 13], sol-gel [14-16], vapor pressure deficit (VPD) [17-19], chemical vapor deposition (CVD) [20-23], electrodeposition [24, 25], electrospinning [26-29], acid-base treatment [30, 31], grafting [32-34], thermal [35-37], plasma [38-41], ion beam irradiation [42-44], and femtosecond laser [45, 46]. Typically, fabricating of superhydrophobic and superoleophilic surfaces can be achieved via either using low surface energy materials or adding roughness or both. The performance of a membrane is affected by important features, such as pore size, wettability, and surface energy [47]. The wettability of a solid surface is controlled by its geometry and chemical composition [28, 48-50]. The main coating techniques introduced in this review are listed in Table 2.2.

2.4.1. Conventional methods

Among these possible coating techniques, dip, spin, and spray coating are the most commonly used methods to generate uniform and high-quality thin film on the substrate surface [51]. Although dip-coating is a cost-benefit and straightforward strategy with low waste, but drawbacks also arise when a coating solution evaporates, or inhomogeneous coating is created when withdrawal speed is too fast [14, 52-54]. Generally, the substrate surface functional groups, withdrawal speed, submersion time, dipping cycle quantity, and environmental humidity are essential factors in the dip-coating technique [55]. The physical properties of the coating solution, such as density, viscosity, surface tension, temperature, and also pH affect the coating quality [56, 57]. One main reason that makes the spin coating a proper candidate for coating a substrate surface

is the possibility for tuning of the coating thickness; It can also be used in repeated cycles to achieve the desired deposition thickness [58, 59]. The rotation speed and solution property are two main factors for tuning the thickness in this method. For example, higher speed leads to a thinner film and/or coating solution with higher viscosity can generate non-uniform film. Compared to dip-coating, less amount of coating solution is needed for the deposition of a film on the substrate surface in the spin coating method, however, more coating solution is wasted at last [51]. The spin coating method is extensively employed for manufacturing superhydrophobic surfaces [5-8]. Spray coating is also a promising technique to fabricate thin-film layers of organic materials. This method is highly scalable and can be used at large-scale industrial applications [60]. Despite the dip-coating and spin-coating, a wide variety of factors are involved in spray coating technique such as spray nozzle aperture, gas pressure, nozzle-substrate distance, and spray angle. However, these factors make the coating process complicated but enable spray coating to generate a tunable thickness on the surface of substrate. On the one hand, the amount of coating solution required for deposition process is significantly lower than dip coating, on the other hand, the waste of coating solution is higher due to over spraying.

Spray coating has also been utilized to perform superhydrophobic–superoleophilic surface fabrication [61, 62]. Similar to spray coating, LbL method allows for tunable coating thickness and controlled functionality [63]. In general, the LbL approach can be combined with other surface modification methods to attain the desired surface structure and chemistry. LbL technique can increase the mechanical properties by providing a multi-layer coating, but it needs a complicated preparation procedure. Another drawback of the LbL method for fabrics is the lack of proper stability. In this regard, the UV-curable resin is used to provide a cross-link between the layers to improve its stability [64]. An in-depth review of the LbL technique is given by Ariga et al. [65].

The homogeneity of the coated layer on the membrane surface is another concern in this field [66]. Sol-gel is a versatile strategy that provides a high purity film owing to mixing at molecular level. The sol-gel technique generates a uniform coating nearly at low-temperature conditions, but the precursors employed in the process enhance the cost of this type of coating [67].

Although more complicated than the previously mentioned techniques, physical vapour deposition (PVD) has been a common strategy to deposit a thin film on the substrate surface. This method provides a widespread choice of materials (organic/inorganic) to be used for coating preparation [68]. The PVD technique can also be utilized for oil-water separation purposes [17-19]. When it comes to the simultaneous deposition of coatings, chemical vapour deposition (CVD) method appears to be an effective strategy for depositing thin films of the desired chemicals onto the surface of a substrate [55]. The CVD approaches were used to prepare silica [328], silica-alumina [329], alumina-zirconia [330], silicon carbide–titanium carbide [331], and composite membranes [55].

Electrodeposition is a versatile conventional surface modification technique, containing an electrochemical cell with a working electrode (cathode) and a counter electrode (anode) to generate a controlled current at a given voltage. Electrodeposition is a cost-effective and simple strategy; it also consumes less energy than other methods since it happens at room temperature. The main challenge in this technique is the fabrication of the electrodes that significantly influence on the shape and size of the coated film [69]. Darmanin et al. [70] provided a systematic review on electrochemical methods for making hydrophobic surfaces.

Electrospinning is an efficient strategy to construct micro-nano fibrous with an adjustable diameter [71]. Superhydrophobic surfaces can be readily fabricated through surface modification of electrospun membranes/fibers; alternatively, electrospun deposition of superhydrophobic fibers

onto various materials can also be employed to functionalize them. In this method, no coagulant or high temperature is needed for the solidification of the coating solution on the surface of substrate. The typical limitations of electrospinning for surface modification are low separation efficiency for gravity-based oil-water separation and low mechanical stability [72]. Applications of electrospinning to manufacture surfaces with a special wettability (e.g., nanofibrous membranes) are widely reported for effective oil-water separation [29, 73, 74].

Grafting is a method in which, either polymer is added to the surface (grafting-on) or monomers are polymerized to the surface through an initiation (grafting-from). In grafting, a polymer can be attached to another polymer surface. This copolymer synthesis not only enhances the thermostability of the final product, but also modify the wettability of the polymers [47, 75]. For example, the oleophilic surface of polyethylene terephthalate (PET) fibers was modified to hydrophilic by grafting functional groups of $-\text{COOH}$, NH , and $-\text{OH}$ [76].

2.4.2. Innovative methods

On the one hand, the low-temperature methods, previously discussed in Section 2.4.1, create high quality and cross-linked coatings. On the other hand, their efficiency is still below that of coatings obtained by thermal treatment of the same material at higher temperatures, or coatings obtained by sol-gel or conventional CVD. Thus, there is still an urgent need for alternative techniques to provide coatings without affecting substrates to high temperatures. The thermal approach is a process in which fine molten or semi-molten particles are sprayed onto the substrate surface without significantly warming the substrate [77, 78]. The source of energy for this method can be electrical arc and combustion [77]. Compared to CVD, this technique can create a thick film (20 μm to several mm) over a large surface area of the substrate. A wide variety of coating materials, that melt without breaking down, can also be used in this method. Although the coated layer is not

consistent (due to lack of access to restricted areas on the surface of the substrate) but the deposition process is repeatable/repairable [79].

One strategy to apply energy into coatings without exposing the substrate is by means of radiation (i.e., ion-beam radiation, plasma radiation, and laser ablation) [51]. Plasma irradiation is one of the most widely used methods for the modification of surfaces [75]. Various functional groups can be added onto the surface of the substrate through plasma irradiation. For example, nitrogen can be used for creating hydrophilicity properties, as referred by Narushima et al. [80]. Likewise, conjugation of hydroxyl groups through the oxygen plasma technique has been suggested by Zimmermann et al. [41], where they coated a silicone nanofilament modified by oxygen plasma irradiation. Figure 2.6 illustrates the significant role of surface roughness on the superhydrophobicity of polymethylmethacrylate (PMMA) [75]. Typically, hydroxylic, carboxylic, and aldehyde groups are created on the surface of PMMA after irradiation with Ar plasma. The hydrophobicity of the PMMA can be increased by employing the plasma texturing before irradiation with Ar plasma that leads to hierarchical structures on the surface.

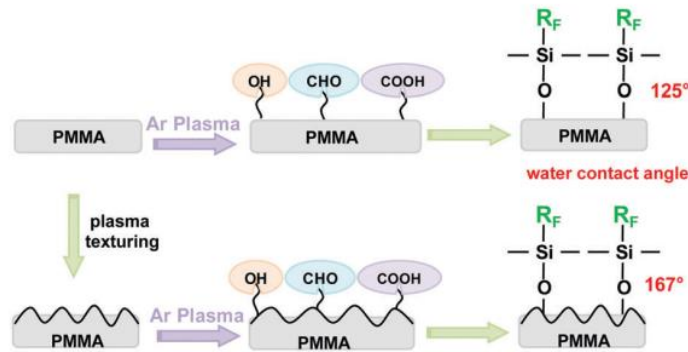


Figure 2.6. Plasma irradiation technique using inorganic gas (Ar) for generating a superhydrophobic surface with WCA of 167°[192].

Ion beam irradiation shoots a high-energy level ion onto the surface of a substrate to generate hydrophobicity features. For instance, Kim and Lee [193] fabricated a superhydrophobic surface by irradiation of Ar⁺ and O²⁺ ions to investigate the impact of the ion irradiation on the wetting

features of PTFE, as depicted in Figure 2.7. The WCA $>150^\circ$ showed the hydrophobicity that was attained by this method. In another study, Chen et al. achieved nano-needle type roughness on the PTFE surface after Xe^+ irradiation, which presented super-hydrophobic features [194].

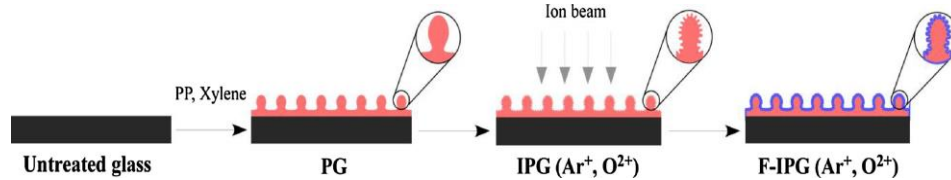


Figure 2.7. Fabrication of superhydrophobic surface using ion beam irradiation technique [193].

In this adjustable and eco-friendly method, the type of ion beams and energy can be altered to achieve desirable surface wetting. For example, high energy ions collisions with one-layer carbon atoms of graphene can induce a graphene nanopores [195]. Since the invention of lasers in 1960, they have found a wide range of applications, including oil-water separation [196, 197]. A femtosecond laser emits ultrashort optical pulses ($1 \text{ fs} = 10^{-15} \text{ s}$). Femtosecond laser, as a promising method to generate hierarchical micro- and nanostructures onto the surface of materials, is employed to induce superhydrophobicity features on SS [198], polymers [199, 200], silicon [201], titanium (Ti) [202], and aluminum [203]. Bhagat and Gupta [18] utilized a femtosecond laser technique to fabricate a superhydrophobic polycarbonate (PC), as depicted in Figure 2.8. The laser technique increased the average height of roughness on the surface of the PC from $1.34 \mu\text{m}$ to $6.68 \mu\text{m}$; as a result, the WCA increased from 82° on smooth PC surface to 155° on femtosecond laser-engraved surface.

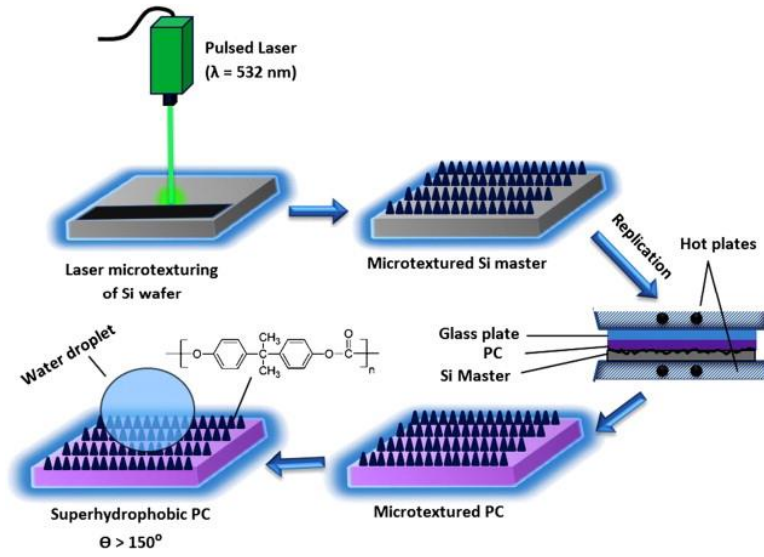


Figure 2.8. Application of femtosecond laser to fabricate superhydrophobic polycarbonate (PC) surface [18].

Table 2.2. Advantages and disadvantages of different methods for the fabrication of superhydrophobic and superoleophilic membranes

Techniques	Advantages	Disadvantages	Remarks	Ref.	
Dip-coating	<ul style="list-style-type: none"> - High-quality and stability thin film - Simple and low-cost strategy - Suitable for complex heterogeneous surfaces 	<ul style="list-style-type: none"> - Process slow - Non-uniformity of film thickness - High-temperature sintering - Unsafe for the environment 	<ul style="list-style-type: none"> - The sol viscosity and withdrawal speed play a crucial role in the thickness of the coating film - Film thickness is between (0.1 and 100 μm) 	[204]	
Spin-coating	<ul style="list-style-type: none"> - Simplicity and uniform coating - Fast drying - Tunable thickness 	<ul style="list-style-type: none"> - Suitable in laboratory scale - Requires large volume of solvent - The single substrate with a low throughput process - Not ideal for nanomaterials that need enough time to crystallize and/or self-assembly 	<ul style="list-style-type: none"> - The ultimate film thickness depends on the concentration of the polymer solution, solvent evaporation rate, surface tension, and spinning speed (for industrial processes, speeds > 1000 rpm leads to best uniformity) 	[204]	
Spray-coating	<ul style="list-style-type: none"> - High-quality and stable coating - Low-cost, time-efficient, and repairable - Large-scale fabrication 	<ul style="list-style-type: none"> - Non-uniform coating thickness 	<ul style="list-style-type: none"> - A uniform coating composition is generated when the surface temperature becomes constant during the spraying 	[204]	
Sol-gel	<ul style="list-style-type: none"> - Controlled particle size and porosity - Better homogeneity and high purity - Energy-intensive - Required inexpensive equipment - Easy operation at the laboratory - Synthesis at ambient temperature 	<ul style="list-style-type: none"> - Expensive precursors - Shrinkage and cracking of wet gel upon drying - Slow deposition - Not suitable to form thick films of NPs on the substrate 	<ul style="list-style-type: none"> - The nature of the precursor solution plays a vital role in the synthesis of the final product - In colloidal gel, non-polymeric particles (with sizes from 1nm to 1μm) are linked with van der Waals force but in polymeric gel, polymer molecules (with dimensions of <1nm) are bonded using covalent forces 	[204, 205]	
Layer by Layer Assembly	<ul style="list-style-type: none"> - Simple and versatile - Controlled thickness and functionality 	<ul style="list-style-type: none"> - Expensive - pH-sensitive - Limited long-term stability 	<ul style="list-style-type: none"> - Surface roughness can also be provided using NPs in the layers that can be obtained at room temperature - The LbL surface modification can also be conducted through immersion, spin, spray, and electrochemical techniques 	[204]	
Chemical Deposition	Vapor	<ul style="list-style-type: none"> - The thickness and uniform coating - Quick deposition process - Solvent-free - Simultaneous deposition of various materials 	<ul style="list-style-type: none"> - Expensive raw materials - Limitation for colloidal and porous materials - The gaseous phase can be toxic, flammable, explosive, and corrosive 	<ul style="list-style-type: none"> - The ultimate thin films in CVD have thicknesses between 1 and 1000 nm - The temperature range for the CVD process is 500–1200 $^{\circ}\text{C}$, but the substrate temperature should be around 500 $^{\circ}\text{C}$ 	[205, 206]
Physical Deposition	Vapor	<ul style="list-style-type: none"> - Environmental-friendly - Applicable to all inorganic and some organic materials 	<ul style="list-style-type: none"> - Slow deposition - Thin coating layer - Needs annealing time - Complicated and expensive process 	<ul style="list-style-type: none"> - Deposited films in PVD have thicknesses from a few nanometers to 1000 nm - In PVD, substrate temperature approximately equals to ambient temperature 	[207, 208]

Techniques	Advantages	Disadvantages	Remarks	Ref.
Electrodeposition	<ul style="list-style-type: none"> - Energy-efficient and cost-benefit method - Large-surface area - Precise geometry 	<ul style="list-style-type: none"> - The template is required for nanostructure fabrications - Applicable only for electrically conductive substrates 	<ul style="list-style-type: none"> - The shape and size of the coated film strongly depend on the electrode substrate characteristics - This technique is performed in ambient temperature 	[209]
Electrospinning	<ul style="list-style-type: none"> - Controlled fiber diameter and structure - A cost-efficient and simple method 	<ul style="list-style-type: none"> - Low mechanical integrity and separation efficiency for gravity-based oil-water separation 	<ul style="list-style-type: none"> - Electrodeposition requires a high-voltage (5 to 50 kV) and a syringe pump to emit a polymer on the surface of the substrate at a constant injection rate 	[210]
Grafting	<ul style="list-style-type: none"> - Deposition of high molecular weight polymers onto the substrate surface - High adhesion and chemical stability of the grafted polymers 	<ul style="list-style-type: none"> - It always needs the surface functional groups - Limited to be applied for high aspect ratio pores 	<ul style="list-style-type: none"> - Covalent force is the crucial factor for the attachment of the grafted polymers onto the substrate surface 	[211]
Thermal approach	<ul style="list-style-type: none"> - Applicable to different coating materials (i.e., ceramics, plastics, alloys, and composites) - Inexpensive with high efficiency - Quick deposition 	<ul style="list-style-type: none"> - Residual stress (due to fast cooling and rapid solidification) leads to short stability of coating layer 	<ul style="list-style-type: none"> - Coating thicknesses from several 50 μm to over 1000 μm - Various techniques, such as wire-arc, high-velocity oxy-fuel, and plasma spraying can be used in this method 	[212]
Plasma irradiation	<ul style="list-style-type: none"> - Ability to add different functional groups onto the surface of the substrate - Applicable to various surface morphologies (nanocone, pinhole, porous, and rough structures) - Faster than UV irradiation 	<ul style="list-style-type: none"> - The deposition process requires a porous substrate and high temperature 	<ul style="list-style-type: none"> - The ion bombardment of surface with high energy levels can trigger a random fragmentation on the surface, further etching or depositing chemicals onto the adsorbent surfaces - Coating film has a thickness between 50 to 200 μm 	[212]
Ion beam irradiation	<ul style="list-style-type: none"> - Controllable, fast, and environmental-friendly 	<ul style="list-style-type: none"> - Expensive equipment - Needs vacuum system - Thermal decomposition (due to the high temperature of the deposition process) 	<ul style="list-style-type: none"> - The type of ion beams and energy can be changed towards a desirable surface wettability. 	[209, 212]
Femtosecond laser	<ul style="list-style-type: none"> - Applicable on any substrate - Environmental-friendly and even more stable than chemically treated surfaces - Automatic operation - Limited heat-affected zone with high precision 	<ul style="list-style-type: none"> - Time-consuming process - Expensive strategy - Micron-scale resolution 	<ul style="list-style-type: none"> - During femtosecond laser, ultra-short pulse width and extremely high peak intensity can cause sharp edge micro-holes - The femtosecond laser can create both rough microstructures and micro-holes on the surface of the substrate 	[213]

2.5. Fabrication of Superhydrophobic and Superoleophilic Membranes

Superhydrophobic and superoleophilic have found great interest in oil-water separation application. The key features of the surface, such as energy, roughness, charge, and functional groups can be engineered to promote simultaneous hydrophobicity and oleophilicity [214]. As it was discussed earlier, by solely changing the surface chemistry of smooth surfaces, a superhydrophobic surface with a $WCA > 150^\circ$ cannot be achieved. Experimental works have shown that even hexagonal close-pack of aligned $-CF_3$ functional groups (that have very low surface energy) on smooth glass surface results in a maximum $WCA = 119^\circ$ [215]. Hierarchical micro- and nano surface roughness are required to produce superhydrophobic surfaces; without surface roughness, the superoleophilic condition cannot be achieved. A schematic of the process to produce simultaneous superhydrophobic and superoleophilic surface as well as their classification with application to oil-water separation are given in Figure 2.9. As it is clear from Figure 11, the wettability modification process is usually conducted in three stages, including pretreatment, morphology modification, and surface chemistry modification. The pretreatment includes steps, namely; cleaning (physical and chemical) and activation where contaminations and weak hydrophilic oxidized films are removed, and new and reactive hydroxyl groups are attached to allow for a better surface chemistry modification. To prepare hierarchical micro- and nano surface roughness, top-down and bottom - up methods are used to create roughness by either removing or adding rough features, respectively. In surface chemistry modification, new chemicals are bonded to the surface. These chemicals can be inorganic, organic, and/or hybrid inorganic-organic materials.

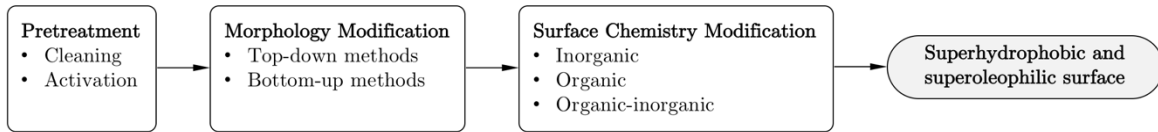


Figure 2.9. A typical process to fabricate superhydrophobic and superoleophilic surfaces.

2.5.1. Pretreatment

The pretreatment process prepares the surface for a better bonding of low surface energy materials, which is usually required to achieve a superhydrophobic and superoleophilic surface. The pretreatment stage generally includes physical and chemical cleaning, and activation. The physical cleaning removes weak boundary layers (loose material) through methods such as abrasion and sandblasting. Similarly, the chemical cleaning stage removes organic surface contaminations as well as old oxide layers [12, 83]. For chemically cleaning of the surface, usually successive cycles of detergent, ethanol, and acetone are implemented to remove the organic contaminations [13]. Utilizing ultrasonic cleaning helps to scrub the surface with ultrasonic energy, leading to a high-quality cleaning [12]. 5–15 minutes ultrasonic solvent cleaning cycles are usually used in the pretreatment stage [216, 217]. A diluted acid solution is used to remove the old surface oxides [97]. After the sample is cleaned, it is usually oven-dried at 80 °C for about 1 hour [93] or dried using N₂ gas [96].

The physical and chemical cleaning methods commonly follow an activation stage in which the old oxidized surfaces are removed and replaced by new and reactive oxide layers. A schematic of the activation process mechanism is depicted in Figure 2.10. The fresh and reactive functional groups will be of critical importance in the surface energy control by chemicals such as silanes. In general, the activation of polymers results in the polar oxygen-based functional groups, as shown in Figure 2.10 [182, 218].

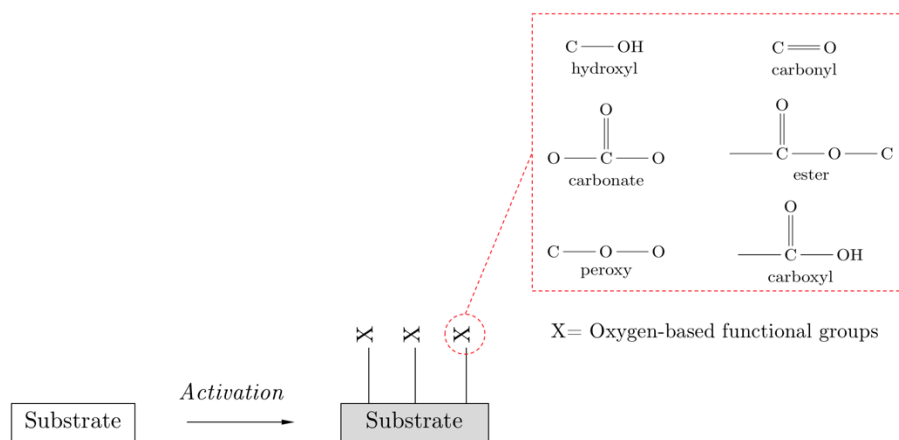


Figure 2.10. A schematic of activation of oxygen based functional groups.

In general, strong oxidizers, such as a mixture of concentrated H_2SO_4 (98 wt%) with concentrated H_2O_2 (30 wt%) or that with CrO_4 (or H_2CrO_4) are used. The mixture of concentrated sulfuric acid and hydrogen peroxide (2:1–7:1) is called piranha solution [12], which is highly reactive and should be handled with extra care [12]. Oxygen or air plasma can be alternatively employed in the activation process. Other methods, such as the use of UV radiation, UV radiation with ozone, and corona method (mainly for plastics) are also utilized for the activation process. The use of air or oxygen plasma has found to be a promising approach that not only gives a superior cleaning and activation, but also provides advantages over wet chemical and UV/ozone activation in terms of the energy input, safety, hazardous waste, corrosion, thermal load, processing time, and versatility in handling a broader range of material surfaces [69]. However, in comparison, the O_2 (or air) plasma activation technique contains a higher number of variables to be optimized.

A comparison between the pretreatment methods was conducted by Lukose [219], where the surfaces of Au and Ag films were treated by different methods including UV irradiation, piranha solution, oxygen plasma, and air plasma. The results for Au film are presented in Figure 2.11 The contact angle of water on Au exposed film after seven days is 106° , as shown in Figure 2.11(a). Upon 10- and 20-min UV irradiation, the contact angle decreases to 78° and 70° , respectively.

Pretreatment with piranha solution and oxygen plasma makes the surface more hydrophilic, as seen in Figure 2.11(d)-(f). The WCAs on surfaces treated with piranha and oxygen plasma are similar. However, air plasma is found superior to all methods, giving a contact angle of 15° (see panel (f) of Figure 2.11) [219]. Similarly, for the case of Ag film, the minimum WCA of 18° was obtained in the case of oxygen plasma [219].

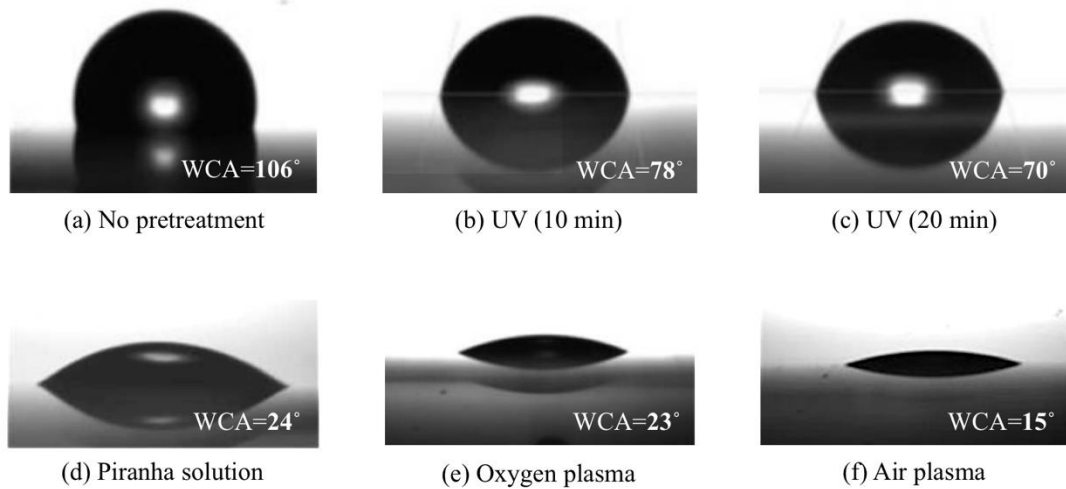


Figure 2.11. Effect of pretreatment method on contact angle of water on Au coated film: (a) no pretreatment, (b) 10 min UV irradiation, (c) 20 min UV irradiation, (d) piranha solution, (e) oxygen plasma, and (f) air plasma [219].

2.5.2. Modifying surface morphology

Surface roughness is found to exhibit a significant role in the wetting characteristics. The effect of hierarchical surface roughness on wetting behavior is studied in several research and review papers [110-116]. The hierarchical surface roughness helps to achieve the superhydrophobicity condition, as explained by the Cassie-Baxter wetting condition. Inspired by lotus leaf, researchers employed the biomimetic hierarchical surfaces to create materials with super-wetting or non-wetting characteristics for different applications, as reported in the literature [74, 191, 220-222]. In general, methods of surface morphology modification can be divided to top-down and bottom-up methods.

In the top-down category, lithography, etching (using chemicals, laser or plasma), annealing, and sandblasting can be included [70-78]. Bottom-up methods of creating hierarchical structures include various approaches, such as LbL assembly, anodizing, hydrothermal, electrodeposition, electrospinning, colloidal assembly, rough polymer films (with micro- and nano roughness features), templating, replication, casting, and 3D printing [71, 72, 74-76, 79, 80]. Samples of modified surface morphology obtained by top-down methods (panels (a)-(d) of Figure 2.12) and bottom-up methods (panels (e)-(h) of Figure 2.12) are given, which demonstrate hierarchical micro- and nano-roughness morphology, as required for the superhydrophobic condition.

2.5.3. Surface chemistry modification

After developing micro- and nano- surface roughness, the surface energy of the building block of the hierarchical material should be controlled to meet the condition of superhydrophobic and superoleophilic; to achieve this criterion, the surface energy should be between the surface energy of oil and water, as explained earlier [190]. If the surface energy of the building block already satisfies this range, further modification is not required. Otherwise, an additional process will be conducted through different methods, such as CVD, spray coating, spin coating, dip coating, LbL assembly, sol-gel, anodizing, hydrothermal, electrospinning, and plasma (laser and UV) irradiation. In general, coating chemicals can be divided into inorganic (metals and non-metals), organic coatings, and hybrid organic-inorganic materials [72, 75].

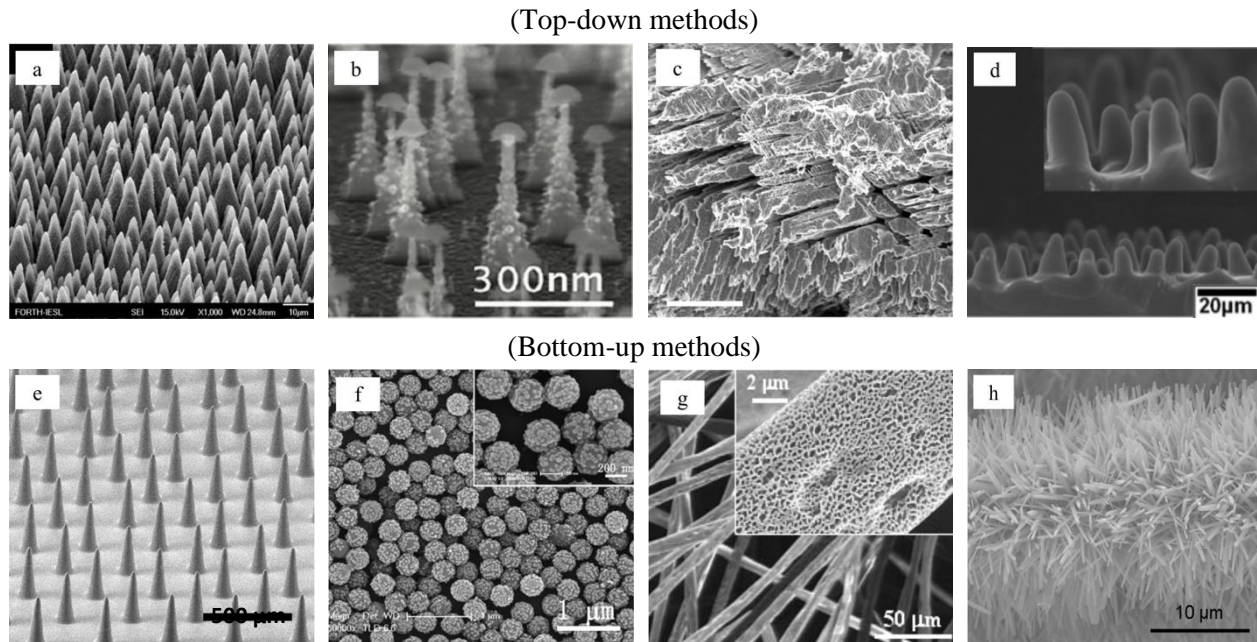


Figure 2.12. Different methods of surface morphology change with application to oil-water separation. Top-down methods: (a) femtosecond laser irradiation on the platinum surface [223], (b) oxygen and bromine plasma etching and reactive ion synthesis [224], (c) SS HF acid etched [225], and (d) lotus-like papillary structure using soft lithography of polydimethylsiloxane (PDMS) [226]. Bottom-up methods: (e) template technique to create PDMS cone array [227], (f) raspberry-like colloidal system of PAA-functionalized PS core with silica NPs [228], (g) PS in tetrahydrofuran (THF)/dimethylformamide (DMF) solvent through electrospun [229], and (h) hydrothermal approach for creating ZnO nanorods [230].

In the class of inorganic coatings, the silicone-based chemicals are the most popular choice. This list includes different types of silanes [75] such as PDMS, methyltrichlorosilane (MTS), trimethyltrichlorosilane, octadecyltrichlorosilane (OTS), MTES, TEOS, perfluoroalkylsilane (PFAS), perfluorooctyltriethoxysilane (PFTOS), hexadecyltrimethoxysilane (HDTMS), HMDS, mercaptopropyltrimethoxysilane (MPTMS), aminoethylaminopropyl polydimethylsiloxane (AEAPS), 1H,1H,2H,2H-perfluorooctyl trimethoxysilane (PFOTMS) and vinyltriethoxysilane (VTES). Other inorganic chemical coatings include graphene, graphene oxide, CNTs, and metallic and metal oxides chemicals (Ag, Al, TiO₂, and CuO). In the category of organic polymer coatings, thiols are the mostly used coatings, for example, *n*-dodecanethiol (DDT), dodecanethiol, *n*-octadecylthiol, and 1H, 1H, 2H, and 2H-perfluorodecanethiol (PFDDT). Other important organic

polymers include PE, PTFE, Teflon AF® or amorphous fluoropolymer, polyvinyl (PV), polyvinylchloride (PVC), polyvinilidene fluoride (PVDF), polystyrene (PS), polybenzoxazine (PBZ), polyimide (PI), and polyethylenimide (PEI).

As described in Figure 2.9, three stages of pretreatment, morphology modification, and surface chemistry modification are required to achieve a superhydrophobic and superoleophilic surface. A summary of different methods for wettability alteration to superhydrophobic and superoleophilic with application to oil-water separation is provided in Table 2.3.

Table 2.3. A summary of available pathways for wettability alteration to superhydrophobic and superoleophilic with implication of oil-water separation.

Process	Common materials and methods	Objectives
Pretreatment	Physical cleaning [12] <ul style="list-style-type: none"> • abrasion and sandblasting 	Removing weak bonds and loose material
	Chemical cleaning [13] <ul style="list-style-type: none"> • solvents (deionized water, acetone, ethanol, chloroform, and detergent) • ultrasonic-aided cleaning 	Removing organic surface contaminations
	Activation [14, 69] <ul style="list-style-type: none"> • piranha solution (H_2SO_4/H_2O_2) • H_2SO_4/H_2CrO_4 (or CrO_3/H_2SO_4 solution) • air or O_2 plasma • UV/ ozone • Corona treatment (for plastics) 	Eliminating the old oxidized layers (or chlorinated, and fluorinated surfaces) and growing fresh and reactive oxide layers.
Surface morphology modification	Top-down methods [70-78] <ul style="list-style-type: none"> • lithography • etching (chemical, plasma or laser) • annealing • sandblasting 	Creating surface roughness, or hierarchical micro- and nano structure to enhance wetting or non-wetting.
	Bottom-up methods [71, 72, 74-76, 79, 80] <ul style="list-style-type: none"> • layer by layer assembly • hydrothermal (crystal growth) • anodizing and electrodeposition • electrospinning • colloidal assembly (micro/nano particles) • rough polymer film • templating, replication, casting, and 3D printing 	
Surface energy modification	Inorganic chemical coatings [75] <ul style="list-style-type: none"> • Si-based (silanes: PDMS, MTES, TEOS, PFAS, HMDS, PFOTMS, and; applied through dip coating, spray coating, spin coating, and LbL assembly) • C-based (graphene, graphene oxide, and CNTs; applied through CVD, phase separation, and solution immersion) • metallic and metallic oxide (Ag, ZnO, Al, TiO_2, and CuO; usually applied through electrodeposition, plasma deposition, anodizing, hydrothermal, and solution immersion) 	Reducing surface energy to promote the superhydrophobic and superoleophilic condition.
	Organic coatings [75]	

Usually applied through the template, dip coating, spin coating, spray coating, electrospinning, and LbL assembly:

- thiols (dodecane, *n*-octadecyl, dodecane, and perfluorodecane)
- PE, PTFE, and Teflon AF®
- fluorinated methacrylates
- PV, PVC, and PVDF
- PS, F-PBZ, PI, and PEI
- fatty acids such as stearic acid

Hybrid inorganic-organic coatings [72, 75]

Usually combined through hydrothermal, dip coating, spray coating, sol-gel, CVD, and LbL assembly.

2.6. Superhydrophobic and Superoleophilic Membranes for Oil-Water Separation

Superhydrophobic and superoleophilic membranes were first proposed in 2004 to be employed for oil-water separation [187]; since then, there are extensive studies on different superhydrophobic and superoleophilic membranes and sorbents. In this section, we only focus on the membranes. First, we classify three different types of superhydrophobic and superoleophilic membranes based on the pore structure, namely, mesh, porous, and film (see Figure 2.13). Each category is divided into sub-categories based on different attributes, found in the literature. This classification is by no means unambiguous. For example, when functionalizing a metal mesh by colloidal assembly, the surface roughness created by the micro- and NPs can grow a porous structure onto a 2D metal mesh; however, we classify it as a mesh-type superhydrophobic and superoleophilic membrane. In the same fashion, we consider a functionalized fabric, single-layer graphene membrane as a mesh-type membrane.

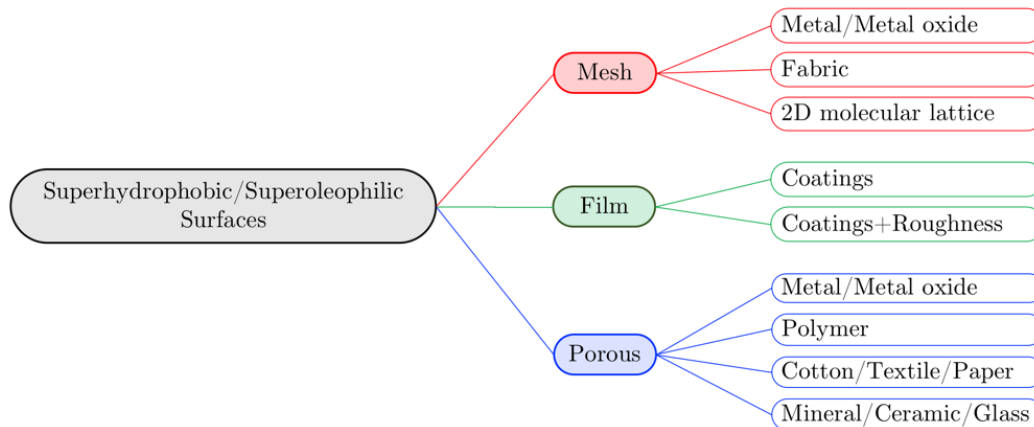


Figure 2.13. Classification of superhydrophobic and superoleophilic membranes with application to oil-water separation.

2.6.1. Mesh-based superhydrophobic and superoleophilic membranes

Over the last decade, functionalized meshes with special wettability have gained exceptional interest for oil-water separation purposes. The metallic mesh material provides good mechanical strength, flexibility and thermal resistance with a low-cost, featuring an excellent substrate to fabricate superhydrophobic and superoleophilic filters [29]. In this section, we first classified mesh-based superhydrophobic and superoleophilic membranes based on the type of substrate (i.e., SS, Cu, and others). For each substrate, chemicals and/or coating methods that are used for surface modification are discussed. A summary of the mesh-based superhydrophobic and superoleophilic membranes with application to oil-water separation is given in Table 2.4.

Stainless steel: Recently, there has been considerable interest to fabricate superhydrophobic and superoleophilic coatings on SS mesh for obtaining a high separation efficiency for water-oil mixtures [11, 231]. The idea of using superhydrophobic surfaces to fabricate superoleophilic SS mesh-based membranes proposed in 2004 by Feng et al. [32]. They coated the SS mesh with a suspension of PTFE particles (30 wt%), PVAC as an adhesive (10 wt%), PVA as a dispersant (8 wt%), SDBS as a surfactant (2 wt%), and water as a thinner (50 wt%) [32]. They cleaned a SS mesh (50-200 μm) and then sprayed the coating solution onto the mesh and cured it at 350°C. The

coated mesh featured a WCA=156.2±2.8°, and a sliding angle of 4°. Furthermore, the OCA using diesel oil showed a zero value. However, the proposed technique has been criticized due to its low thermal and mechanical stability [214]. The SS mesh-based superhydrophobic and superoleophilic membranes are extensively cited in the literature [11, 13, 17, 20, 33-48]. The PTFE-coated SS meshes are found to promote superhydrophobicity and superoleophilicity, leading to a reasonable oil-water separation efficiency [35, 36, 103]. By default, PTFE exhibits hydrophobicity (with a WCA in the range of 98° to 112°). Also, it has excellent thermal, chemical, and abrasion resistances; thus, PTFE-coated SS mesh can be used under harsh conditions (e.g., acidic-basic solutions, corrosive compounds, abrasive mixtures, and high temperatures). The PTFE robustness makes it a promising organic-based coating for superhydrophobic and superoleophilic surfaces. However, this excellent chemical resistance can be a drawback when it is used to dissolve PTFE into solvent for being used in electrospinning technique [118]. Qin et al. [103] modified Feng's experimental method of using PTFE suspension by adding polypropylene sulfide (PPS) and achieved a similar WCA of 156°. Some researchers used stearic acid ($\text{CH}_3(\text{CH}_2)_{16}\text{COOH}$) as a surface chemistry modifier to induce superhydrophobic and superoleophilic properties on the metal mesh via immersion method [11, 13, 42] and spray coating [34, 48]. Stearic acid is an organic-based coating material that can also be applied for enhancing the corrosion resistance [232]. In other studies, stearic acid used along with various NPs, such as $\text{Mg}(\text{OH})_2$ [34], Cu crystals [42], and ZnO [11, 232] to create superhydrophobic and superoleophilic SS mesh-based membranes. Li et al. [13] and Liu et al. [42] coated a SS mesh by mixture of stearic acid and Al/ZnO and Cu NPs via immersion approach and created superhydrophobic and superoleophilic membranes with a WCA of 156° and 153°, respectively. Zhang et al. [11] grew a hierarchical ZnO micro-nano structure and applied immersion coating in stearic acid to obtain a superhydrophobic

and superoleophilic SS mesh for oil-water separation application. The functionalized mesh featured a WCA of 156° and a separation efficiency of 95% where up to 10 separation cycles were performed. The prepared mesh was also stable under harsh operating conditions, such as acidic-basic conditions, and corrosive and saline solutions [11]. Wu et al. [22] applied ZnO nanoparticle on an SS mesh through the spin coating method with the aid of Teflon® AF as a surface chemistry modifier, where a WCA of 157° was achieved for the superhydrophobic and superoleophilic membrane. A similar WCA 160° was obtained using ZnO crystals on the surface under a dip coating method by Wang et al. [232].

Several inorganic materials have been applied to functionalize SS meshes. For example, CNTs with a low density (1.4 g/cm^3) and tubular network exhibit a high strength (46 M.Nm/kg) which is 300 times higher than SS metals. Furthermore, CNTs have been widely recommended for synthesis of superhydrophobic coated surfaces due to their high thermal conductivity, stability, and nanoscale dimensions. Given these properties and superhydrophobic and superoleophilic characteristics, CNT coating on SS mesh can be used to facilitate oil-water separation [102]. CNT has been applied to modify both the surface roughness [36] and chemistry [40, 102, 109] in the fabrication of superhydrophobic and superoleophilic mesh. For instance, Hsieh et al. [40] fabricated a fluorinated CNT onto carbon fabric using spin coating method, and obtained 99.7% separation efficiency, and 165° WCA. The fluorination of CNT contributes to the high separation efficiency. In a similar study, Lee et al. [36] grew CNT on the SS surface via CVD technique and fabricated a superhydrophobic and superoleophilic mesh with a WCA of 163° . Cerium oxide (CeO_2) is a rare earth chemical oxide that is widely applied in glass polishing, optical devices, humidity sensors, and solid oxide fuel cells. Due to its inherent hydrophobicity, it also has gained

attention in oil-water separation. Matin et al. [43] spray-coated a suspension of CeO₂ to fabricate an SS mesh with a WCA of 153° and an OCA of 0°.

Moreover, a variety of coating techniques are used to fabricate superhydrophobic and superoleophilic SS meshes with application to oil-water separation; the techniques include rough polymer and colloidal assembly [20, 21, 24, 33, 35, 38, 43, 47, 81, 83-86, 89, 90, 93, 103, 104, 118-124], spray coating [32, 34, 36, 43, 44, 47, 48, 84], electrodeposition [37, 41], CVD [36, 102], and immersion [25, 42]. Using a colloidal assembly is a common method of fabricating superhydrophobic and superoleophilic SS mesh-based membranes. Polymeric materials are suitable to bond NPs, such as CNT [36], silica [41], ZnO [11], particle clusters of Cu, Ni, and Fe [20], CeO₂ [43], attapulgite [33], and Mg(OH)₂ [34]; the NPs were used to modify micro-nano hierarchical structures on the mesh surface. Researchers have also used other polymeric materials such as PTFE [35, 36, 103], Teflon® AF [22], PFTOS [41], PU [104], polydopamine (PDA), and *n*-dodecylmercaptan [20]. Although various superhydrophobic and superoleophilic coatings have been successfully fabricated using the colloidal assembly, significant limitations remain. For instance, materials with a low-surface-energy are required in the coating composite, which are expensive with a short life. Alternatively, high-temperature curing and UV post-treatments are needed to improve the stability and mechanical strength of the coating film [233]. Spray coating has shown a high separation efficiency for oil-water mixtures in the literature. For example, Baig et al. [44] manufactured an SS membrane using spray coating that exhibited a high separation efficiency of 99% and a WCA of around 150°. Moreover, the coated membrane had a high potential to remove organic pollutants due to its high photocatalytic performance under UV irradiation. Cao et al. [34] applied spray coating of a mixture of phenol formaldehyde and Mg(OH)₂ NPs in stearic acid to obtain a superhydrophobic and superoleophilic SS mesh-based membrane with a WCA of

about 151.4°; the mesh was used to remove soybean oil from the water with a separation efficiency of 94.6% for up to 10 cycles. They concluded that the separation efficiency of an oil depends on its viscosity and volatility. They examined different oils such as trichloromethane, petroleum ether, *n*-hexane, toluene, and soybean oil. Trichloromethane resulted in a relatively lower separation efficiency (92.1%), which was attributed to its high volatility. Soybean oil featured the highest separation efficiency (94.6%) due to its high viscosity that tend to stick to the tubes wall and mesh [34]. Yang et al. [33] used different types of oils, such as lubrication oil, hexadecane, and proline to estimate the potential separation efficiency of their fabricated SS mesh. They spray-coated epoxy/attapulgitite (44.4 wt%) on the SS mesh surface; the superhydrophobic and superoleophilic membrane was used for oil-water separation purposes. The WCA was consistently at 160°± 1, even after 30 separation cycles, with a separation efficiency of 98%; the technique led to excellent properties of the superhydrophobic and superoleophilic mesh. For the stability tests, they exposed the mesh to harsh conditions (95% relative humidity, 150 °C for 48 h, washing, and drying), after which no significant decrease in the WCA of the coated mesh was observed [33]. Xiang et al. [20] used one-step electrodeposition approach to deposit particle clusters of nickel (Ni), Cu, and iron (Fe) on the surface of SS. Simultaneously, *n*-dodecyl mercaptan (NDM) was grafted on the substrate surface, using PDA, to modify the surface chemistry. The prepared mesh demonstrated a WCA of 162° and 98.6% separation efficiency for oil-water mixtures. After ten separation cycles, the obtained efficiency and WCA slightly reduced to 97.8% and 155°, respectively. The mesh also showed a high mechanical stability upon abrading tests, and immersion in solutions with different magnitudes of pH and salinity content. Dip coating method is commonly employed as a facile strategy to create superhydrophobic and superoleophilic properties on SS mesh [37, 41, 232, 234]. For instance, Wang et al. [234] immersed SS meshes into a sol-gel based solution containing

perfluoroalkyltriethoxysilane; they obtained a superhydrophobic and superoleophilic surface with a WCA 148° . The sol-gel featured room temperature condition, and provided a homogeneous coating [235]. Du et al. [48] employed the dip coating technique to fabricate a superhydrophobic and superoleophilic SS mesh. The coated mesh exhibited a WCA of 152° with an excellent stability under acidic and basic conditions, and/or hot water. It also showed at least 97% separation efficiency for kerosene-water mixtures after 40 cycles.

Copper meshes: Cu is another material that is widely used to create superhydrophobic and superoleophilic surfaces [26, 28, 83, 84, 96-99, 104-108] owing to its excellent chemical and physical properties [84], malleability [107], extensibility, thermal conductivity, and adjustable pore sizes [28]. Some researchers used Cu oxide or Cu hydroxide to create micro-nano structures on the Cu-based surfaces along with chemicals to obtain superhydrophobic and superoleophilic membranes [107]. La et al. [236] fabricated a superhydrophobic and superoleophilic Cu mesh with $\text{Cu}(\text{OH})_2$ nanoneedle arrays via the electrochemical method, followed by 1H,1H, 2H, and 2H-PFTOS surface chemistry modification. Later, Cao and Cheng [98] developed flower-like clusters composed of nano-sized ginkgo-leaf-like lamellas on the surface of the Cu mesh after modification with DDT. The prepared mesh had a WCA of 155° and an OCA of 0° ; the superhydrophobic and superoleophilic mesh was used to separate oil/water emulsions. The designed mesh demonstrated a separation efficiency of 98% that was stable after 10 cycles. Pi et al. [84] developed a superhydrophobic and superoleophilic Cu mesh-based membrane where the Cu_2S and Cu_2O micro- and nano-roughness structures were modified with PDMS. The prepared mesh showed an oil-water separation efficiency of over 99.2% for free oil (light and heavy). Their mesh was stable under harsh conditions, such as exposure to hot water, hyper-saline solutions, strongly acidic systems, and basic solutions [84]. Cao et al. [104] investigated hot water repellency using

superhydrophobic Cu mesh. They used hydrophobized SiO₂ NPs and a waterborne PU modified with AEAPS to improve the mechanical stability of the SiO₂ NPs deposited onto the surface of Cu mesh. Although the methodology to spray composite silica-PU solution was simple, the coated mesh did not resist against basic, acidic and hypersaline solutions for 24 h. The superhydrophobic and superoleophilic coated mesh provided a WCA of 162.5° and a high recyclability with 95.5% separation efficiency even after 40 separation cycles.

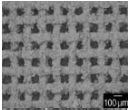
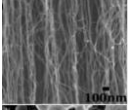
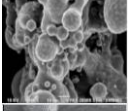
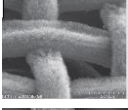
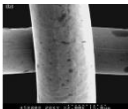
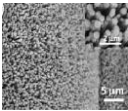
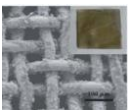
According to the literature review, electrochemical deposition is another widely used method that can be combined with other methods, such as dip coating [83], grafting [100], and vapour deposition [106]. For instance, Cao et al. [106] constructed a superhydrophobic mesh via electrodeposition and vapor deposition techniques on a candle soot (carbon NPs). In this electrode-based system under DC voltage (−0.5 V), Cu mesh and platinum sheet acted as the cathode and anode, respectively. Chain-like structures of agglomerated soot (C) NPs were grown on the Cu mesh. The fabricated mesh with a WCA 150° separated oil from water with an efficiency of around 90% after at least 30 separation cycles. Dip coating has also been employed with Cu-based superhydrophobic and superoleophilic meshes [84, 96, 97]. Pan et al. [97] immersed a Cu mesh into an aqueous solution of NaOH and K₂S₂O₈ and subsequently modified it with DDT. Over 97% of the oil was separated from water at experimental conditions. Yanlonga et al. [99] prepared a superhydrophobic and superoleophilic Cu mesh membrane through annealing at 400 °C and subsequently, immersion coating in DDT. The WCA was approximately 162°, and the separation efficiency of more than 95% for oil-water mixtures was achieved. Yang et al. [28], employed the immersion technique to coat a Cu mesh with stearic acid and ethanol solution. The separation efficiency of more than 97% with at least 20 times repeatability for the coated mesh was obtained, where the WCA was 155.8°. The fabricated mesh demonstrated high stability under acidic-basic

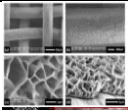
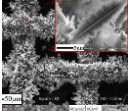
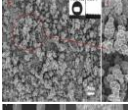
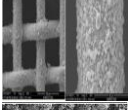
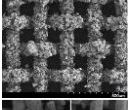
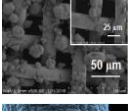
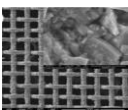
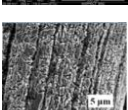
and salty solution conditions. Zhang et al. [107] used the immersion techniques to coat a Cu mesh using a solution of NaOH and $(\text{NH}_4)_2\text{S}_2\text{O}_8$, which resulted in peony flower-like $\text{Cu}(\text{OH})_2$ on the surface of the Cu mesh. The superhydrophobic and superoleophilic Cu mesh exhibited a separation efficiency of 95% after 10 cycles.

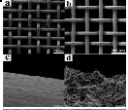
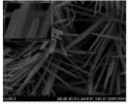
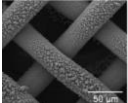
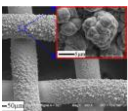
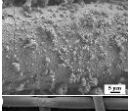
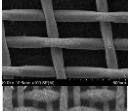
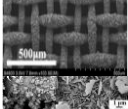
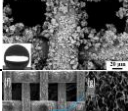
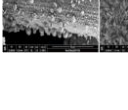
Other metal meshes: The SS- and Cu-based meshes dominate superhydrophobic and superoleophilic membranes that are used for oil-water separation applications. Other metal-based meshes, such as Ni [26], Fe [237], and Ti [121] have also been employed to prepare special wettable materials for oil-water separation. For example, Ni mesh is used due to its malleability, durability, air permeability, anticorrosion, and thermal tolerance. The base material is prepared through hydrothermal method where Ni_3S_2 nano-rods are created; later, the hierarchical rough structure is coated with 1-octadecanethiol [101]. Also, hydrothermal and chemical etching techniques are used to create hierarchical micro- and nanostructures, including nanorods, nanoneedles, and nanowires on the Ni mesh surfaces. For example, Jian et al. [26] utilized Ni meshes that were modified with 1-octadecanethiol and used for oil-water separation. Their superhydrophobic and superoleophilic mesh led to an efficiency more than 94% after ten cycles even under immersion test in 3.5% NaCl solution for two days. Fe mesh is a cheap, available, and highly durable candidate for the SS meshes. Yu et al. [237] used an Fe-based mesh that was coated with bismuth. The process created coral-like bismuth oxide structures and irregular petal folds. The Fe mesh was also etched in the acid to create additional surface roughness. The final coated mesh exhibited excellent wettability and durability in cyclic oil-water separations. Ti is light, flexible, and thermally stable; hence, it has been used as a base material to create superhydrophobic and superoleophilic membranes with application to oil-water separation [292]. Yu et al. [121] coated Ti with Cu oxides to fabricate a superhydrophobic and superoleophilic metal mesh. The

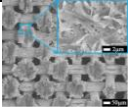
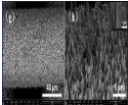
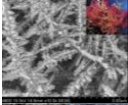
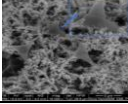
superhydrophobic and superoleophilic Ti mesh resulted in a separation efficiency of more than 96% after at least 20 cycles. The Ti mesh exhibited outstanding stability and durability after subjecting to water and air atmosphere for the lab-based corrosion test.

Table 2.4. Superhydrophobic and superoleophilic mesh-based membranes for oil-water separation.

Chemistry	Surface modification		Morphology	Pore opening	WCA (OCA)	Oil state (Separation tests)	Ref.
	Roughness	Method					
			SS mesh				
PTFE suspension (30% wt)	PS spheres (2–5 μm)	spray coating		30–420 μm	156 (0)	free	[35]
PTFE 35	CNT (100 μm average, 0–970 μm)	spray coating, CVD (CNT)		100 nm (spacing CNT)	163 (0)	free, o/w emulsion	[36]
PTFE-PPS	composite (nm/ μm) suspension film	spray coating		26–440 μm (mesh)	156.3 (0)	free	[103]
CNTs	CVD of CNT on SS with Al_2O_3 barrier (OD=10–30 nm, length >5 μm)	CVD		44 μm (325 mesh)	145–150 (0)	free, w/o emulsion	[102]
PFTOS	silica NPs (220 nm), agglomerates (1–5 μm)	dip coating, sol-gel		75 μm	154.8 (n/a)	o:w	[41]
PFAS	acid erosion	dip coating, (in PFAS sol-gel)		40–1500 mesh	148 (0)	o:w	[17]
Teflon® AF	ZnO rod or flower-like micron and nano structure (1–2 μm)	spin coating		200 μm	157 (0)	o:w	[22]
stearic acid	ZnO crystal growth on SS mesh (hydrothermal reaction)	dip coating		38–600 μm	160 (0)	o:w	[37]
ZnO, stearic acid	clustered structure consisting of nanosheets	immersion		50 μm	156 (0)	o:w (1:1 vol)	[11]

Chemistry	Surface modification		Morphology	Pore opening	WCA (OCA)	Oil state (Separation tests)	Ref.
	Roughness	Method					
stearic acid	Al film deposition and ZnO 2D nano/micro flakes (width=1.5 μm, height=2 μm)	immersion		25–600 μm	156.3 (0)	o:w	[13]
stearic acid	hierarchical micro-nano scale structure of Cu crystals	immersion		100 μm	153 ± 3 (0)	o:w (1:1 vol)	[42]
PDA, NDM	particle clusters of Cu and Ni irons	simultaneous electrodeposition/polymerization		200 μm	162± 1 (0)	oil/water mixtures	[20]
CeO ₂ NPs	deposited CeO ₂ particles (100–500 nm)	spray coating		50, 75 μm	~153 (n/a)	o:w (1:1 vol)	[43]
epoxy/attapulgite nanocomposite	attapulgite particles (320 mesh)	spray coating		150 μm	160 ± 1 (0)	oil/water	[33]
stearic acid/phenol formaldehyde/Mg(OH) ₂	Mg(OH) ₂ particles	spray coating, calcination		150–500 mesh	155.2 (n/a)	o:w (1:1 vol)	[34]
stearoyl chloride (through acylation reaction)	polyaniline and polypyrrole	electrochemical deposition (pulse electro polymerization)		30 μm	154±1.5 (0)	o:w (1:3 vol)	[46]
hexadecanethiol	ytterbium oxide (Yb ₂ O ₃)	spray coating, annealing (200°C)		Micron-sized	~ 150 (0)	oil-water mixture	[47]
stearic acid	HF acid etching, Ag micro/nano hierarchical structures	spray coating		500 mesh	152 (0)	o:w (1:1 vol)	[48]
Cu mesh							
<i>n</i> -DDT	Cu(OH) ₂ nano needles (7 μm long, 150–300 nm diameter)	dip coating, solution immersion		50–1000 μm	151 (0)	o:w (1:1 vol)	[97]

Chemistry	Surface modification		Morphology	Pore opening	WCA (OCA)	Oil state (Separation tests)	Ref.
	Roughness	Method					
dexadecanethiol	acid corrosion (HNO ₃ 4M)	dip coating, solution immersion		44–490 mesh	153 (0)	o:w mixture	[96]
PFAS	Cu(OH) ₂ nano needles (200 nm from anodizing)	electrochemical anodizing, dip coating		389 μm	170 (0)	free	[83]
<i>n</i> -octadecylthiol	Cu NPs (2 μm film thickness)	thiol grafting, electrochemical deposition of Cu		n/a	154.1 (0)	o:w mixture	[100]
lauric acid	Cu clusters	electrodeposition with lauric acid		80–124 μm	155.5 ± 3 (0)	o:w mixture	[105]
dodecanethiol	CuO through annealing (400 °C)	immersion coating		400 μm	162 (n/a)	free	[99]
PDMS	micro/nano binary structure by Cu ₂ S and Cu ₂ O composite	dip coating		n/a	153.3 ± 0.7 (0)	o:w (1:1 vol)	[84]
carbon NPs (candle soot)	electrodeposition, chain-like structures of agglomerated soot (C) NPs formed	electrodeposition, vapor deposition		n/a	153 (<5)	o:w (1:1 vol)	[106]
modified PU, AEAPS, hydrophobic silica NPs	silica NPs	spray coating		85 μm	162.5 (0)	o:w (1:1 vol)	[104]
Cu@Ag modification with DDT	flower-like clusters composed of nano-sized ginkgo-leaf-like lamellas	acid etching		60–200 mesh	155 ± 1 (0)	w/o emulsions	[98]
stearic acid	etched wire, and dense polymer sheets (width=3–10 μm, thickness=300 nm)	immersion		120 μm	155.8 ± 1.1 (0)	o:w (1:1 vol)	[28]
alkaline solution of NaOH and (NH ₄) ₂ S ₂ O ₈	peony flower-like structures by Cu(OH) ₂	immersion		~58 μm	154.39 (0)	o:w (1:1 vol)	[107]

Surface modification		Morphology	Pore opening	WCA (OCA)	Oil state (Separation tests)	Ref.
Chemistry	Roughness					
cupric myristate $\text{Cu}(\text{CH}_3(\text{CH}_2)_{12}\text{COO})_2$	coral shape micro-nano-binary hierarchical structure after anodization	one-step anodization process		70 μm	153 (0)	w:o mixture [108]
Other metal meshes						
Ni mesh 1-octadecanethiol	Ni_3S_2 nanorods	hydrothermal		75 μm	151 (n/a)	o:w (1:1 vol) [26]
Fe mesh bismuth coating	coral-like bismuth oxide structures and irregular petal folds	chemical etching, immersion, anneal (160 °C)		n/a	163 (0)	o:w (1:1 vol) [237]
Ti mesh (Cu-coated) CuCl_2 aqueous solution	micro/nanostructures of TiO_2 and CuO , CuO_2	HF etching, immersion, annealing (160 °C)		n/a	158 (0)	o:w mixture [121]

2.6.2. Superhydrophobic and superoleophilic porous membranes

Utilization of porous materials (filters) for oil-water separation has been a conventional practice in some chemical and energy industries [238]. Porous materials have attracted considerable interest to be used as raw materials for the fabrication of superhydrophobic and superoleophilic surfaces [239]. In this part, we review superhydrophobic and superoleophilic porous materials that are categorized based on their material, including polymers, cotton/textile, filter paper, metals, minerals, ceramics, glasses, carbon-based, and composites. A summary of the superhydrophobic and superoleophilic porous membranes is provided in Table 2.5.

Porous polymers: Membrane surface modification by incorporating numerous types of NPs into the polymeric membrane is also used in fabrication of superhydrophobic and superoleophilic membranes. One of common polymers that is used for oil-water separation is PVDF due to its favorable properties, such as low surface energy, high mechanical strength, and high physical and chemical stabilities [240-242]. These membranes may have limitations for separation of surfactant-stabilized emulsions when the membrane pore size is large [243, 244]. The properties of the modified membrane are affected by incorporating polymeric materials as well as NPs. Commonly NPs such as Ti (oxide) [85, 120] and silica [81] are used in the matrix of porous polymer membrane. Ti is a light nanoparticle with high thermal stability and superhydrophobic properties, which has been widely utilized in oil-water separation [85, 120]; it also features a self-cleaning character [23]. However, in some cases, a superhydrophobic TiO₂ surface can become hydrophilic, for example, under UV exposure [245]. Zhang et al. [120] used TiO₂ NPs with PBZ on polyester non-woven fabrics using dip coating and thermal curing with application to oil-water separation. PBZ is a cost-effective and low surface energy material with high thermal stability and good resistance to harsh environment and UV irradiation. Moreover, it generates a surface with

hydrophobic and oleophilic properties [120]. Similarly, Yu et al. [85] utilized TiO₂ NPs and dip coating technique with TEOS, and VTES. The coated surfaces provided an oil-water separation efficiency of 98% and 95%, respectively [85]. Using low-cost silane coupling agents (TEOS/VTES) resulted in a stable membrane even after 24 separation cycles [85].

Silica NPs are also promising in fabrication of superhydrophobic and superoleophilic porous membranes. They are common NPs that are relatively inexpensive and can be produced with controlled particle size and surface energy to be integrated in modifying superhydrophobic and superoleophilic porous PVDF membranes [81, 122] and PET textile [86]. As the impermeable and dense adhesive layers can reduce the permeate flux [246], Wei et al. [122] used delayed phase inversion method to immobilize the SiO₂ NPs on the PVDF membrane without using adhesive; they achieved a high separation efficiency (99.95%). A functional PU foam is another modified superhydrophobic and superoleophilic porous membrane that can be fabricated through dip coating; these functionalized foams can float on the water due to low density and light weight; it may be used for the capture of oil spills. The PU foam modified with PFAS is chemically stable and reusable that can have a separation efficiency over 95% after 10 cycles [23]. Spray coating as an alternative surface modification strategy is employed to a much less extent with superhydrophobic and superoleophilic polymeric porous membranes. Li et al. [87] fabricated a porous polymer membrane using a fluorinated polyarylester polydimethylsiloxane block copolymer (PAR-b-PDMS) through spray coating. The modified membrane exhibited a stable superhydrophobicity that can effectively treat oil-water mixtures (99%) with at least 50 cycles reusability.

Electrospinning is becoming a widely used technique in the category of superhydrophobic and superoleophilic porous membranes [25, 118, 247]. For instance, a WCA of 153° was achieved

using electrospinning method and applying N, N-DMF/acetone on the ultrathin electrospun fibrous PVDF membranes [247] and PFDT/PI nanofibers [25]. Both research studies reported an excellent separation efficiency of above 99%. Also, the PFDT/PI nanofiber showed excellent recyclability (at least 20 cycles) with consistent superhydrophobicity and good durability under harsh operating conditions. In another study, a hybrid PVA/PTFE nanofibrous membrane was prepared through electrospinning technique [118]. The developed PTFE membrane showed superhydrophobic behavior with a WCA around 155° and efficient gravity-driven oil-water separation. The robust membrane mechanical strength was a result of the sintering process that caused the stability of nanofiber in the membrane under a high vibration environment [118].

Cotton and paper: Cotton textiles have attracted great interest in oil-water separation due to particular characteristics such as easy handling, flexibility, biodegradability, environmentally-friendly, low cost, and high efficiency [88]. The cotton fabrics can be wetted by water and oil simultaneously due to their hydroxyl functional groups on the surfaces. Typically, superhydrophobic cotton textiles are designed for water-repelling or self-cleaning purposes [76, 248]. Only a few studies in the literature employed superhydrophobic textiles for oil-water separation [249, 250]. As the cotton-based materials lose their superhydrophobicity due to the lack of a strong attachment between the cotton fibers and low surface energy materials, it is important to find a robust coating with high mechanical stability for large-scale and long-term applications [251]. Silane, as an inorganic chemical, has been commonly utilized for coating surfaces through covalent attachments consisting of one or more silicons [252]. Singh et al. [88] generated superhydrophobic and superoleophilic cotton fabric via immersion and drying methods. They used HDTMS and stearic acid with zirconia particles, followed by AgBr modification (for constructing surface roughness). The zirconia particles have a high bond dissociation energy and strong

covalent characteristic that can enhance durability. The AgBr can be used when a visible light photocatalyst is needed to degrade the organic compounds. The prepared coated fabric could effectively separate a wide range of oil-water mixtures with high efficiency (>99%) even after 10 cycles [88]. It was noticeable that the modified cotton retained its properties under harsh environmental conditions, such as acidic, alkaline, salty, and UV irradiation. Zhang et al. [89] used solution immersion to coat cotton and PS fabrics with MPTMS and SiO₂ NPs. The superhydrophobic and superoleophilic fabric was used for oil-water separation. The coated surface exhibited mechanical durability, easy repairability, and anti-fouling behavior with the ability of self-cleaning of the organic solvents. Moreover, the prepared surface illustrated a significant performance to separate liquids with different surface tensions and temperatures where the separation efficiency was above 95%. Zhou et al. [253] applied fluorinated alkylsilane onto the cotton fabric. The modified superhydrophobic and superoleophilic cotton demonstrated high separation efficiency of the oil-water mixture. PDMS is a silicon rubber with a high flexibility and mechanical, which is used to coat cotton fabrics without using any adhesives [188]. Liu et al. [24] fabricated a superhydrophobic and superoleophilic cotton fabric through spray coating PDMS, and PMMA in THF solution. The modified cotton fabric displayed a WCA of 157.5° with excellent stability in the harsh environment. The as-prepared cotton provided a high performance in oil-water emulsion separation, anti-fouling, and self-cleaning [24]. Self-polymerization of dopamine under alkaline conditions leads to form PDA, which has a strong adhesive force [20]. Xu et al. [254] used PDA and Ag NPs to fabricate a superhydrophobic cotton fabric for separation of oil and water mixtures with self-cleaning properties. Cellulose is an abundant natural organic polymer that is known as an environmentally friendly and biocompatible material. The cellulose-based filter papers are used in the fabrication of superhydrophobic and superoleophilic surfaces [27, 94, 255].

For instance, modification of filter paper with a PS solution in toluene [38] created a superhydrophobic and superoleophilic membrane with a WCA around 157° . Fluorinated PBZ [119], coated with silica NPs, formed nanoscale roughness and increased the WCA up to 161° . Both fabricated surfaces demonstrated a good performance with the separation efficiency above 96% for different oil/water volume ratios. Huang et al. [256] used dodecafluoroheptyl methacrylate to fabricate a superhydrophobic and superoleophilic filter paper, using dip coating. Wu et al. [255] employed F-based materials, such as polyperfluorooctylethylmethacrylate (PFOEMA) through grafting onto filter papers. The covalent chemical bond between the low surface energy fluorinated materials and filter paper provides a high chemical resistance with a promising performance in oil-water separation. The cellulose- perfluorooctyl ethyl methacrylate porous membrane showed over 95% oil-water separation efficiency with excellent reusability (10 times) [255]. However, as fluorinated compounds are nonbiodegradable, they are considered as environmentally undesirable materials [88]. Stearic acid, as a low-surface-energy material with self-assembly capability, can be alternatively deposited onto the filter paper/cellulose-based surface to exhibit superhydrophobic and superoleophilic feature [27, 94].

Porous metals: The three-dimensional porous metal foams provide a large specific area with a well-developed porous structure, high strength, and low cost in comparison with the traditional two-dimensional materials; they have been alternatively used to fabricate superhydrophobic and superoleophilic membranes for treatment of oily-water systems [257-259]. Liu et al. [95] designed a superhydrophobic and superoleophilic Fe foam using annealing and chemical etching to create micro-nano hierarchical structures on the substrate surface. The surface energy was reduced through coating with stearic acid. The modified superhydrophobic and superoleophilic Fe foam exhibited a high separation efficiency (more than 95%) with exceptional physical and chemical

stability [95]. Also, a porous Cu foam was fabricated, through growing Cu(OH)₂ nanowires on the surface of a Cu mesh via electrodeposition, followed by chemical modification with NDM through immersion approach [260]. The as-prepared foam exhibited a high durability, and a high performance in continuous separation of oil-water systems at a high flux. The modified foam showed the ability of demulsification due to having the cage-like structure; this membrane pore structure resulted in the collision and coalescence of micron-size water droplets [260].

Porous minerals, ceramic, and glass: These materials feature high density, fragility, and incompressibility (their volume is not affected by changing temperature and pressure), compared to the other materials. However, they can be applied in the harsh environment due to their excellent thermal stability and erosion resistance [261]. Sponges as the three-dimensional superhydrophobic and superoleophilic materials are frequently used due to low weight, low price, high mechanical stability, high flexibility, and high separation capacity [238]. However, superhydrophobic and superoleophilic sponges are usually used as a sorbent rather than a filter in oil-water separation. Mi et al. [123] fabricated a superhydrophobic and superoleophilic silica sponge, using cobalt (Co) NPs and PDMS as a surface modifier; the sponge was used in oil-water separation both as a sorbent and a filter. The Co NPs provided hierarchical microstructures and added remote controllability of modified sponge by imparting magnetic properties. The modified silica sponge showed excellent superhydrophobicity and superoleophilicity with high surface area, good thermal resistance, good flexibility, and reasonable durability. The as-prepared sponge exhibited a separation efficiency up to 99.9%, which decreased to 97% after ten cycles of separation test [123]. Ceramic membranes feature excellent mechanical strength, high chemical resistance, and exceptional thermal stability [262]. Indeed, the alumina membrane with excellent resistance in the harsh chemical cleaning can be applied in the different ranges of pH and temperature for oil-water separation applications. Yao

et al. [117] fabricated nanostructured alumina membrane through electrochemical anodization in the oxalic-acid electrolyte. In this morphology dependent technique, a superhydrophobic and superoleophilic alumina film is created without using low energy chemicals. Tang et al. [263] fabricated a superhydrophobic and superoleophilic alumina membrane with PTFE through thermal decomposition (sintering). The modified alumina membrane led to higher than 97% water rejection over four hours.

Carbon-based porous membranes: Shi et al. [109] used free-standing, single-wall CNTs to fabricate a thin membrane (70–120 nm thick) for oil-water separation application. The membrane was superoleophilic, and hydrophobic with a WCA of 94°. One of the features of this thin membrane is its exceptionally high permeate flux up to 100,000 L/(m².h.bar), which is up to three orders of magnitude higher than that for the commercial filters. They used the filter to separate emulsions with and without surfactant; it was possible to separate the emulsified oil with 99.95% efficiency, even after 20 cycles [109]. The membrane also had a high chemical resistance to acid and base (except for strong oxidizing acids). Hsieh et al. [264] used carbon fabrics with fabric diameter of 0.3–0.9 mm in the presence and absence of multi-wall CNTs for oil-water separation purposes. The CNTs were used to add nano-roughness, with an average diameter 30–50 nm that were synthesized through catalytic CVD method. The prepared membrane was spin coated with perfluoroalkyl methacrylic copolymer (Zonyl® 8740, Dupont™) and exhibited superhydrophobic and superoleophilic properties with a WCA of 165° [264]. The membrane was capable of separating oil from water up to 99.7% efficiency. Their results showed a dramatic decrease in the separation efficiency when the diameter of carbon fibers was increased from 0.3 mm to 0.9 mm, as shown in Figure 2.14. This reduction in separation efficiency was more pronounced for the fabric without CNTs, compared to the carbon fiber with CNTs. For example, the separation

efficiencies of 0.9 mm fabric with and without CNTs were decreased to 90%, and 70%, respectively [264]. The permeate flux was also significantly affected by the diameter of the carbon fibers. However, permeability reduction due to an increase in the fiber thickness was more pronounced in the membrane decorated with CNTs, as observed in Figure 2.14. This study suggests opposite effects of the (hierarchical) surface roughness on separation efficiency and permeate flux; a process optimization is thus required to find an optimal roughness on superhydrophobic and superoleophilic membranes, especially for high throughput applications. Also, this study highlights the importance of membrane thickness on oil-water separation efficiency and membrane flux. Both the separation efficiency and the permeate flux will increase as the membrane thickness decreases. For this reason, ultrathin mesh-based membranes and 2D molecular lattice (such as graphene) seem to be promising.

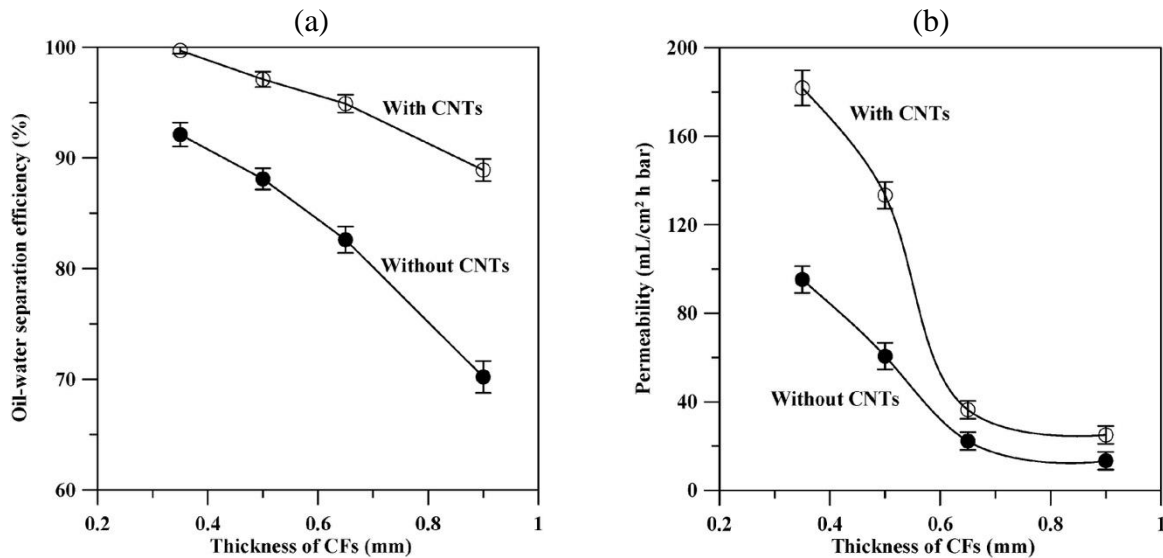
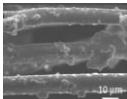
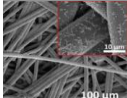
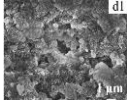
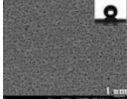
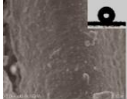
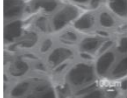
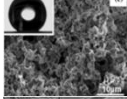
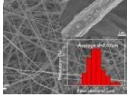
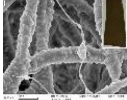


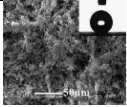
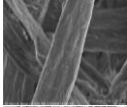
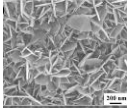
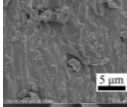
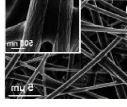
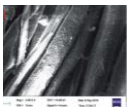
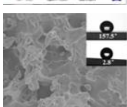
Figure 2.14. Impact of carbon fiber thickness (membrane thickness) and multi-wall CNTs roughness on: (a) separation efficiency and (b) membrane flux, for a superhydrophobic and superoleophilic membrane [264].

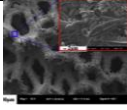
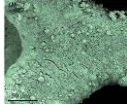
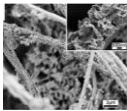
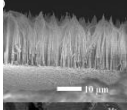
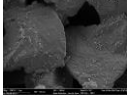
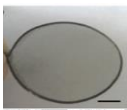
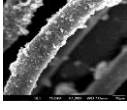
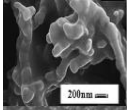
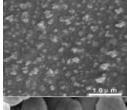
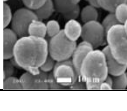
Porous composite membranes: Another practical alternative to fabricate superhydrophobic and superoleophilic surfaces is nanocomposites. Chakradhar et al. [90] prepared a ZnO-PDMS nanocomposite through a simple spray coating and combustion. The ZnO provided micro and

nanostructure that is necessary to achieve superhydrophobic condition. The WCA of the ZnO coating was around 108° , which increased to 155° after modification with PDMS. ZnO/PS cotton textile modified with stearic acid is also utilized for fabricating superhydrophobic and superoleophilic composite membranes [93]. Moreover, using the casting method, PP/methyl silicone membrane was constructed for oil-water separation purposes [124].

Table 2.5. Superhydrophobic and superoleophilic porous membranes for oil-water separation.

Type	Surface modification			Structure	Pore size	WCA (OCA)	Oil state	Ref.
	Chemical	Roughness	Method					
polyester textile (fabric)	TEOS/VTES	TiO ₂ NPs	Polymer-based dip coating		5–10 (μm)	152.4 (n/a)	o:w mixture	[85]
polyester non-woven fabrics	PBZ	TiO ₂ NPs	dip coating, thermal curing		18.9 (μm)	155 ± 1 (0)	o:w mixture	[120]
PVDF	PVDF/DMF	hydrophobic silica NPs (7–40 nm)	immersion polymerization (delayed phase inversion)		n/a	157 ± 2 (0)	w/o emulsion	[122]
PVDF-MF	hexamethyldisilazane	hydrophobic silica NPs	dip coating		0.45 (μm)	>150 (0)	w/o emulsion	[81]
PET textile membrane	TEOS, HMDS	hydrophobic silica NPs (10 nm)	sol gel, dip coating		n/a	150 (0)	o:w mixture	[86]
PU foam	FAS/ethanol	acid etching	dip coating		n/a	155 (0)	o:w mixture	[23]
PAR-b-PDMS (polyarylester)	fluorinated PAR-b-PDMS	hierarchical micro/nano (PAR-b-PDMS)	spray coating		0.1–0.8 (μm)	163 ± 2.3 (0)	o:w (3:7 vol)	[87]
PVDF membrane	PVDF powders, N,N-DMF/acetone	fibrous PVDF	electrospinning		2.02±0.31 (μm)	153 (0)	w/o emulsion	[247]
PVA/PTFE nanofiber	PVA/PTFE	PTFE	electrospinning, sintering		n/a	155 (0)	o:w (1:1)	[118]
PI nanofiber	1H, 1H, 2H, 2H- PFDT	micro/nano-scale hierarchical (300 nm fiber)	electrospinning, dip coating		n/a	153 (0)	o:w (1:1), w/o emulsion	[25]

Type	Surface modification			Structure	Pore size	WCA (OCA)	Oil state	Ref.
	Chemical	Roughness	Method					
PVC membrane	PVC in THF, glacial acetic acid	n/a	pouring and drying		10-50 (nm)	151.5 (8)	n/a	[265]
filter paper	PS/toluene	hydrophobic silica NPs (14 nm)	dip coating		n/a	157 (0)	o:w mixture	[38]
filter paper	Dodecafluoroheptyl methacrylate	n/a	dip coating		40 (nm)	152 (0)	w/o emulsion	[256]
filter paper	stearic acid	Cu(OH) ₂ micro/nano structure	adsorption, immersion		n/a	153 (0)	w/o emulsion	[94]
filter paper	PFOEMA	PFOEMA grated chains	grafting, atom transfer radical polymerization		n/a	157.5 (n/a)	o:w mixture	[255]
cellulose-based	stearic acid	layered double hydroxide uniform crystals	immersion, crystal growth		150 (nm)	154 ± 1.8 (0)	o:w (1:1 vol)	[27]
cellulose acetate	fluorinated poly benzoxazine	silica NPs (7-40 nm)	electrospinning, in-situ polymerization		40 (nm)	161 (3)	o:w (1:1 vol)	[119]
cotton fabric	non-fluorinated hydrophobic reagents (HDTMS and stearic acid)	zirconia particles subsequently AgBr	immersing & dried		n/a	153 (0)	o:w (1:1 vol)	[88]
cotton fabric	PDMS, PMMA, THF	n/a	spray-coating		n/a	157.5 (0)	o:w emulsion	[24]
cotton and PS fabrics	PS, MPTMS	hydrophobic silica NPs	solution immersion metals		n/a	154-156 (0)	o:w mixture	[89]

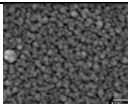
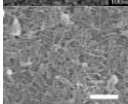
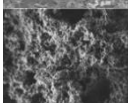
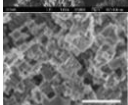
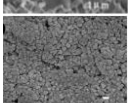
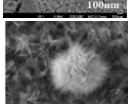
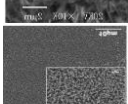
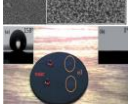
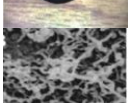
Type	Surface modification			Structure	Pore size	WCA (OCA)	Oil state	Ref.
	Chemical	Roughness	Method					
Fe foam	stearic acid	micron-sized leafy crystals and nano-scale particles	chemical etching, annealing		300-500 (μm)	157 (0)	o:w (2:1 vol)	[95]
Cu foam	NDM	$\text{Cu}(\text{OH})_2$	electrodeposition, immersion		<150	154 (0)	o:w emulsion	[260]
silica sponge	Co NPs/ PDMS	hierarchical Co microstructures	minerals/ceramic/glass self-assembly electrospinning and calcination, controlled particle precipitation, and surface coating		fiber diameter of 2.5 μm	156.9 (n/a)	o:w mixture	[123]
alumina membrane	n/a	alumina nano pyramids (2–3 μ high, 1 μ spacing)	high field anodizing		180 (nm)	152.4 (0)	n/a	[117]
alumina membranes	PTFE	decomposed PTFE particles	thermal decomposition (sintering)		0.10 (μm)	155 (0)	o:w mixture	[263]
single-wall CNT	n/a	CNTs	C-based vacuum filtration		n/a	94 (0)	w/o emulsion	[109]
CNTs	perfluoroalkyl metacrylate (Zonyl® 8740, Dupont™)	CNTs micro/nano	spin coating		n/a	165 (0)	o:w (1:1 vol)	[264]
ZnO/PDMS nano composite	PDMS	hydrophobic ZnO NPs (14 nm)	Composites spray coating, combustion		n/a	155 (<2)	n/a	[90]
ZnO/PS cotton textile	PS, stearic acid	hydrophobic ZnO NPs (150 nm)	drop coating, hydrothermal reaction		11 (μm)	155 (0)	o:w mixture	[93]
PP/methyl-silicone membrane	PP/methyl-silicone (in tetrachloroethane)	PP granules (15–20 μ)	casting		n/a	152 (0)	o:w (1:1 vol)	[124]

2.6.3. Superhydrophobic and superoleophilic films

In this section, we review superhydrophobic and superoleophilic films that have applications in oil-water separation. Various substrates, such as polymers [21, 91, 266], metals [92, 267, 268], NPs [269], and silanes [82] can be employed to prepare superhydrophobic and superoleophilic films. Several methods including electrodeposition [21], solution immersion [270], CVD [271], dip coating [82], and spray coating [91] are usually used to make superhydrophobic and superoleophilic films. In an interesting study, Wang et al. [271] fabricated PTFE hierarchical network film and polytetrafluoroethylene-perfluoropropylvinylethers (PFA) particle rough structure; the first film was oleophobic with an OCA of 138° , while the second film was superoleophilic with an OCA near zero [271]. Both films were superhydrophobic with a $WCA > 150^\circ$. They justified this difference due to different conformation of the $-\text{CF}_2$ functional groups on the film surface. The surface was pretreated by plasma etching, followed by CVD. The result showed 156° WCA. Tang et al. [267] successfully prepared a superhydrophobic and superoleophilic film on a boehmite substrate by a thermal pretreatment and crystal growth (2–3 μm roughness). They obtained a WCA around 152.8° . Pei et al. [268] reported a higher WCA when oxidized Cu was employed as the base substrate. To manipulate the film surface wettability, the surface can be textured with nanomaterials, such as CNTs [269] or TiO_2 [270]. Two forces play a significant role in constructing superhydrophobic and superoleophilic CNT films: 1) van der Waals force to cover the CNT surface with low surface energy chemicals via attachment, and 2) covalent forces to attach the hydrophobic groups onto the CNT surface [272]. Darmanin et al. [21] used electrodeposition to create a rough film of polyheptylendioxythiophene; the film featured a WCA of 156° and an $\text{OCA} < 5^\circ$. Li et al. [92] etched the Al surface with acid immersion and reduced the surface energy, using MTS [92]; their results revealed promising advantages of organosilane

to create stable superhydrophobic film with a high WCA of 169.7°. Zimmermann et al. [82] used plasma treatment and applied dip coating with OTS, and perfluorooctyltrichlorosilane (PFOTS); they observed excellent water repellency with a WCA of 165°. Zhang et al. [91] spray coated trimethylchlorosilane (TMS) and dimethylsiloxane (DMS) on the surface of the polymer film, using NPs for creating roughness on the film, resulting in a WCA of 168°. Table 2.6 summarizes important information (e.g., type and chemical nature/structure) on the superhydrophobic and superoleophilic films for oil/water separation.

Table 2.6. Superhydrophobic and superoleophilic surfaces for oil-water separation application (Film)

Type	Surface modification			Structure	WCA (OCA)	Ref.
	Chemical	Roughness	Technique			
PFA film	PFA	plasma-etched channels (3 μm , 6 μm spacing)	plasma etch, CVD		156 (0)	[271]
surface TiO ₂ nanowires and PDMS	TiO ₂ nanowires (Width: 20–40 nm Length: 5– >10 μ)	Solution immersion	PDMS in THF (10 g/L)		158 (0)	[270]
polymer film	polyehtylendioxythiophene	rough film	electrodepositing		156 (<5)	[21]
modified Al surface	MTS	etched/corroded Al	acid etch, solution immersion		169.7 (0)	[92]
polymer film	TMS, DMS	hydrophobic silica NPs	spray coating		168 (0)	[91]
oxidized cu	n/a	Cu petal like (1–4 μm thick, 20-70 nm slices)	chemical oxidation of cu		158 (<5)	[268]
Beoehmite surface	n/a	crystal growth (2–3 μm)	thermal, crystal growth		152.8 (0)	[267]
multiwall-CNT	alkyl-pyrene	CNTs	noncovalent functionalization		158±2 (0)	[269]
silicone nanofilament	OTS, PFOTS	film	plasma treatment, dip coating		165 (2)	[82]

2.7. Challenges and Future Perspective of Superhydrophobic and Superoleophilic Membranes for Oil-Water Separation

Superhydrophobic and superoleophilic membranes have found great applications in oil-water separation, such as oil spills and oily wastewater treatment. However, they have limited capabilities to separate volatile components as well as systems with potential fouling [273]. Also, the membrane stability under harsh operating condition such as strong acids, bases, oxidizers, and saline solutions is uncertain; the hydrophobicity can decrease at high temperature conditions. The effects of operating parameters including temperature, cross-flow velocity, pH, trans-membrane pressure, and the molecular size of solute in separation membranes should not be underestimated, especially in the presence of solid particles that cause rapid fouling. Furthermore, pH influence on membrane material and larger molecular size of solute augments rejection is still complicated and contradictory results have been reported in the open sources [273]. Systematic investigation of important aspects (e.g., wettability impact, separation mechanisms, and fouling phenomenon) in superhydrophobic and superoleophilic membranes is overlooked in the literature.

For a given oil-water mixture, the separation efficiency is related to the membrane thickness, pore size, wetting state, and surface roughness. A decrease in the membrane thickness increases the separation efficiency, permeate flux, and energy consumption. Therefore, the use of an ultra-thin membrane with a good mechanical strength can be accepted as a promising future trend in membrane filtration. The use of 2D molecular lattice (atom thick membrane) of graphene and single-wall CNTs, and/or other meshes with ultra-thin fibers is expected to be a part of future studies in this area.

Utilization of controlled hierarchical surface roughness is favored in separating dispersed and emulsified oil contaminations from an oil-water mixture. The surface roughness improves the oil

separation efficiency but it also reduces the maximum permeate flux. Therefore, an optimal design of surface roughness is required. Such an optimal design should include the effect of hierarchical surface roughness on membrane fouling for a realistic and effective operation. Using lithography technique and micromachining, it is possible to fabricate a desired surface roughness structure; however, with the current technology, large scale production is expensive, which would be a limiting factor. Perhaps the advancement of 3D printers with high resolutions can improve the scalability of hierarchical roughness that is imperative in fabricating superhydrophobic and superoleophilic membranes.

2.8. Conclusions

This paper systematically reviews the conventional separation methods, fundamental theories, coating techniques, surface energy and morphology modifiers, and recent advancement in superhydrophobic and superoleophilic membranes (mesh, porous, and film) for the oil-water separation applications. A systematic overview of superhydrophobic and superoleophilic sorbents is of great interest in the oil-spill application and can be studied in a separate review paper. The following conclusions are made from our extensive literature review:

- Metallic mesh-based membranes are considered as alternatives to the porous membranes due to greater mechanical integrity, lower pressure drop, and higher permeability and porosity.
- Membrane wettability is changed towards superhydrophobicity and superoleophilicity after modifying the surface energy and morphology. Stearic acid, different silanes, different thiols, and PE-derived (co-) polymers are mainly used to modify the surface energy of the superhydrophobic and superoleophilic membranes. The colloidal assembly

has been suggested as a facile, energy-efficient, and cost-benefit approach to construct surface morphology.

- In most previous studies, the surface topology is modified first. Facile methods are also utilized that simultaneously modify both conditions. Given the simplicity, scalability, and cost of the colloidal assembly and rough polymer films to create superhydrophobic and superoleophilic membranes, these methods can be potentially employed in large-scale applications.
- Among common surface pretreatment methods, air plasma is the best option due to its safety and capability to create fresh reactive sites. In terms of technical and non-technical aspects, the order is as follows: air plasma > oxygen plasma > piranha solution > UV irradiation.
- Selecting an appropriate method for coating SHSO membranes depends on many factors such as budget, environmental values, time, stability, uniformity, simplicity, scalability, and the repairability of the coating film.
- Dip-coating, spin-coating, spray-coating, and sol-gel are the most widely utilized methods that provide a uniform coating with low-cost, and minimum environmental pollutants. Spin coating, spray coating, LbL, and electrospinning methods also provide tunable thickness. Innovative methods (e.g., ion-beam radiation, plasma radiation, and laser ablation) have been developed to provide more stability for coating without decomposition of the coated film.
- The superhydrophobic and superoleophilic membranes are commonly characterized with tests such as contact angle measurement, oil-water separation test, oil permeation flux, breakthrough capillary pressure, SEM, XPS, XRD, AFM, and FTIR.

- Micro- nano- surface structures, account for hydrophobicity of membranes, can be damaged under external mechanical forces and harsh conditions (hot water, brine, acidic, and basic solutions). Therefore, a guideline/standard is urgently needed to measure/compare the stability and durability of the superhydrophobic-superoleophilic membranes.
- Although superhydrophobic-superoleophilic membranes separated around 99% oil from oil-water mixtures, it is not yet desirable, as most of the researchers employed pure oil for their experiments. Instead, oils processed in industries contain contaminations and solids that block membrane pores and reduce the performance of separation. Hence, the antifouling feature, recyclability, and reusability of membranes should be enhanced. The factors mentioned above directly affect the service life of membranes.
- Further technology development in large-scale femtosecond laser ablation, high-resolution 3D printing, and the use of 2D materials such as graphene are expected to cause a breakthrough in the use of superhydrophobic and superoleophilic membranes with application to oil-water separation.

Acknowledgements

The financial support of Suncor Energy Inc. /Terra Nova Young Innovator, Memorial University (Canada), and the Natural Sciences and Engineering Research Council of Canada (NSERC) is acknowledged.

Nomenclatures

Acronyms

- | | |
|-------|--|
| AEAPS | - Aminoethylaminopropyl polydimethylsiloxane |
| API | - American petroleum institute |

APP	- Ammonium polyphosphate
CeO ₂	- Cerium oxide
CNT	- Carbon nanotube
Cu	- Copper
Cu	- Copper
CVD	- Chemical Vapor deposition
DDT	- Dodecanethiol
DMF	- N, N-dimethylformamide
DMS	- Dimethylsiloxane
Fe	- Iron
FL	- Functional layer
HDMS	- Hexamethyldisilazine
HDTMS	- Hexadecyltrimethoxy silane
LbL	- Layer by Layer
MF	- Microfiltration
MPTMS	- Mercaptopropyltrimethoxysilane
MTES	- Methyltrimethoxysilane
MTS	- Methyltrichlorosilane
Ni	- Nickel
NPs	- Nanoparticles
o/w	- Oil in water
OCA	- Oil contact angle
OTS	- Octadecyltrichlorosilane

PAR-b-PDMS	Polyarylester polydimethylsiloxane block copolymer
PBZ	- Polybenzoxazine
PDA	- Polydopamine
PDDA	- Polydiallyldimethyl ammonium chloride
PDMS	- Polydimethylsiloxane
PE	- Polyethylene
PEI	- Polyethylenimide
PFA	- Polytetrafluoroethylene-perfluoropropylvinylethers
PFAS	- Perfluoroalkylsilane
PFDT	- Perfluorodecanethiol
PFOEMA	- polyperfluorooctylethylmethacrylate
PFOTS	- Perfluorooctyltrichlorosilane
PFTOS	- Perfluorooctyltriethoxysilane
PI	- Polyimide
PMMA	- Polymethylmethacrylate
PPS	- Polypropylene sulfide
PS	- Polystyrene
PTFE	- Polytetrafluoroethylene
PU	- Polyurethane
PV	- Polyvinyl
PVA	- Polyvinyl alcohol
PVAC	- Polyvinyl acetate
PVC	- Polyvinylchloride

PVD	- Physical Vapor Deposition
PVDF	- Polyvinylidene fluoride
RO	- Reverse osmosis
SDBS	- Sodium dodecylbenzanesulfonate
SS	- Stainless steel
TEOS	- Tetraethylorthosilicate
THF	- Tetrahydrofuran
Ti	- Titanium
TMCS	- Trimethyltrichlorosilane
UF	- Ultrafiltration
UV	- Ultraviolet
VTES	- Vinyltriethoxysilane
w/o	- Water in oil
WCA	- Water contact angle

Variables/Symbols

f_1	- The total area of the solid under the liquid drop per unit projected area below the drop	(m ²)
f_2	- The total area of the air under the liquid drop per unit projected area below the drop	(m ²)
r	- The ratio of the actual rough surface area to that of the smooth area	

Greek Letters

γ	- Surface energy	(mN/m)
θ	- Static contact angle	(°)

Subscript

<i>App</i>	-	Apparent
<i>CB</i>	-	Cassie-Baxter
<i>LG</i>	-	Liquid-gas
<i>LS</i>	-	Liquid-solid
<i>OA</i>	-	Oil-air
<i>SG</i>	-	Solid-gas
<i>W</i>	-	Wenzel
<i>WA</i>	-	Water-air
<i>Y</i>	-	Young

References

- [1] Pendashteh AR, Fakhru'l-Razi A, Madaeni SS, Abdullah LC, Abidin ZZ, Biak DRA. Membrane foulants characterization in a membrane bioreactor (MBR) treating hypersaline oily wastewater. *Chemical Engineering Journal*. 2011;168:140-50.
- [2] Rubio J, Souza ML, Smith RW. Overview of flotation as a wastewater treatment technique. *Minerals Engineering*. 2002;15:139-55.
- [3] Zhong J, Sun X, Wang C. Treatment of oily wastewater produced from refinery processes using flocculation and ceramic membrane filtration. *Separation and Purification Technology*. 2003;32:93-8.
- [4] Gupta RK, Dunderdale GJ, England MW, Hozumi A. Oil/water separation techniques: a review of recent progresses and future directions. *Journal of Materials Chemistry A*. 2017;5:16025-58.
- [5] Doble M, Kruthiventi AK. CHAPTER 9 - Industrial Examples. In: Doble M, Kruthiventi AK, (editors). *Green Chemistry and Engineering*. Burlington: Academic Press; 2007. p. 245-96.

- [6] Cheryan M, Rajagopalan N. Membrane processing of oily streams. Wastewater treatment and waste reduction. *Journal of Membrane Science*. 1998;151:13-28.
- [7] Li Q, Kang C, Zhang C. Waste water produced from an oilfield and continuous treatment with an oil-degrading bacterium. *Process Biochemistry*. 2005;40:873-7.
- [8] Liu D, Yu Y, Chen X, Zheng Y. Selective separation of oil and water with special wettability mesh membranes. *RSC Advances*. 2017;7:12908-15.
- [9] Unno H, Saka H, Akehata T. OIL SEPARATION FROM OIL-WATER MIXTURE BY A POROUS POLY(TETRAFLUOROETHYLENE) (PTFE) MEMBRANE. *Journal of Chemical Engineering of Japan*. 1986;19:281-6.
- [10] Saththasivam J, Loganathan K, Sarp S. An overview of oil–water separation using gas flotation systems. *Chemosphere*. 2016;144:671-80.
- [11] Zhang Y, Wang X, Wang C, Liu J, Zhai H, Liu B, et al. Facile fabrication of zinc oxide coated superhydrophobic and superoleophilic meshes for efficient oil/water separation. *RSC Advances*. 2018;8:35150-6.
- [12] Ebnesajjad S. Material Surface Preparation Techniques. *Handbook of Adhesives and Surface Preparation*: Elsevier; 2011. p. 49-81.
- [13] Li H, Zheng M, Ma L, Zhu C, Lu S. Two-dimensional ZnO nanoflakes coated mesh for the separation of water and oil. *Materials Research Bulletin*. 2013;48:25-9.
- [14] Li L, Li B, Dong J, Zhang J. Roles of silanes and silicones in forming superhydrophobic and superoleophobic materials. *Journal of Materials Chemistry A*. 2016;4:13677-725.
- [15] Wen N, Miao X, Yang X, Long M, Deng W, Zhou Q, et al. An alternative fabrication of underoil superhydrophobic or underwater superoleophobic stainless steel meshes for oil-water

separation: Originating from one-step vapor deposition of polydimethylsiloxane. *Separation and Purification Technology*. 2018;204:116-26.

[16] Zhang X, Zheng F, Ye L, Xiong P, Yan L, Yang W, et al. A one-pot sol-gel process to prepare a superhydrophobic and environment-resistant thin film from ORMOSIL nanoparticles. *RSC Advances*. 2014;4:9838-41.

[17] Wang Q, Cui Z, Xiao Y, Chen Q. Stable highly hydrophobic and oleophilic meshes for oil-water separation 2007.

[18] Bhagat SD, Gupta MC. Superhydrophobic microtextured polycarbonate surfaces. *Surface and Coatings Technology*. 2015;270:117-22.

[19] Xu Z, Jiang D, Wei Z, Chen J, Jing J. Fabrication of superhydrophobic nano-aluminum films on stainless steel meshes by electrophoretic deposition for oil-water separation. *Applied Surface Science*. 2018;427:253-61.

[20] Xiang M, Jiang M, Zhang Y, Liu Y, Shen F, Yang G, et al. Fabrication of a novel superhydrophobic and superoleophilic surface by one-step electrodeposition method for continuous oil/water separation. *Applied Surface Science*. 2018;434:1015-20.

[21] Darmanin T, Nicolas M, Guittard F. Electrodeposited polymer films with both superhydrophobicity and superoleophilicity. *Physical Chemistry Chemical Physics*. 2008;10:4322-6.

[22] Wu J, Chen J, Qasim K, Xia J, Lei W, Wang B-p. A hierarchical mesh film with superhydrophobic and superoleophilic properties for oil and water separation. *Journal of Chemical Technology & Biotechnology*. 2012;87:427-30.

[23] Zhang X, Li Z, Liu K, Jiang L. Bioinspired Multifunctional Foam with Self-Cleaning and Oil/Water Separation. *Advanced Functional Materials*. 2013;23:2881-6.

- [24] Liu H, Huang J, Chen Z, Chen G, Zhang K-Q, Al-Deyab SS, et al. Robust translucent superhydrophobic PDMS/PMMA film by facile one-step spray for self-cleaning and efficient emulsion separation. *Chemical Engineering Journal*. 2017;330:26-35.
- [25] Ma W, Zhao J, Oderinde O, Han J, Liu Z, Gao B, et al. Durable superhydrophobic and superoleophilic electrospun nanofibrous membrane for oil-water emulsion separation. *Journal of Colloid and Interface Science*. 2018;532:12-23.
- [26] Jian S, Qi Z, Sun S, Zeng Y, Liu Z, Liu Y, et al. Design and fabrication of superhydrophobic/superoleophilic Ni₃S₂-nanorods/Ni-mesh for oil–water separation. *Surface and Coatings Technology*. 2018;337:370-8.
- [27] Yue X, Li J, Zhang T, Qiu F, Yang D, Xue M. In situ one-step fabrication of durable superhydrophobic-superoleophilic cellulose/LDH membrane with hierarchical structure for efficiency oil/water separation. *Chemical Engineering Journal*. 2017;328:117-23.
- [28] Yang C, Wang Y, Fu H, Yang S, Zhu Y, Yue H, et al. A stable eco-friendly superhydrophobic/superoleophilic copper mesh fabricated by one-step immersion for efficient oil/water separation. *Surface and Coatings Technology*. 2019;359:108-16.
- [29] Wang H, Hu X, Ke Z, Du CZ, Zheng L, Wang C, et al. Review: Porous Metal Filters and Membranes for Oil–Water Separation. *Nanoscale Research Letters*. 2018;13:284.
- [30] Yuzhang Z, Dong W, Lei J, Jian J. Recent progress in developing advanced membranes for emulsified oil/water separation. *NPG Asia Materials*. 2014;6:e101.
- [31] Kaur H, Bulasara VK, Gupta RK. Influence of pH and temperature of dip-coating solution on the properties of cellulose acetate-ceramic composite membrane for ultrafiltration. *Carbohydrate Polymers*. 2018;195:613-21.

- [32] Feng L, Zhang Z, Mai Z, Ma Y, Liu B, Jiang L, et al. A Super-Hydrophobic and Super-Oleophilic Coating Mesh Film for the Separation of Oil and Water. *Angewandte Chemie International Edition*. 2004;43:2012-4.
- [33] Yang J, Tang Y, Xu J, Chen B, Tang H, Li C. Durable superhydrophobic/superoleophilic epoxy/attapulgite nanocomposite coatings for oil/water separation. *Surface and Coatings Technology*. 2015;272:285-90.
- [34] Cao W-T, Liu Y-J, Ma M-G, Zhu J-F. Facile preparation of robust and superhydrophobic materials for self-cleaning and oil/water separation. *Colloids and Surfaces A: Physicochemical and Engineering Aspects*. 2017;529:18-25.
- [35] Feng L, Zhang Z, Mai Z, Ma Y, Liu B, Jiang L, et al. A Super-Hydrophobic and Super-Oleophilic Coating Mesh Film for the Separation of Oil and Water. *Angewandte Chemie*. 2004;116:2046-8.
- [36] Lee C, Baik S. Vertically-aligned carbon nano-tube membrane filters with superhydrophobicity and superoleophilicity. *Carbon*. 2010;48:2192-7.
- [37] Wang C-F, Tzeng F-S, Chen H-G, Chang C-J. Ultraviolet-Durable Superhydrophobic Zinc Oxide-Coated Mesh Films for Surface and Underwater–Oil Capture and Transportation. *Langmuir*. 2012;28:10015-9.
- [38] Wang S, Li M, Lu Q. Filter Paper with Selective Absorption and Separation of Liquids that Differ in Surface Tension. *ACS Applied Materials & Interfaces*. 2010;2:677-83.
- [39] Yang H, Pi P, Cai Z-Q, Wen X, Wang X, Cheng J, et al. Facile preparation of superhydrophobic and super-oleophilic silica film on stainless steel mesh via sol–gel process. *Applied Surface Science*. 2010;256:4095-102.

- [40] Hsieh C-T, Hsu J-P, Hsu H-H, Lin W-H, Juang R-S. Hierarchical oil–water separation membrane using carbon fabrics decorated with carbon nanotubes 2016.
- [41] Yang H, Zhang X, Cai Z-Q, Pi P, Zheng D, Wen X, et al. Functional silica film on stainless steel mesh with tunable wettability. *Surface and Coatings Technology*. 2011;205:5387-93.
- [42] Liu Y, Zhang K, Yao W, Liu J, Han Z, Ren L. Bioinspired structured superhydrophobic and superoleophilic stainless steel mesh for efficient oil-water separation. *Colloids and Surfaces A: Physicochemical and Engineering Aspects*. 2016;500:54-63.
- [43] Matin A, Baig U, Gondal MA, Akhtar S, Zubair SM. Superhydrophobic and superoleophilic surfaces prepared by spray-coating of facile synthesized Cerium(IV) oxide nanoparticles for efficient oil/water separation. *Applied Surface Science*. 2018;462:95-104.
- [44] Baig U, Matin A, Gondal MA, Zubair SM. Facile fabrication of superhydrophobic, superoleophilic photocatalytic membrane for efficient oil-water separation and removal of hazardous organic pollutants. *Journal of Cleaner Production*. 2019;208:904-15.
- [45] Li J, Guan P, Zhang Y, Xiang B, Tang X, She H. A diatomite coated mesh with switchable wettability for on-demand oil/water separation and methylene blue adsorption. *Separation and Purification Technology*. 2017;174:275-81.
- [46] Xiao C, Si L, Liu Y, Guan G, Wu D, Wang Z, et al. Ultrastable coaxial cable-like superhydrophobic mesh with self-adaption effect: facile synthesis and oil/water separation application. *Journal of Materials Chemistry A*. 2016;4:8080-90.
- [47] Matin A, Baig U, Gondal MA, Akhtar S, Zubair SM. Facile fabrication of superhydrophobic/superoleophilic microporous membranes by spray-coating ytterbium oxide particles for efficient oil-water separation. *Journal of Membrane Science*. 2018;548:390-7.

- [48] Du Z, Ding P, Tai X, Pan Z, Yang H. Facile Preparation of Ag-Coated Superhydrophobic/Superoleophilic Mesh for Efficient Oil/Water Separation with Excellent Corrosion Resistance. *Langmuir*. 2018;34:6922-9.
- [49] Dunderdale GJ, Urata C, Sato T, England MW, Hozumi A. Continuous, High-Speed, and Efficient Oil/Water Separation using Meshes with Antagonistic Wetting Properties. *ACS applied materials & interfaces*. 2015;7:18915-9.
- [50] Ezazi M, Shrestha B, Kim SI, Jeong B, Gorney J, Hutchison K, et al. Selective Wettability Membrane for Continuous Oil–Water Separation and In Situ Visible Light-Driven Photocatalytic Purification of Water. *Global challenges*. 2020;4:2000009-n/a.
- [51] Yuliwati E, Ismail AF. Effect of additives concentration on the surface properties and performance of PVDF ultrafiltration membranes for refinery produced wastewater treatment. *Desalination*. 2011;273:226-34.
- [52] Garcia-Jares C, Becerril-Bravo E, Sanchez-Prado L, Lamas JP, Dagnac T, Llompart M. Analysis of different high production volume chemicals and their chlorination by-products in waters by ultrasound-assisted emulsification–microextraction. *International Journal of Environmental Analytical Chemistry*. 2014;94:1-15.
- [53] Joye SB. Deepwater Horizon, 5 years on. *Science*. 2015;349:592.
- [54] Kintisch E. Gulf Oil Spill. An audacious decision in crisis gets cautious praise. *Science*. 2010;329:735-6.
- [55] Dubansky B, Whitehead A, Miller JT, Rice CD, Galvez F. Multitissue Molecular, Genomic, and Developmental Effects of the Deepwater Horizon Oil Spill on Resident Gulf Killifish (*Fundulus grandis*). *Environmental Science & Technology*. 2013;47:5074-82.

- [56] Panchanathan D. Photoinduced Wetting Kinetics of Water on Immersed Nanoporous Titania Surfaces with Application to Oil-Water Separation: Massachusetts Institute of Technology; 2015.
- [57] Abdurahman H. Nour FSM, Rosli M. Yunus and A. Arman, . Demulsification of Virgin Coconut Oil by Centrifugation Method: A Feasibility Study. *International Journal of Chemical Technology*. 2009;1:59-64.
- [58] Liu M, Chen J, Cai X, Han Y, Xiong S. Oil–water pre-separation with a novel axial hydrocyclone. *Chinese Journal of Chemical Engineering*. 2018;26:60-6.
- [59] Rocha e Silva FCP, Rocha e Silva NMP, da Silva IA, Ferreira Brasileiro PP, Luna JM, Rufino RD, et al. Oil removal efficiency forecast of a Dissolved Air Flotation (DAF) reduced scale prototype using the dimensionless number of Damköhler. *Journal of Water Process Engineering*. 2018;23:45-9.
- [60] Kwon W-T, Park K, Han SD, Yoon SM, Kim JY, Bae W, et al. Investigation of water separation from water-in-oil emulsion using electric field. *Journal of Industrial and Engineering Chemistry*. 2010;16:684-7.
- [61] Teh CY, Budiman PM, Shak KPY, Wu TY. Recent Advancement of Coagulation–Flocculation and Its Application in Wastewater Treatment. *Industrial & Engineering Chemistry Research*. 2016;55:4363-89.
- [62] Diaz de Tuesta JL, Silva AMT, Faria JL, Gomes HT. Removal of Sudan IV from a simulated biphasic oily wastewater by using lipophilic carbon adsorbents. *Chemical Engineering Journal*. 2018;347:963-71.
- [63] Huang L, Deng S, Guan J, Chen M, Hua W. Development of a novel high-efficiency dynamic hydrocyclone for oil–water separation. *Chemical Engineering Research and Design*. 2018;130:266-73.

- [64] Kundu P, Mishra IM. Removal of emulsified oil from oily wastewater (oil-in-water emulsion) using packed bed of polymeric resin beads. *Separation and Purification Technology*. 2013;118:519-29.
- [65] Matara MR. Mpumalanga province mining operations expansion below old oil bunkers impacts on water quality: Petroleum oil bioremediation strategies: University of Pretoria; 2015.
- [66] Ramseur JL. *Oil Spills: Background and Governance*. 2107.
- [67] McNutt MK, Chu S, Lubchenco J, Hunter T, Dreyfus G, Murawski SA, et al. Applications of science and engineering to quantify and control the Deepwater Horizon oil spill. *Proceedings of the National Academy of Sciences*. 2012;109:20222-8.
- [68] Kostka JE, Prakash O, Overholt WA, Green SJ, Freyer G, Canion A, et al. Hydrocarbon-Degrading Bacteria and the Bacterial Community Response in Gulf of Mexico Beach Sands Impacted by the Deepwater Horizon Oil Spill. *Applied and Environmental Microbiology*. 2011;77:7962.
- [69] Kaya S, Rajan P, Dasari H, Ingram DC, Jadwisienczak W, Rahman F. A systematic study of plasma activation of silicon surfaces for self assembly. *ACS applied materials & interfaces*. 2015;7:25024-31.
- [70] Wang B, Liang W, Guo Z, Liu W. Biomimetic super-lyophobic and super-lyophilic materials applied for oil/water separation: a new strategy beyond nature. *Chemical Society Reviews*. 2015;44:336-61.
- [71] Wang H, Hu X, Ke Z, Du CZ, Zheng L, Wang C, et al. Porous Metal Filters and Membranes for Oil–Water Separation. *Nanoscale research letters*. 2018;13:284.

- [72] Li X-M, Reinhoudt D, Crego-Calama M. What do we need for a superhydrophobic surface? A review on the recent progress in the preparation of superhydrophobic surfaces. *Chemical Society Reviews*. 2007;36:1350-68.
- [73] Yang X-Y, Chen L-H, Li Y, Rooke JC, Sanchez C, Su B-L. Hierarchically porous materials: synthesis strategies and structure design. *Chemical Society Reviews*. 2017;46:481-558.
- [74] Bellanger H, Darmanin T, Taffin de Givenchy E, Guittard F. Chemical and physical pathways for the preparation of superoleophobic surfaces and related wetting theories. *Chemical reviews*. 2014;114:2694-716.
- [75] Si Y, Guo Z. Superhydrophobic nanocoatings: from materials to fabrications and to applications. *Nanoscale*. 2015;7:5922-46.
- [76] Xue C-H, Jia S-T, Zhang J, Ma J-Z. Large-area fabrication of superhydrophobic surfaces for practical applications: an overview. *Science and Technology of Advanced Materials*. 2010;11:033002.
- [77] Xu Z-W, Zhang Y-K, Chen T-H, Chang J-H, Lee T-H, Li P-Y, et al. Enhancement on the surface hydrophobicity and oleophobicity of an organosilicon film by conformity deposition and surface fluorination etching. *Materials*. 2018;11:1089.
- [78] Li Y, Pan Y, Zhao X. Interface conditions of roughness-induced superoleophilic and superoleophobic surfaces immersed in hexadecane and ethylene glycol. *Beilstein journal of nanotechnology*. 2017;8:2504-14.
- [79] Xing R, Huang R, Qi W, Su R, He Z. Three-dimensionally printed bioinspired superhydrophobic PLA membrane for oil-water separation. *AIChE Journal*. 2018;64:3700-8.

- [80] Yang Y, Li X, Zheng X, Chen Z, Zhou Q, Chen Y. 3D-Printed Biomimetic Super-Hydrophobic Structure for Microdroplet Manipulation and Oil/Water Separation. *Advanced materials*. 2018;30:1704912.
- [81] Ju J, Wang T, Wang Q. A facile approach in fabricating superhydrophobic and superoleophilic poly (vinylidene fluoride) membranes for efficient water–oil separation. *Journal of Applied Polymer Science*. 2015;132.
- [82] Zimmermann J, Rabe M, Artus GRJ, Seeger S. Patterned superfunctional surfaces based on a silicone nanofilament coating. *Soft Matter*. 2008;4:450-2.
- [83] La D-D, Nguyen TA, Lee S, Kim JW, Kim YS. A stable superhydrophobic and superoleophilic Cu mesh based on copper hydroxide nanoneedle arrays. *Applied Surface Science*. 2011;257:5705-10.
- [84] Pi P, Hou K, Zhou C, Li G, Wen X, Xu S, et al. Superhydrophobic Cu₂S@Cu₂O film on copper surface fabricated by a facile chemical bath deposition method and its application in oil-water separation. *Applied Surface Science*. 2017;396:566-73.
- [85] Yu L, Zhang S, Zhang M, Chen J. Superhydrophobicity construction with dye-sensitised TiO₂ on fabric surface for both oil/water separation and water bulk contaminants purification. *Applied Surface Science*. 2017;425:46-55.
- [86] Xue C-H, Ji P-T, Zhang P, Li Y-R, Jia S-T. Fabrication of superhydrophobic and superoleophilic textiles for oil–water separation. *Applied Surface Science*. 2013;284:464-71.
- [87] Li H, Zhao X, Wu P, Zhang S, Geng B. Facile preparation of superhydrophobic and superoleophilic porous polymer membranes for oil/water separation from a polyarylester polydimethylsiloxane block copolymer. *Journal of Materials Science*. 2016;51:3211-8.

- [88] Singh AK, Singh JK. Fabrication of zirconia based durable superhydrophobic–superoleophilic fabrics using non fluorinated materials for oil–water separation and water purification. *RSC Advances*. 2016;6:103632-40.
- [89] Zhang X, Geng T, Guo Y, Zhang Z, Zhang P. Facile fabrication of stable superhydrophobic SiO₂/polystyrene coating and separation of liquids with different surface tension. *Chemical Engineering Journal*. 2013;231:414-9.
- [90] Chakradhar RPS, Kumar VD, Rao JL, Basu BJ. Fabrication of superhydrophobic surfaces based on ZnO–PDMS nanocomposite coatings and study of its wetting behaviour. *Applied Surface Science*. 2011;257:8569-75.
- [91] Zhang X, Guo Y, Zhang P, Wu Z, Zhang Z. Superhydrophobic and Superoleophilic Nanoparticle Film: Synthesis and Reversible Wettability Switching Behavior. *ACS Applied Materials & Interfaces*. 2012;4:1742-6.
- [92] Li S, Jin M, Yu C, Liao M. Wetting behavior of superhydrophobic surface in the liquid influenced by the existing of air layer. *Colloids and Surfaces A: Physicochemical and Engineering Aspects*. 2013;430:46-50.
- [93] Zhang M, Wang C, Wang S, Li J. Fabrication of superhydrophobic cotton textiles for water–oil separation based on drop-coating route. *Carbohydrate polymers*. 2013;97:59-64.
- [94] Cao C, Cheng J. A novel Cu(OH)₂ coated filter paper with superhydrophobicity for the efficient separation of water-in-oil emulsions. *Materials Letters*. 2018;217:5-8.
- [95] Liu Y, Zhan B, Zhang K, Kaya C, Stegmaier T, Han Z, et al. On-demand oil/water separation of 3D Fe foam by controllable wettability. *Chemical Engineering Journal*. 2018;331:278-89.

- [96] Wang C, Yao T, Wu J, Ma C, Fan Z, Wang Z, et al. Facile approach in fabricating superhydrophobic and superoleophilic surface for water and oil mixture separation. *ACS applied materials & interfaces*. 2009;1:2613-7.
- [97] Pan Q, Wang M, Wang H. Separating small amount of water and hydrophobic solvents by novel superhydrophobic copper meshes. *Applied Surface Science*. 2008;254:6002-6.
- [98] Cao C, Cheng J. Fabrication of robust surfaces with special wettability on porous copper substrates for various oil/water separations. *Chemical Engineering Journal*. 2018;347:585-94.
- [99] Yanlong S, Wu Y, Xiaojuan F, Yongsheng W, Guoren Y, Shuping J. Fabrication of superhydrophobic-superoleophilic copper mesh via thermal oxidation and its application in oil–water separation. *Applied Surface Science*. 2016;367:493-9.
- [100] Wang B, Guo Z. Superhydrophobic copper mesh films with rapid oil/water separation properties by electrochemical deposition inspired from butterfly wing. *Applied Physics Letters*. 2013;103:063704.
- [101] Bigos A. Electrodeposition and characterisation of Ni-based anticorrosive coatings. *J Geophys Res Biogeosci*. 2005;116:944-56.
- [102] Lee CH, Johnson N, Drelich J, Yap YK. The performance of superhydrophobic and superoleophilic carbon nanotube meshes in water–oil filtration. *Carbon*. 2011;49:669-76.
- [103] Qin F, Yu Z, Fang X, Liu X, Sun X. A novel composite coating mesh film for oil-water separation. *Frontiers of Chemical Engineering in China*. 2009;3:112-8.
- [104] Cao M, Luo X, Ren H, Feng J. Hot water-repellent and mechanically durable superhydrophobic mesh for oil/water separation. *Journal of Colloid and Interface Science*. 2018;512:567-74.

- [105] Liu Y, Zhang K, Yao W, Zhang C, Han Z, Ren L. A Facile Electrodeposition Process for the Fabrication of Superhydrophobic and Superoleophilic Copper Mesh for Efficient Oil–Water Separation. *Industrial & Engineering Chemistry Research*. 2016;55:2704-12.
- [106] Cao H, Fu J, Liu Y, Chen S. Facile design of superhydrophobic and superoleophilic copper mesh assisted by candle soot for oil water separation. *Colloids and Surfaces A: Physicochemical and Engineering Aspects*. 2018;537:294-302.
- [107] Zhang K, Li H, Yin X, Wang Z. Oil/water separation on structure-controllable Cu mesh: Transition of superhydrophilic-superoleophilic to superhydrophobic-superoleophilic without chemical modification. *Surface and Coatings Technology*. 2019;358:416-26.
- [108] Zhang D, Li L, Wu Y, Sun W, Wang J, Sun H. One-step method for fabrication of superhydrophobic and superoleophilic surface for water-oil separation. *Colloids and Surfaces A: Physicochemical and Engineering Aspects*. 2018;552:32-8.
- [109] Shi Z, Zhang W, Zhang F, Liu X, Wang D, Jin J, et al. Ultrafast Separation of Emulsified Oil/Water Mixtures by Ultrathin Free-Standing Single-Walled Carbon Nanotube Network Films. *Advanced Materials*. 2013;25:2422-7.
- [110] Bhushan B, Nosonovsky M, Chae Jung Y. Towards optimization of patterned superhydrophobic surfaces. *Journal of the Royal Society Interface*. 2007;4:643-8.
- [111] Jung YC, Bhushan B. Wetting transition of water droplets on superhydrophobic patterned surfaces. *Scripta Materialia*. 2007;57:1057-60.
- [112] Bhushan B, Jung YC. Wetting, adhesion and friction of superhydrophobic and hydrophilic leaves and fabricated micro/nanopatterned surfaces. *Journal of Physics: Condensed Matter*. 2008;20:225010.

- [113] Bhushan B, Jung YC, Koch K. Micro-, nano-and hierarchical structures for superhydrophobicity, self-cleaning and low adhesion. *Philosophical Transactions of the Royal Society A: Mathematical, Physical and Engineering Sciences*. 2009;367:1631-72.
- [114] Bell MS, Shahraz A, Fichthorn KA, Borhan A. Effects of hierarchical surface roughness on droplet contact angle. *Langmuir*. 2015;31:6752-62.
- [115] Bottiglione F, Carbone G. An effective medium approach to predict the apparent contact angle of drops on super-hydrophobic randomly rough surfaces. *Journal of Physics: Condensed Matter*. 2014;27:015009.
- [116] Cai Y, Chang W, Luo X, Qin Y. Superhydrophobicity of microstructured surfaces on zirconia by nanosecond pulsed laser. *Journal of Micromanufacturing*. 2018:2516598418799933.
- [117] Yao L, Zheng M, Ma L, Li W, Li M, Shen W. Self-assembly of diverse alumina architectures and their morphology-dependent wettability. *Materials Research Bulletin*. 2011;46:1403-8.
- [118] Qing W, Shi X, Deng Y, Zhang W, Wang J, Tang CY. Robust superhydrophobic-superoleophilic polytetrafluoroethylene nanofibrous membrane for oil/water separation. *Journal of Membrane Science*. 2017;540:354-61.
- [119] Shang Y, Si Y, Raza A, Yang L, Mao X, Ding B, et al. An in situ polymerization approach for the synthesis of superhydrophobic and superoleophilic nanofibrous membranes for oil–water separation. *Nanoscale*. 2012;4:7847-54.
- [120] Zhang W, Lu X, Xin Z, Zhou C. A self-cleaning polybenzoxazine/TiO₂ surface with superhydrophobicity and superoleophilicity for oil/water separation. *Nanoscale*. 2015;7:19476-83.
- [121] Yu T, Lu S, Xu W, Boukherroub R. Preparation of superhydrophobic/superoleophilic copper coated titanium mesh with excellent ice-phobic and water-oil separation performance. *Applied Surface Science*. 2019;476:353-62.

- [122] Wei C, Dai F, Lin L, An Z, He Y, Chen X, et al. Simplified and robust adhesive-free superhydrophobic SiO₂-decorated PVDF membranes for efficient oil/water separation. *Journal of Membrane Science*. 2018;555:220-8.
- [123] Mi H-Y, Jing X, Xie H, Huang H-X, Turng L-S. Magnetically driven superhydrophobic silica sponge decorated with hierarchical cobalt nanoparticles for selective oil absorption and oil/water separation. *Chemical Engineering Journal*. 2018;337:541-51.
- [124] Hou W, Mu B, Wang Q. Studies on wettability of polypropylene/methyl-silicone composite film and polypropylene monolithic material. *Journal of Colloid and Interface Science*. 2008;327:120-4.
- [125] Duong PHH, Chung T-S. Application of thin film composite membranes with forward osmosis technology for the separation of emulsified oil–water. *Journal of Membrane Science*. 2014;452:117-26.
- [126] Genc A, & Bakirci, B. Treatment of emulsified oils by electrocoagulation: Pulsed voltage applications. . *Water Science and Technology*. 2015;71:1196-202.
- [127] Tawalbeh M, Al Mojily A, Al-Othman A, Hilal N. Membrane separation as a pre-treatment process for oily saline water. *Desalination*. 2018;447:182-202.
- [128] Awaleh MO SY. Waste Water Treatment in Chemical Industries: The Concept and Current Technologies. *Hydrology: Current Research*. 2014;5.
- [129] Cheremisinoff PN. Oil water Separation *The National Environmental Journal*. 1993.
- [130] Fakhru'l-Razi A, Pendashteh A, Abdullah LC, Biak DRA, Madaeni SS, Abidin ZZ. Review of technologies for oil and gas produced water treatment. *Journal of Hazardous Materials*. 2009;170:530-51.

- [131] Bavar B. The removal of fats, oils and grease (FOG) from food industry wastewater by magnetic coagulation: Ryerson University; 2011.
- [132] Blewett TA, Delompré PLM, He Y, Folkerts EJ, Flynn SL, Alessi DS, et al. Sublethal and Reproductive Effects of Acute and Chronic Exposure to Flowback and Produced Water from Hydraulic Fracturing on the Water Flea *Daphnia magna*. *Environmental Science & Technology*. 2017;51:3032-9.
- [133] Suchanek TH. Oil Impacts on Marine Invertebrate Populations and Communities. *American Zoologist*. 1993;33:510-23.
- [134] Blackburn M, C. A. S. Mazzacano, C. Fallon, and S. H. Black. Oil in Our Oceans. A Review of the Impacts of Oil Spills on Marine Invertebrates.: The Xerces Society for Invertebrate Conservation.; 2014. p. 152.
- [135] Bechmann RK, Larsen BK, Taban IC, Hellgren LI, Moller P, Sanni S. Chronic exposure of adults and embryos of *Pandalus borealis* to oil causes PAH accumulation, initiation of biomarker responses and an increase in larval mortality. *Marine pollution bulletin*. 2010;60:2087-98.
- [136] Maj A. Combined effect of ocean acidification, ocean warming and oil spill on aspects of development of marine invertebrates University of Plymouth; 2016.
- [137] Epstein PR SJ. Oil: A Life Cycle Analysis of Its Health and Environmental Impacts. . Harvard Medical School; 2002.
- [138] Doyle J, Friends of the Earth - United S. Crude awakening : the oil mess in America : wasting energy, jobs & the environment. Washington, D.C.: Friends of the Earth; 1994.
- [139] Kassotis CD, Iwanowicz LR, Akob DM, Cozzarelli IM, Mumford AC, Orem WH, et al. Endocrine disrupting activities of surface water associated with a West Virginia oil and gas industry wastewater disposal site. *Science of The Total Environment*. 2016;557-558:901-10.

- [140] Lester Y, Ferrer I, Thurman EM, Sitterley KA, Korak JA, Aiken G, et al. Characterization of hydraulic fracturing flowback water in Colorado: Implications for water treatment. *Science of The Total Environment*. 2015;512-513:637-44.
- [141] Kassotis CD, Nagel SC, Stapleton HM. Unconventional oil and gas chemicals and wastewater-impacted water samples promote adipogenesis via PPAR γ -dependent and independent mechanisms in 3T3-L1 cells. *Science of The Total Environment*. 2018;640-641:1601-10.
- [142] Yost EE, Stanek J, DeWoskin RS, Burgoon LD. Overview of Chronic Oral Toxicity Values for Chemicals Present in Hydraulic Fracturing Fluids, Flowback, and Produced Waters. *Environmental Science & Technology*. 2016;50:4788-97.
- [143] Bolden AL, Kwiatkowski CF, Colborn T. Correction to New Look at BTEX: Are Ambient Levels a Problem? *Environmental Science & Technology*. 2015;49:11984-9.
- [144] Webb E, Bushkin-Bedient S, Cheng A, Kassotis CD, Balise V, Nagel SC. Developmental and reproductive effects of chemicals associated with unconventional oil and natural gas operations. *Reviews on Environmental Health*. 2014;29:307-18.
- [145] Zoeller RT, Brown TR, Doan LL, Gore AC, Skakkebaek NE, Soto AM, et al. Endocrine-Disrupting Chemicals and Public Health Protection: A Statement of Principles from The Endocrine Society. *Endocrinology*. 2012;153:4097-110.
- [146] Huang G, Xu H, Wu L, Li X, Wang Y. Research of novel process route and scale-up based on oil-water separation flotation column. *Journal of Water Reuse and Desalination*. 2017;8:111-22.
- [147] Wang C, Alpatova A, McPhedran KN, Gamal El-Din M. Coagulation/flocculation process with polyaluminum chloride for the remediation of oil sands process-affected water: Performance and mechanism study. *Journal of Environmental Management*. 2015;160:254-62.

- [148] Zahrim AY, Dexter ZD, Joseph CG, Hilal N. Effective coagulation-flocculation treatment of highly polluted palm oil mill biogas plant wastewater using dual coagulants: Decolourisation, kinetics and phytotoxicity studies. *Journal of Water Process Engineering*. 2017;16:258-69.
- [149] Bhatia S, Othman Z, Ahmad AL. Coagulation–flocculation process for POME treatment using *Moringa oleifera* seeds extract: Optimization studies. *Chemical Engineering Journal*. 2007;133:205-12.
- [150] Tansel B, Vilar F. Enhancement of media filter performance with coagulant use for treatment of diesel oil contaminated surface water. *Desalination*. 2005;173:69-76.
- [151] Gobbi LCA, Nascimento IL, Muniz EP, Rocha SMS, Porto PSS. Electrocoagulation with polarity switch for fast oil removal from oil in water emulsions. *Journal of Environmental Management*. 2018;213:119-25.
- [152] Angelova D, Uzunov I, Uzunova S, Gigova A, Minchev L. Kinetics of oil and oil products adsorption by carbonized rice husks. *Chemical Engineering Journal*. 2011;172:306-11.
- [153] Jamaly S, Giwa A, Hasan SW. Recent improvements in oily wastewater treatment: Progress, challenges, and future opportunities. *Journal of Environmental Sciences*. 2015;37:15-30.
- [154] Mhatre S, Vivacqua V, Ghadiri M, Abdullah AM, Al-Marri MJ, Hassanpour A, et al. Electrostatic phase separation: A review. *Chemical Engineering Research and Design*. 2015;96:177-95.
- [155] Radetić MM, Jocić DM, Jovančić PM, Petrović ZL, Thomas HF. Recycled Wool-Based Nonwoven Material as an Oil Sorbent. *Environmental Science & Technology*. 2003;37:1008-12.
- [156] Tsai C-K, Liao C-Y, Wang HP, Chien Y-C, Jou C-JG. Pyrolysis of spill oils adsorbed on zeolites with product oils recycling. *Marine Pollution Bulletin*. 2008;57:895-8.

- [157] Bayat A, Aghamiri SF, Moheb A, Vakili-Nezhaad GR. Oil Spill Cleanup from Sea Water by Sorbent Materials. 2005;28:1525-8.
- [158] Wang H, Wang E, Liu Z, Gao D, Yuan R, Sun L, et al. A novel carbon nanotubes reinforced superhydrophobic and superoleophilic polyurethane sponge for selective oil–water separation through a chemical fabrication. *Journal of Materials Chemistry A*. 2015;3:266-73.
- [159] Wang L. PVDF Membranes with Stable, Ultrathin Graphene Oxide (GO) Functional Coatings for Antifouling Oil/Water Separation under Cross-Flow Condition: University of South Carolina; 2016.
- [160] Ahmad NA, Leo CP, Ahmad AL, Ramli WKW. Membranes with Great Hydrophobicity: A Review on Preparation and Characterization. *Separation & Purification Reviews*. 2015;44:109-34.
- [161] Ismail NH, Salleh WNW, Ismail AF, Hasbullah H, Yusof N, Aziz F, et al. Hydrophilic polymer-based membrane for oily wastewater treatment: A review. *Separation and Purification Technology*. 2020;233:116007.
- [162] Fella Jahromi A, Elektorowicz M. Electrokinetically assisted oil-water phase separation in oily sludge with implementing novel controller system. *Journal of Hazardous Materials*. 2018;358:434-40.
- [163] Egazar'yants S, Vinokurov V, Vutolkina A, Talanova M, Frolov V, Karakhanov E. Oil Sludge Treatment Processes. *Chemistry & Technology of Fuels & Oils*. 2015;51:506-15.
- [164] Wahi R, Chuah LA, Choong TSY, Ngaini Z, Nourouzi MM. Oil removal from aqueous state by natural fibrous sorbent: An overview. *Separation and Purification Technology*. 2013;113:51-63.
- [165] Yang C-L. Electrochemical coagulation for oily water demulsification. *Separation and Purification Technology*. 2007;54:388-95.

- [166] Almojjly A, Johnson D, Oatley-Radcliffe DL, Hilal N. Removal of oil from oil-water emulsion by hybrid coagulation/sand filter as pre-treatment. *Journal of Water Process Engineering*. 2018;26:17-27.
- [167] Nonato TCM, Schöntag JM, Burgardt T, Alves AAdA, Broock WF, Dalsasso RL, et al. Combination of electroflotation process and down-flow granular filtration to treat wastewater contaminated with oil. *Environmental Technology*. 2018;39:717-24.
- [168] Young T. III. An essay on the cohesion of fluids. *Philosophical Transactions of the Royal Society of London*. 1805;95:65-87.
- [169] Wenzel RN. RESISTANCE OF SOLID SURFACES TO WETTING BY WATER. *Industrial & Engineering Chemistry*. 1936;28:988-94.
- [170] Cassie ABD, Baxter S. Wettability of porous surfaces. *Transactions of the Faraday Society*. 1944;40:546-51.
- [171] Milne A, Amirfazli A. The Cassie equation: How it is meant to be used. *Advances in colloid and interface science*. 2012;170:48-55.
- [172] Marmur A, Bittoun E. When Wenzel and Cassie are right: reconciling local and global considerations. *Langmuir*. 2009;25:1277-81.
- [173] Kim D, Pugno NM, Ryu S. Wetting theory for small droplets on textured solid surfaces. *Scientific reports*. 2016;6:37813.
- [174] Bormashenko E, Pogreb R, Whyman G, Erlich M. Resonance Cassie– Wenzel wetting transition for horizontally vibrated drops deposited on a rough surface. *Langmuir*. 2007;23:12217-21.
- [175] Marmur A. The lotus effect: superhydrophobicity and metastability. *Langmuir*. 2004;20:3517-9.

- [176] Onda T, Shibuichi S, Satoh N, Tsujii K. Super-water-repellent fractal surfaces. *Langmuir*. 1996;12:2125-7.
- [177] Roach P, Shirtcliffe NJ, Newton MI. Progress in superhydrophobic surface development. *Soft matter*. 2008;4:224-40.
- [178] Wang Z, Elimelech M, Lin S. Environmental applications of interfacial materials with special wettability. *Environmental science & technology*. 2016;50:2132-50.
- [179] Fujishima A, Rao TN, Tryk DA. Titanium dioxide photocatalysis. *Journal of photochemistry and photobiology C: Photochemistry reviews*. 2000;1:1-21.
- [180] Otitoju T, Ahmad A, Ooi B. Superhydrophilic (superwetting) surfaces: A review on fabrication and application. *Journal of industrial and engineering chemistry*. 2017;47:19-40.
- [181] Sarbada S, Shin YC. Superhydrophobic contoured surfaces created on metal and polymer using a femtosecond laser. *Applied Surface Science*. 2017;405:465-75.
- [182] Drelich J, Chibowski E, Meng DD, Terpilowski K. Hydrophilic and superhydrophilic surfaces and materials. *Soft Matter*. 2011;7:9804-28.
- [183] Remington JP. *Remington: the science and practice of pharmacy*: Lippincott Williams & Wilkins; 2006.
- [184] Lee TR, Carey RI, Biebuyck HA, Whitesides GM. The wetting of monolayer films exposing ionizable acids and bases. *Langmuir*. 1994;10:741-9.
- [185] Ha C-S, Nagappan S. *Hydrophobic and Superhydrophobic Organic-Inorganic Nano-Hybrids*: Pan Stanford; 2018.
- [186] Brown PS, Bhushan B. Bioinspired, roughness-induced, water and oil super-philic and super-phobic coatings prepared by adaptable layer-by-layer technique. *Scientific reports*. 2015;5:14030.

- [187] Feng L, Zhang Z, Mai Z, Ma Y, Liu B, Jiang L, et al. A super-hydrophobic and superoleophilic coating mesh film for the separation of oil and water. *Angewandte Chemie (International ed in English)*. 2004;43:2012-4.
- [188] Jin Y, Jiang P, Ke Q, Cheng F, Zhu Y, Zhang Y. Superhydrophobic and superoleophilic polydimethylsiloxane-coated cotton for oil–water separation process: An evidence of the relationship between its loading capacity and oil absorption ability. *Journal of Hazardous Materials*. 2015;300:175-81.
- [189] Yeh K-Y, Chen L-J, Chang J-Y. Contact angle hysteresis on regular pillar-like hydrophobic surfaces. *Langmuir*. 2008;24:245-51.
- [190] Xue Z, Cao Y, Liu N, Feng L, Jiang L. Special wettable materials for oil/water separation. *Journal of Materials Chemistry A*. 2014;2:2445-60.
- [191] Shahabadi SMS, Brant JA. Bio-inspired superhydrophobic and superoleophilic nanofibrous membranes for non-aqueous solvent and oil separation from water. *Separation and Purification Technology*. 2019;210:587-99.
- [192] Hetemi D, Pinson J. Surface functionalisation of polymers. *Chemical Society Reviews*. 2017;46:5701-13.
- [193] Kim D-H, Lee D-H. Effect of irradiation on the surface morphology of nanostructured superhydrophobic surfaces fabricated by ion beam irradiation. *Applied Surface Science*. 2017.
- [194] Chen Y, Zhao Z, Dai J, Liu Y. Topological and chemical investigation on superhydrophobicity of PTFE surface caused by ion irradiation. *Applied Surface Science*. 2007;254:464-7.

- [195] Wu X, Zhao H, Pei J. Fabrication of nanopore in graphene by electron and ion beam irradiation: Influence of graphene thickness and substrate. *Computational Materials Science*. 2015;102:258-66.
- [196] Yong J, Fang Y, Chen F, Huo J, Yang Q, Bian H, et al. Femtosecond laser ablated durable superhydrophobic PTFE films with micro-through-holes for oil/water separation: Separating oil from water and corrosive solutions. *Applied Surface Science*. 2016;389:1148-55.
- [197] Yin K, Chu D, Dong X, Wang C, Duan J-A, He J. Femtosecond laser induced robust periodic nanoripple structured mesh for highly efficient oil–water separation. *Nanoscale*. 2017;9:14229-35.
- [198] Wu B, Zhou M, Li J, Ye X, Li G, Cai L. Superhydrophobic surfaces fabricated by microstructuring of stainless steel using a femtosecond laser. *Applied Surface Science*. 2009;256:61-6.
- [199] Jin M, Feng X, Xi J, Zhai J, Cho K, Feng L, et al. Super-Hydrophobic PDMS Surface with Ultra-Low Adhesive Force. *Macromolecular Rapid Communications*. 2005;26:1805-9.
- [200] Cardoso MR, Tribuzi V, Balogh DT, Misoguti L, Mendonça CR. Laser microstructuring for fabricating superhydrophobic polymeric surfaces. *Applied Surface Science*. 2011;257:3281-4.
- [201] Baldacchini T, Carey JE, Zhou M, Mazur E. Superhydrophobic Surfaces Prepared by Microstructuring of Silicon Using a Femtosecond Laser. *Langmuir*. 2006;22:4917-9.
- [202] Fadeeva E, Truong VK, Stiesch M, Chichkov BN, Crawford RJ, Wang J, et al. Bacterial Retention on Superhydrophobic Titanium Surfaces Fabricated by Femtosecond Laser Ablation. *Langmuir*. 2011;27:3012-9.
- [203] Jagdheesh R, Pathiraj B, Karatay E, Römer GRBE, Huis in't Veld AJ. Laser-Induced Nanoscale Superhydrophobic Structures on Metal Surfaces. *Langmuir*. 2011;27:8464-9.

- [204] Meena MK, Tudu BK, Kumar A, Bhushan B. Development of polyurethane-based superhydrophobic coatings on steel surfaces. *Philosophical transactions Series A, Mathematical, physical, and engineering sciences*. 2020;378:20190446-.
- [205] Varshney G, Kanel SR, Kempisty DM, Varshney V, Agrawal A, Sahle-Demessie E, et al. Nanoscale TiO₂ films and their application in remediation of organic pollutants. *Coordination Chemistry Reviews*. 2016;306:43-64.
- [206] Hamedani Y, Macha P, Bunning TJ, Naik RR, Vasudev MC. Plasma-enhanced chemical vapor deposition: Where we are and the outlook for the future: InTech; 2016.
- [207] Faraji G, Kim HS, Kashi HT. Introduction. In: Faraji G, Kim HS, Kashi HT, (editors). *Severe Plastic Deformation*: Elsevier; 2018. p. 1-17.
- [208] Aliofkhazraei M, Ali N. 7.05 - Fabrication of Micro/Nanostructured Coatings by CVD Techniques. In: Hashmi S, Batalha GF, Van Tyne CJ, Yilbas B, (editors). *Comprehensive Materials Processing*. Oxford: Elsevier; 2014. p. 85-117.
- [209] Schmidt M, Nazneen F, Georgiev Y, Herzog G, Galvin P, Petkov N. Fib patterning of stainless steel for the development of nano-structured stent surfaces for cardiovascular applications. *Journal of Physics: Conference Series*. 2012;371:012065.
- [210] Merritt SR, Exner AA, Lee Z, von Recum HA. Electrospinning and Imaging. *Advanced Engineering Materials*. 2012;14:B266-B78.
- [211] Lee D. *Surface Engineering Using Layer-by-Layer Assembly of pH-Sensitive Polymers and Nanoparticles*: Massachusetts Institute of Technology; 2007.
- [212] Sukhodub LF, Yanovska G, Sukhodub L, Kuznetsov V, Stanislavov O. Nanocomposite apatite-biopolymer materials and coatings for biomedical applications. *Journal of Nano- and Electronic Physics*. 2014;6:01001 (16pp).

- [213] Yong J, Yang Q, Guo C, Chen F, Hou X. A review of femtosecond laser-structured superhydrophobic or underwater superoleophobic porous surfaces/materials for efficient oil/water separation. *RSC Advances*. 2019;9:12470-95.
- [214] Cai Y, Li S, Cheng Z, Xu G, Quan X, Zhou Y. Facile fabrication of super-hydrophobic FAS modified electroless Ni-P coating meshes for rapid water-oil separation. *Colloids and Surfaces A: Physicochemical and Engineering Aspects*. 2018;540:224-32.
- [215] Nishino T, Meguro M, Nakamae K, Matsushita M, Ueda Y. The lowest surface free energy based on- CF₃ alignment. *Langmuir*. 1999;15:4321-3.
- [216] Deng D, Prendergast DP, MacFarlane J, Bagatin R, Stellacci F, Gschwend PM. Hydrophobic meshes for oil spill recovery devices. *ACS applied materials & interfaces*. 2013;5:774-81.
- [217] Wang JM, Wang LD, Feng L. One-step fabrication of fluoropolymer transparent films with superhydrophobicity by dry method. *Journal of Applied Polymer Science*. 2011;120:524-9.
- [218] O'Hare LA, Leadley S, Parbhoo B. Surface physicochemistry of corona-discharge-treated polypropylene film. *Surface and Interface Analysis: An International Journal devoted to the development and application of techniques for the analysis of surfaces, interfaces and thin films*. 2002;33:335-42.
- [219] Lukose J. Design and development of surface plasmon resonance spr instrument for sensing applications: Manipal University; 2016.
- [220] Yao H-B, Fang H-Y, Wang X-H, Yu S-H. Hierarchical assembly of micro-/nano-building blocks: bio-inspired rigid structural functional materials. *Chemical Society Reviews*. 2011;40:3764-85.

- [221] Yan YY, Gao N, Barthlott W. Mimicking natural superhydrophobic surfaces and grasping the wetting process: A review on recent progress in preparing superhydrophobic surfaces. *Advances in colloid and interface science*. 2011;169:80-105.
- [222] Liu K, Yao X, Jiang L. Recent developments in bio-inspired special wettability. *Chemical Society Reviews*. 2010;39:3240-55.
- [223] Stratakis E. Nanomaterials by ultrafast laser processing of surfaces. *Science of Advanced Materials*. 2012;4:407-31.
- [224] Chen Y, Xu Z, Gartia MR, Whitlock D, Lian Y, Liu GL. Ultrahigh throughput silicon nanomanufacturing by simultaneous reactive ion synthesis and etching. *ACS nano*. 2011;5:8002-12.
- [225] Li L, Breedveld V, Hess DW. Creation of superhydrophobic stainless steel surfaces by acid treatments and hydrophobic film deposition. *ACS applied materials & interfaces*. 2012;4:4549-56.
- [226] Liu B, He Y, Fan Y, Wang X. Fabricating super-hydrophobic lotus-leaf-like surfaces through soft-lithographic imprinting. *Macromolecular rapid communications*. 2006;27:1859-64.
- [227] Li K, Ju J, Xue Z, Ma J, Feng L, Gao S, et al. Structured cone arrays for continuous and effective collection of micron-sized oil droplets from water. *Nature communications*. 2013;4:2276.
- [228] Qian Z, Zhang Z, Song L, Liu H. A novel approach to raspberry-like particles for superhydrophobic materials. *Journal of Materials Chemistry*. 2009;19:1297-304.
- [229] Miyauchi Y, Ding B, Shiratori S. Fabrication of a silver-ragwort-leaf-like super-hydrophobic micro/nanoporous fibrous mat surface by electrospinning. *Nanotechnology*. 2006;17:5151.
- [230] Wang K, Han DS, Yiming W, Ahzi S, Abdel-Wahab A, Liu Z. A windable and stretchable three-dimensional all-inorganic membrane for efficient oil/water separation. *Scientific reports*. 2017;7:16081.

- [231] Liu Y, Liu F, Ni L, Meng M, Meng X, Zhong G, et al. A modeling study by response surface methodology (RSM) on Sr(ii) ion dynamic adsorption optimization using a novel magnetic ion imprinted polymer. *RSC Advances*. 2016;6:54679-92.
- [232] Ng WF, Wong MH, Cheng FT. Stearic acid coating on magnesium for enhancing corrosion resistance in Hanks' solution. *Surface and Coatings Technology*. 2010;204:1823-30.
- [233] Wang X, Li X, Lei Q, Wu Y, Li W. Fabrication of superhydrophobic composite coating based on fluorosilicone resin and silica nanoparticles. *Royal Society Open Science*.5:180598.
- [234] Wang Q, Cui Z, Xiao Y, Chen Q. Stable highly hydrophobic and oleophilic meshes for oil–water separation. *Applied Surface Science*. 2007;253:9054-60.
- [235] Eo Y-J, Kim D-J, Bae B-S, Song K-C, Lee T-Y, Song S-W. Coating of Tetraethylorthosilicate (TEOS)/Vinyltriethoxysilane (VTES) Hybrid Solution on Polymer Films. *Journal of Sol-Gel Science and Technology*. 1998;13:409-13.
- [236] D.D. La TAN, S. Lee, J.W. Kim, S.K. Yong. A stable superhydrophobic and superoleophilic Cu mesh based on copper hydroxide nanoneedle arrays. *Appl Surf Sci.*, 2011;257:5705-10.
- [237] Yu T, Lu S, Xu W. A reliable filter for oil-water separation: Bismuth coated superhydrophobic/superoleophilic iron mesh. *Journal of Alloys and Compounds*. 2018;769:576-87.
- [238] Ke Q, Jin Y, Jiang P, Yu J. Oil/Water Separation Performances of Superhydrophobic and Superoleophilic Sponges. *Langmuir*. 2014;30:13137-42.
- [239] Gao X, Wang X, Ouyang X, Wen C. Flexible Superhydrophobic and Superoleophilic MoS₂ Sponge for Highly Efficient Oil-Water Separation. *Scientific Reports*. 2016;6:27207.

- [240] Chen L, Si Y, Zhu H, Jiang T, Guo Z. A study on the fabrication of porous PVDF membranes by in-situ elimination and their applications in separating oil/water mixtures and nano-emulsions. *Journal of Membrane Science*. 2016;520:760-8.
- [241] Shi H, He Y, Pan Y, Di H, Zeng G, Zhang L, et al. A modified mussel-inspired method to fabricate TiO₂ decorated superhydrophilic PVDF membrane for oil/water separation. *Journal of Membrane Science*. 2016;506:60-70.
- [242] Wang Y, Lin H, Xiong Z, Wu Z, Wang Y, Xiang L, et al. A silane-based interfacial crosslinking strategy to design PVDF membranes with versatile surface functions. *Journal of Membrane Science*. 2016;520:769-78.
- [243] Zhang W, Shi Z, Zhang F, Liu X, Jin J, Jiang L. Superhydrophobic and Superoleophilic PVDF Membranes for Effective Separation of Water-in-Oil Emulsions with High Flux. *Advanced Materials*. 2013;25:2071-6.
- [244] Zhou Z, Wu X-F. Graphene-beaded carbon nanofibers for use in supercapacitor electrodes: Synthesis and electrochemical characterization. *Journal of Power Sources*. 2013;222:410-6.
- [245] Rathousky J, Kalousek V, Kolar M, Jirkovsky J. Mesoporous films of TiO₂ as efficient photocatalysts for the purification of water. *Photochemical & photobiological sciences : Official journal of the European Photochemistry Association and the European Society for Photobiology*. 2011;10:419-24.
- [246] Xiong Z, Lin H, Zhong Y, Qin Y, Li T, Liu F. Robust superhydrophilic polylactide (PLA) membranes with a TiO₂ nano-particle inlaid surface for oil/water separation. *Journal of Materials Chemistry A*. 2017;5:6538-45.
- [247] Zhou Z, Wu X-F. Electrospinning superhydrophobic–superoleophilic fibrous PVDF membranes for high-efficiency water–oil separation. *Materials Letters*. 2015;160:423-7.

- [248] Synytska A, Khanum R, Ionov L, Cherif C, Bellmann C. Water-Repellent Textile via Decorating Fibers with Amphiphilic Janus Particles. *ACS Applied Materials & Interfaces*. 2011;3:1216-20.
- [249] Li J, Shi L, Chen Y, Zhang Y, Guo Z, Su B-l, et al. Stable superhydrophobic coatings from thiol-ligand nanocrystals and their application in oil/water separation. *Journal of Materials Chemistry*. 2012;22:9774-81.
- [250] Zhang L, Zhang Z, Wang P. Smart surfaces with switchable superoleophilicity and superoleophobicity in aqueous media: toward controllable oil/water separation. *Npg Asia Materials*. 2012;4:e8.
- [251] Sasaki K, Tenjimabayashi M, Manabe K, Shiratori S. Asymmetric Superhydrophobic/Superhydrophilic Cotton Fabrics Designed by Spraying Polymer and Nanoparticles. *ACS Applied Materials & Interfaces*. 2016;8:651-9.
- [252] Zareei Pour F, Karimi H, Madadi Avargani V. Preparation of a superhydrophobic and superoleophilic polyester textile by chemical vapor deposition of dichlorodimethylsilane for Water–Oil separation. *Polyhedron*. 2019;159:54-63.
- [253] Wang J, Geng G. Simple and eco-friendly fabrication of superhydrophobic textile for oil/water separation. *Environmental Technology*. 2016;37:1591-6.
- [254] Xu Z, Miyazaki K, Hori T. Fabrication of polydopamine-coated superhydrophobic fabrics for oil/water separation and self-cleaning. *Applied Surface Science*. 2016;370:243-51.
- [255] Wu H, Wu L, Lu S, Lin X, Xiao H, Ouyang X, et al. Robust superhydrophobic and superoleophilic filter paper via atom transfer radical polymerization for oil/water separation. *Carbohydrate Polymers*. 2018;181:419-25.

- [256] Huang X, Wen X, Cheng J, Yang Z. Sticky superhydrophobic filter paper developed by dip-coating of fluorinated waterborne epoxy emulsion. *Applied Surface Science*. 2012;258:8739-46.
- [257] Li J, Li D, Li W, She H, Feng H, Hu D. Facile fabrication of three-dimensional superhydrophobic foam for effective separation of oil and water mixture. *Materials Letters*. 2016;171:228-31.
- [258] Zhu H, Gao L, Yu X, Liang C, Zhang Y. Durability evaluation of superhydrophobic copper foams for long-term oil-water separation. *Applied Surface Science*. 2017;407:145-55.
- [259] Luo Z-Y, Chen K-X, Wang J-H, Mo D-C, Lyu S-S. Hierarchical nanoparticle-induced superhydrophilic and under-water superoleophobic Cu foam with ultrahigh water permeability for effective oil/water separation. *Journal of Materials Chemistry A*. 2016;4:10566-74.
- [260] Wang Z, Xiao C, Wu Z, Wang Y, Du X, Kong W, et al. A novel 3D porous modified material with cage-like structure: fabrication and its demulsification effect for efficient oil/water separation. *Journal of Materials Chemistry A*. 2017;5:5895-904.
- [261] Tan JC, Cheetham AK. Mechanical properties of hybrid inorganic–organic framework materials: establishing fundamental structure–property relationships. *Chemical Society Reviews*. 2011;40:1059-80.
- [262] Pan Y, Wang T, Sun H, Wang W. Preparation and application of titanium dioxide dynamic membranes in microfiltration of oil-in-water emulsions. *Separation and Purification Technology*. 2012;89:78-83.
- [263] Tang H, Hao L, Chen J, Wang F, Zhang H, Guo Y. Surface Modification to Fabricate Superhydrophobic and Superoleophilic Alumina Membranes for Oil/Water Separation. *Energy & Fuels*. 2018;32:3627-36.

- [264] Hsieh C-T, Hsu J-P, Hsu H-H, Lin W-H, Juang R-S. Hierarchical oil–water separation membrane using carbon fabrics decorated with carbon nanotubes. *Surface and Coatings Technology*. 2016;286:148-54.
- [265] Kang Y, Wang J, Yang G, Xiong X, Chen X, Yu L, et al. Preparation of porous superhydrophobic and super-oleophilic polyvinyl chloride surface with corrosion resistance property. *Applied Surface Science*. 2011;258:1008-13.
- [266] Wang L, Yang S, Wang J, Wang C, Chen L. Fabrication of superhydrophobic TPU film for oil–water separation based on electrospinning route. *Materials Letters*. 2011;65:869-72.
- [267] Tang K, Yu J, Zhao Y, Liu Y, Wang X, Xu R. Fabrication of super-hydrophobic and super-oleophilic boehmite membranes from anodic alumina oxide film via a two-phase thermal approach. *Journal of Materials Chemistry*. 2006;16:1741-5.
- [268] Pei M-D, Wang B, Li E, Zhang X-h, Song X-m, Yan H. The fabrication of superhydrophobic copper films by a low-pressure-oxidation method. *Applied Surface Science*. 2010;256:5824-7.
- [269] Huang T-C, Li P, Yao H, Sue H-J, Kotaki M, Tsai M-H. Highly efficient oil–water separators based on dual superhydrophobic and superoleophilic properties of multiwall-carbon nanotube filtration films. *RSC Advances*. 2016;6:12431-4.
- [270] Zhang X, Guo Y, Zhang Z, Zhang P. Self-cleaning superhydrophobic surface based on titanium dioxide nanowires combined with polydimethylsiloxane. *Applied Surface Science*. 2013;284:319-23.
- [271] Wang J-M, Wang L-D, Feng L. One-step fabrication of fluoropolymer transparent films with superhydrophobicity by dry method. *Journal of Applied Polymer Science*. 2011;120:524-9.

[272] Chu C-C, White KL, Liu P, Zhang X, Sue H-J. Electrical conductivity and thermal stability of polypropylene containing well-dispersed multi-walled carbon nanotubes disentangled with exfoliated nanoplatelets. *Carbon*. 2012;50:4711-21.

[273] Padaki M, Surya Murali R, Abdullah MS, Misdan N, Moslehyani A, Kassim MA, et al. Membrane technology enhancement in oil–water separation. A review. *Desalination*. 2015;357:197-207.

3. CHAPTER THREE

Design, Fabrication, and Characterization of a Facile Superhydrophobic and Superoleophilic Mesh-Based Membrane for Selective Oil-Water Separation

Abstract

Superhydrophobic and superoleophilic (SHSO) membranes have found great attention in oil-water separation application. We fabricate a SHSO stainless steel mesh-based membrane, using a facile one-stage dip-coating technique, and investigate the effects of silane alkyl chain, and ratio of micro-to-nanoparticle in the coating. The long-silane features a higher water contact (WCA) at all solid compositions. Increasing ratio of nano-to-microparticles increases the WCA with long-chain silane. Maximum WCAs are attained with both silanes when coating solid is composed of 75 wt% nanoparticles and 25 wt% microparticles. Increasing concentration of nanoparticles to 100% decreases hydrophobicity, which is more pronounced for the short-chain silane. Flower-like hierarchical roughness structures are observed for the coating solution with only nanoparticles. Except for exposure to 1.0 M NaOH solution, the membranes are stable ($\text{WCA} > 145^\circ$) in H_2SO_4 , NaOH, and NaCl solutions over four weeks. Using the fabricated mesh, the macroscopic separation efficiency of kerosene from water is $> 99\%$.

Keywords: Superhydrophobic, Superoleophilic, Oil/Water Separation, Contact Angle, Mesh

3.1. Introduction

Superhydrophobic and superoleophilic (SHSO) surfaces are commonly used in the form of porous or mesh material in oil-water separation applications such as treatment of oily wastewater and oil spill removal. The mesh-based SHSO membranes feature a higher permeability and mechanical strength, and a lower pressure drop compared to the porous membranes. Among the metallic mesh substrates, stainless steel (SS) and copper materials are commonly used as the base substrate; its wettability is altered to SHSO condition by modifying surface morphology and chemistry. In the literature of SHSO SS mesh membranes, methods such as acid erosion [1-3], colloidal assembly

[4-12], rough polymer film [13,14], crystal growth [15-17], and chemical vapor deposition (CVD) [18-20] are used to create hierarchical micro- and nano roughness features. For the SS mesh membranes, chemicals such as fluoropolymers [17,18, 21], silanes [1, 11], stearic acid [2, 5, 6, 9, 12, 15], and thiols [10] are commonly used to adjust the surface energy to achieve SHSO wetting. In this section, we present a history of SHSO SS mesh membranes that are used in oil-water separation application. The first SHSO membrane was fabricated by Feng et al. [4] in 2004 through spray-coating a mixture of polytetrafluoroethylene (PTFE) particles, polyvinyl acetate (as an adhesive), polyvinyl alcohol (as a dispersant), water (as a thinner), and sodium dodecylbenzylsulfate (as a surfactant) on SS mesh. The coating gel was cured at 350°C to improve the coating stability; the coated mesh featured a water contact angle (WCA) of 156.2°, an oil contact angle (OCA) of zero, and a sliding angle of 4° [4]. Since 2004, different facile approaches, including rough polymer films and colloidal assemblies, were employed to prepare SHSO membranes [7-8, 10, 13, 14, 21-40]. For example, Yang et al. [13] coated a SS mesh with epoxy/attapulgitite (44.4 wt%) through spray-coating, resulting in a WCA of 160 ± 1 and 98% oil-water separation efficiency. Xiang et al. [7] coated Ni, Fe, and Cu clusters onto a SS mesh, by grafting *n*-dodecyl mercaptan through polydopamine solution, and using electrodeposition process. They observed popcorn-like micro- and nano-roughness structures that were obtained by the particle clusters [7]. The as-prepared mesh exhibited a WCA of $162 \pm 1^\circ$, with 98.6% oil-water separation efficiency. Cao et al. [9] spray-coated a mixture of phenol formaldehyde and Mg(OH)₂ nanoparticles (NPs) in stearic acid, onto a SS mesh. They found a WCA of 151.4°, and oil-water separation efficiency of 94.6% (for soy oil) up to 10 separation cycles [9]. Matin et al. [8] spray-coated a suspension of CeO₂ NPs in tetrahydrofuran (THF) onto a SS mesh, following calcination at 200°C (without further chemical modifications). The CeO₂ NPs agglomerates with size

distribution 100–500 nm provided the condition for SHSO with a WCA of 153° and an OCA of 0°. Du et al. [2] used HF acid etching, following dip coating in a solution of stearic acid and Ag NPs. The SHSO SS mesh featured a WCA of 152° with an excellent stability against chemicals and hot water; they also observed over 97% oil-water separation efficiency (up to 40 cycles). In several studies, carbon nano tube (CNT) has been also used to fabricate the SHSO SS mesh [19, 41, 42]. Lee et al. [18] grew vertically aligned multi-wall CNTs on the SS surface via CVD in the presence of Al₂O₃ diffusion barrier. The fabricated SHSO mesh resulted in a WCA up to 150°; the mesh also successfully separated oil-in-water emulsions with an oil droplet size 3–100 μm, and oil concentration of 5–10 wt.%. Fluorinated (co)polymers such as PTFE or Teflon AF[®] have high chemical, thermal, and mechanical stabilities (against abrasion) that are naturally hydrophobic and oleophilic. With adding hierarchical micro- and nano roughness structure, the condition of SHSO can be achieved. Wu et al. [17] used hierarchical rod- and flower-like roughness features of ZnO (1–2 μm) onto SS mesh, and coated it with Teflon AF[®]. ZnO was first seeded onto a SS mesh, by spraying 0.2 M zinc acetate solution. Using hydrothermal method, the hierarchical features were grown. The SHSO mesh had a WCA of 157° and the mesh was used for oil-water separation [17]. Varshney et al. [3] employed a mixture of hydrochloric acid and nitric acid to create microstructure surface roughness, and then applied lauric acid to adjust the surface energy. The as prepared mesh was SHSO with a WCA of 171°, and a sliding angle of 4°; over 99% oil-water separation efficiency was achieved in their work [3].

Dip-coating into a colloidal solution combines the surface morphology and surface energy modification steps in one step when fabricating the SHSO membranes [43, 44]. This technique is simple, controllable, and reliable in which high-quality thin films with a thickness of 0.1–100 μm can be achieved [45]. Using a mixture of microparticles (MPs) and nanoparticles (NPs) in the

coating solution increases surface roughness heterogeneity, and improves mechanical stability of the coated meshes [24, 46]. Despite extensive investigations on developing SHSO membranes for oil-water separation, the effect of size distribution of solids (MPs and NPs) in the colloidal coating solution has been overlooked in previous research studies. Zhang et al. [47] examined the effect of roughness by adding micro- and nanoparticles of CaCO₃ solids. They employed a two-step coating method where the surface roughness was first created and then treated with stearic acid. They used spin-coating to first deposit the rough features from a suspension of solids in poly(vinylpyrrolidone) onto a glass slide; after the film was dried, the glass slide was dipped into 20 mM stearic acid in *n*-hexane for a period of 10 days to change the surface energy. It was found that the optimum concentration of solids is 40 wt% and that the best superhydrophobicity is achieved using 2 wt% MPs and 38 wt% NPs (meaning that 95% of the solid is NP). Zhang et al. [47] concluded that among all compositions tested, only one solid composition satisfies the sliding angle < 10° condition for the hydrophobic surfaces [47,48]. One issue with the experimental methodology is that the centrifugation force is expected to cause heterogeneity in the size of solid aggregates deposited onto the glass slide; larger particles will be pushed away from the rotation center.

We use a simplified one-step coating procedure where the surface roughness features (MPs and NPs of silica) and surface modification chemicals (two different organoalkylsilanes with short- and long alkyl-chains) are simultaneously present in the coating solution. We use Dynasylan[®] F8261 as long silane, and Dynasylan[®] SIVO 408 as the short silane; there is no study in the literature on SHSO SS mesh membranes using the shorter silane. Organoalkylsilanes with a longer fluorinated alkyl chain are known to be more hydrophobic. However, fluorine (F) is harmful to the environment and it is desired to use less F in the coating solution. One practical implication from

our research is that it is possible to use a shorter silane and to compensate its lower hydrophobicity by controlling the surface morphology—through adjusting the ratio of micro- and nanoparticles in the coating solution. We also conduct systematic long-term stability of SHSO membranes in concentrated alkaline, acidic and brine solutions.

The structure of the paper is designed as follows. After the introduction part in Section 1, materials and methods for fabricating and characterizing the superhydrophobic and superoleophilic membranes are discussed in Section 2. The results and conclusions are provided in Section 3 where the results of WCA, sliding angle, transmission electron microscopy (TEM), scanning electron microscope (SEM), X-ray diffraction (XRD), Fourier-transform infrared spectroscopy (FTIR), energy-dispersive X-ray spectroscopy (EDX), and separation efficiency analyses are presented. Finally, in Section 4, the key conclusion remarks are summarized.

3.2. Materials and Methods

3.2.1. Materials

Stainless steel 316 meshes (woven, 34% open area and 75 μm opening, and 53.3 μm wire diameter) are purchased from McMaster-Carr. Sulfuric acid (H_2SO_4 , 98 wt%) is purchased from Caledon Laboratory Ltd. Hydrochloric acid (HCl, 37 wt%), hydrogen peroxide (H_2O_2 , 30 wt%), and acetone (99.5 wt%) are obtained from ACP Chemicals. Dynasylan[®] F8261 solution (long-chain alkyl silane), Dynasylan[®] SIVO 408 (short-chain alkyl silane), hydrophobic SiO_2 nanoparticles (NPs) of AEROSIL[®] R812 (7 nm), and microparticles (MPs) of SIPERNAT[®] D13 (10.5 μm) are provided from Evonik Industries AG. Acetone and ethanol (> 99.5 wt%) are utilized for cleaning. Kerosene is purchased locally, and is used in oil-water separation tests. All chemicals are used

without any purification. Compressed air is used for pre-drying. Deionized water (DI, 18.2 M Ω .cm) is produced in the lab (RODI-C-12A, Aqua Solution[®]).

3.2.2. Fabricating SHSO mesh

The fabrication process includes four main stages of a) cleaning, b) activation, c) solution preparation, and d) coating, as shown in Figure 3.1.

Cleaning: SS mesh samples (1 cm wide, 5 cm long) are cut and rinsed with DI water. The organic contaminants on the SS mesh surface are first ultrasonically cleaned (for 30 min) in acetone, rinsed with DI water, ultrasonically cleaned (for 30 min) in ethanol, and rinsed with DI water again, as shown in Figure 3.1 (a). The mesh is pre-dried with compressed air and dried on hot plate at 120°C for 30 min.

Activation: The old oxide layers on the SS mesh are replaced with fresh and reactive hydroxyl groups. We activate the cleaned mesh using piranha solution (see Figure 3.1 (b)). A 3:1 (by volume) mixture of H₂SO₄ (98 wt%) and H₂O₂ (30 wt%) is prepared for activation. The cleaned meshes are placed in the piranha solution heated to 80°C for 30 min, while continuously stirred the piranha solution under a hood. The piranha solution is extremely reactive and requires extreme safety cautions. After this stage, we remove the mesh from the solution, and submerge it in DI water. Then, the activated mesh is rinsed with the DI water, pre-dried with compressed air, and dried on a hot plate at 120°C for 30 min. Some studies used a 1:1 mixture of acetone and ethanol for chemical cleaning [5].

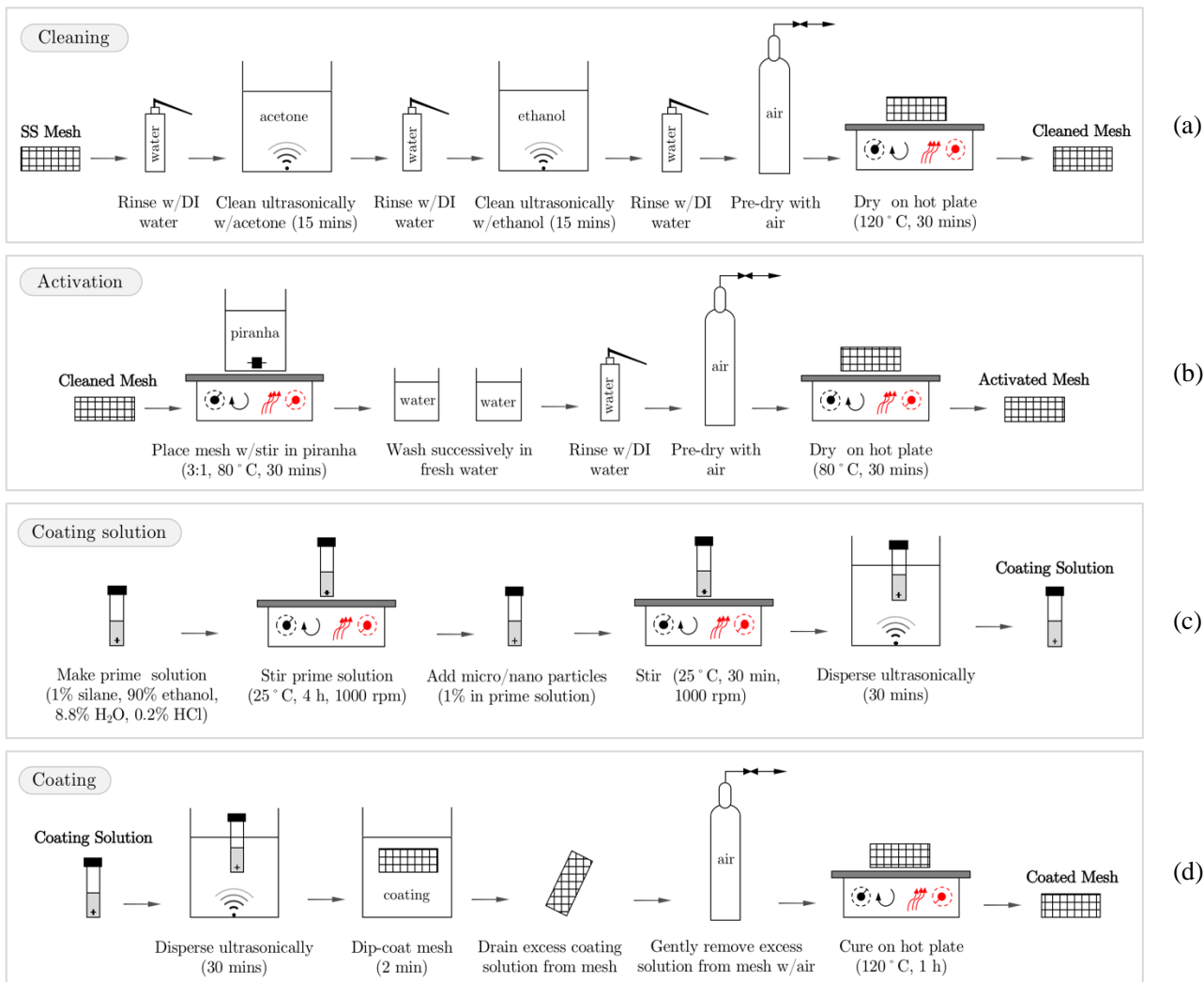


Figure 3.1. Schematics of the experimental procedures for (a) stainless steel mesh cleaning, (b) mesh activation, (c) coating solution preparation, and (d) mesh coating.

Coating solutions: Different coating solutions are prepared as depicted in Table 3.1 (c). The prime solution contains ethanol, silane, H₂O, and HCl at concentrations 90, 1, 8.8, and 0.2 wt%, respectively. The prime solution is mixed at room condition, using a magnet stirrer at 900–1200 rpm to obtain a homogeneous solution. In this study, we use two different types of silanes, namely Dynasylan[®] F8216 (long-chain), and SIVO 408 (short-chain). Other coating solutions are prepared, by adding 1% solid (MPs and NPs) to the prime solutions. For NPs and MPs, Aerosil[®] R812 (hydrophobic, 7 nm diameter) and SIPERNAT[®] D13 (hydrophobic, D₅₀ = 10.5 μm),

respectively, are utilized. After adding solids, the coating solution is mixed at 1000 rpm for 30 min, and ultrasonically dispersed for 30 min. 12 coating formulations are obtained as summarized in Table 3.1. All coatings contain 1 wt% silane in the prime solution. For the samples containing solids, the overall solid concentration (NP, MP, or both) in the prime solution is 1 wt%.

Table 3.1. Coating formulations with different silanes and solid particles.

Coating Formulation	Silane Type (Dynasylan®)	Solid Composition (wt%)	
		Aerosil® R812 (7 nm)	SIPERNAT® D13 (10.5 µm)
F1 (Prime)		0	0
F2	Dynasylan®	0	100
F3	SIVO 408	25	75
F4	(short-silane)	50	50
F5		75	25
F6		100	0
F7 (Prime)		0	0
F8	Dynasylan®	0	100
F9	F8261	25	75
F10	(long-silane)	50	50
F11		75	25
F12		100	0

Mesh coating procedure: We use dip-coating method to fabricate the SHSO mesh (see Figure 3.1 (d)). This SHSO coating technique has been employed by other researchers in oil-water separation applications [11, 15, 24, 45, 49-51]. The coating solution is ultrasonically dispersed for 30 min, and the mesh samples are dipped into the coating solution for 2 min. The excess coating solution is allowed to drain under gravity. The coating solution is carefully dried with air, and placed on the top of a heat plate to be cured at 120°C for 1 h. The curing improves the coating stability [52]. The reaction mechanism between the hydroxyl groups on activated stainless steel mesh and silane is given in a series of reactions [53], namely, hydrolysis, condensation, adsorption, and covalent bonding (grafting), as given in Figure 3.2. First the silane (Dynasylan® R8261) undergoes hydrolysis reaction in the presence of an acid (HCl in our study) to produce silanol and three moles of ethanol. Then, three silanol molecules condense, and two moles of water is produced. The

condensed silanol molecules adsorb onto the activated SS mesh surface; in this stage, hydrogen bonds form between the oxygen and hydrogen molecules on hydroxyl groups and those on the adsorbed silanol molecules. Finally, upon heating, covalent bonds are formed (grafted) between the silane and SS surface. The fluorinated functional group $[-(\text{CF}_2)_5-\text{CF}_3]$ are exposed on the surface of SS mesh, providing it with a hydrophobic property.

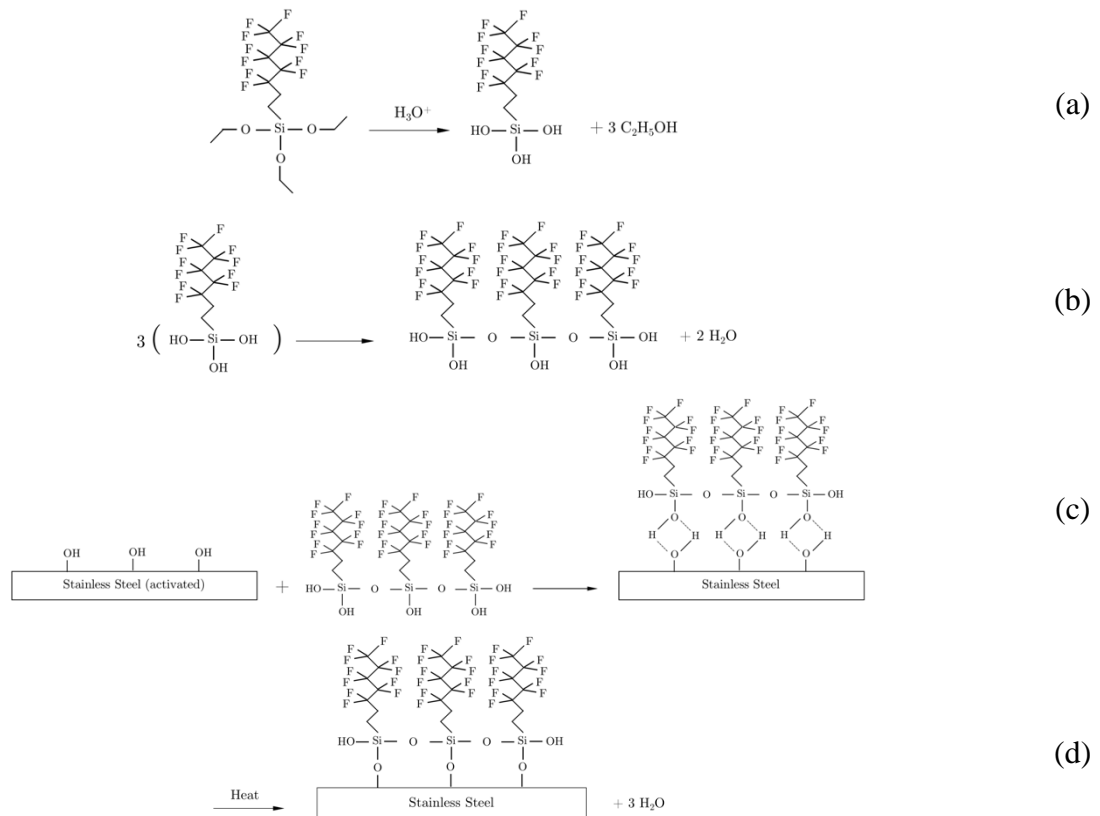


Figure 3.2. Mechanism of bonding between silane (Dynasylan® R8261) and activated stainless steel mesh (modified after Mostafaei et al. [53]). In this figure different steps are given: (a) hydrolysis, (b) condensation, (c) adsorption through hydrogen bonding, and (d) covalent bonding (or, grafting).

3.2.3. Characterizing SHSO mesh

We characterize the SHSO mesh, using static contact angle, sliding angle, stability analysis, transmission electron microscopy (TEM), scanning electron microscope (SEM), X-ray diffraction

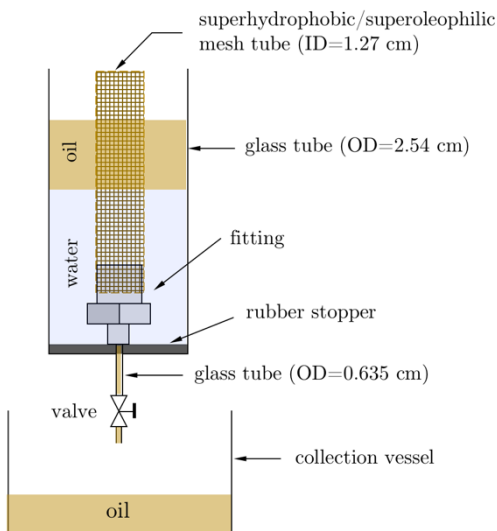
(XRD), Fourier-transform infrared spectroscopy (FTIR), energy-dispersive X-ray spectroscopy (EDX), and oil-water separation tests. Except for the static contact angle measurements, other characterization tests are conducted on the mesh samples coated with F12 (see Table 3.1). All experiments are conducted at ambient conditions. We measure WCA and OCA on dry mesh in the presence of air (OCA 15EC, DataPhysics Instruments GmbH, Germany). First, two pictures are taken from the top and front views to assure that the mesh is held straight and that the mesh openings are not stretched in any directions. Water droplets of 10 μL are dispensed, using a Hamilton[®] syringe with a 20-gauge needle. For each mesh sample, we dispense three drops on different parts of the mesh, and report the average contact angle for each mesh. Also, for each drop, the right and left contact angles are measured and the average value is reported. For the sliding angle tests, the mesh holder assembly is tilted until the droplet starts to roll-off; receiving and advancing contact angles at the sliding state are measured at 34 fps.

For the stability tests, the SHSO mesh samples (coated with F12 formulation) are aged in 0.1 M and 1 M H_2SO_4 , NaOH, and NaCl solutions for a period of up to four weeks. For each week, there are five replicated mesh samples in a sealed bottle, containing a chemical. The tests for 1 M chemicals are analyzed for one week.

The morphology and elemental analysis are characterized using FEI MLA 650FEG SEM equipped with Bruker EDX. In the SEM and EDX tests, we gold-sputter the coated mesh samples, and use a double-side carbon tape to attach them to an aluminum stub. The XRD patterns for the cleaned, silanized, and coated mesh samples (with F12) are conducted, using Rigaku Ultima-IV (40 kV and 44 mA). The scan starting angle and angle step are 30° and 0.02° , respectively. FTIR test is performed, using Tensor II spectrometer (Bruker Instruments, Karlsruhe, Germany). We scratch the cured coating gel F12 of the mesh samples, and use it for the FTIR analysis.

The oil-water separation test is conducted according to Figure 3.3. A 1.27 cm ID (1/2 inch) mesh tube is functionalized with F12 coating solution, and is employed to separate free-oil from an oil-water mixture under gravity. The mesh is supported on a Swagelok® reducer fitting and is sealed with Teflon® shrink tube and a clamp. A 0.635 cm OD (1/4 inch) tube is attached to the reducer fitting, and is passed through a rubber stopper that seals the bottom of a 2.54 cm (1 inch) glass tube. A valve is connected to the bottom of the separator. The hollow space between the tube mesh and the glass tube is filled with known amounts of kerosene and water with valve closed. Then by opening the valve, oil is drained in the coated mesh tube. By comparing weights of the initial oil and collected oil, the separation efficiency is determined.

(a)



(b)

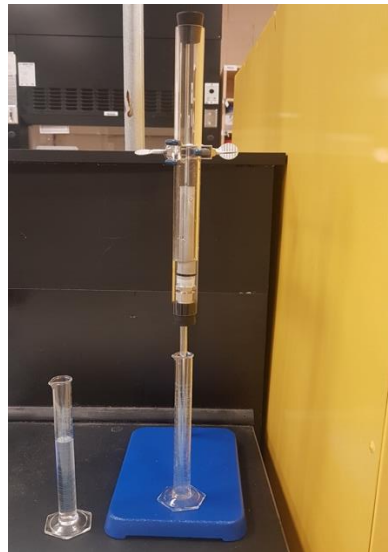


Figure 3.3. Oil-water separation experimental set up using SHSO mesh tube: (a) schematic picture, and (b) actual set up. Oil is shown in brown and water is shown in light blue color.

3.3. Results and Discussions

This section reports wettability and stability assessments through contact angle measurements, surface characterization using TEM, SEM, XRD, FTIR, and EDX as well as oil-water separation efficiency.

3.3.1. Mesh wettability analysis

The activated SS mesh samples are coated with 12 different coatings F1–F12 (see Table 3.1). In all cases, the same SS mesh material is used. The oil (hexane) perfectly wets the mesh, giving a contact angle of zero. The effects of silane chain-length and solid (NPs and MPs) composition are investigated. The results of static WCA in the presence of air are demonstrated in Figure 3.4 based on the average WCA for three drops repeated on three different mesh samples (a total of nine drops). The x-axis of Figure 3.4 shows the solid composition in the coating solution. The WCA results for the prime coatings F1 and F7 (0% NPs and 0% MPs) are also highlighted in Figure 4. The blue bars and gray bars represent the WCA results for the long-chain silane (Dynasylan[®] F8261) and the short-chain silane (Dynasylan[®] SIVO 408), respectively. $WCA=124.3^{\circ}\pm 2.8^{\circ}$ and $134.2^{\circ}\pm 1.8^{\circ}$ for the coatings with short silane (F1) and long silane (F7), respectively, are found. This observation is in agreement with findings in the literature that hydrophobicity increases with the length of the silane functional chain [54, 55]. According to Figure 3.4, with increasing the fraction of the NPs in the coating within the range 0–75 wt%, the WCA increases. At the same level of wt%, the surface covered by the NPs (m^2 rough area/ m^2 smooth area) is expected to be higher in the case of NPs. The hierarchical roughness pores can trap air to promote the condition for superhydrophobicity [24]. The increase in the WCA with the percentage of NPs (in the solid part) is more pronounced in the case of long-chain silane. For the short silane, the difference in the WCA within the range of NPs 0–50 wt% is statistically insignificant. There is a maximum WCA

at the solid composition of 75% NPs and 25% MPs (see Figure 3.4). In all coatings that include solid, there is 1 wt% solid in the prime solution. At 75% NPs and 25% MPs solid composition, the WCA on the coating containing the short silane (F5) is $164.2^{\circ} \pm 2.2^{\circ}$ and that on the long silane (F11) is $165.8^{\circ} \pm 2.0^{\circ}$. By conducting a statistical t-test, it appears that the difference between the maximum contact angle achieved in long- and short-chain silanes (at 75% NPs and 25% MPs) is not statistically significant at 95% confidence level.

By increasing the NPs contribution in the solid to 100%, the contact angle on the coating with short silane (F6) decreases considerably, to $155.5^{\circ} \pm 2.2^{\circ}$, and that for the long silane (F12) decreases slightly, to $163.8^{\circ} \pm 1.8^{\circ}$. Therefore, among the solid concentration levels tested, the case containing 75% NPs and 25% MPs provides the highest hydrophobicity. Similarly, we conduct a t-test analysis at 95% confidence level on differences between the means of the two populations (for both silanes), to assess whether the optimality in the WCA on the coating with 75% NPs and 25% MPs is statistically different from that with 100% NPs only. Although the WCA difference is statistically significant (at 95% confidence) for the case of short-chain silane, it is not significant for the case of the long-chain silane. One problem in using a mixture of MPs and NPs in the dip-coating method is the likelihood of gravity settling for the larger particles. This may bring the concern with the coating homogeneity in terms of the solid particles on the mesh surface. Therefore, we use the coating solution F12 (with only NPs) for the remaining of analysis to achieve a more homogeneous coating [56]; the long-chain silane also provides a slightly better hydrophobicity for which the difference between the WCAs on the coatings F11 (75% NPs) and F12 (100% NPs) is not statistically significant.

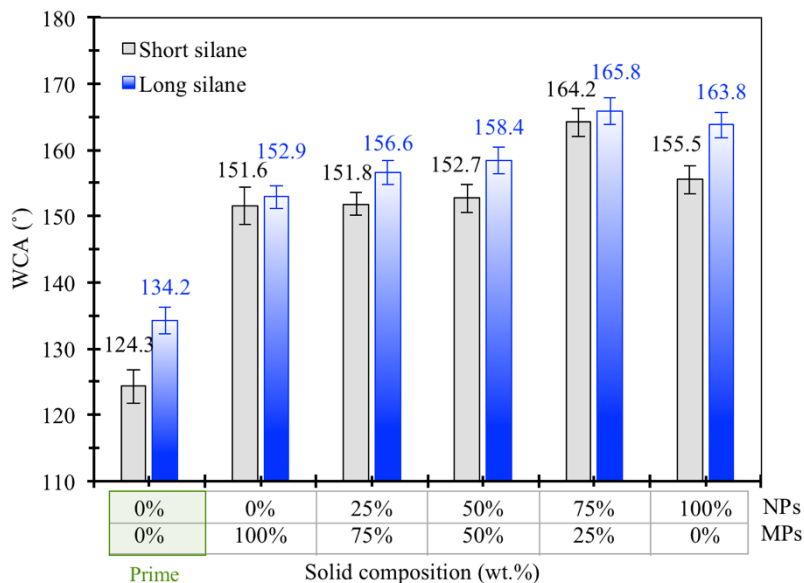


Figure 3.4. Static WCA on coated stainless steel mesh in the presence of air at ambient condition. The wt% of the NPs and MPs in the solid are given in the x-axis. The contact angle results are averaged for three replicates.

The results for the sliding angle measurements are shown in Figure 3.5. Right before water droplet sliding (see Figure 3.5 (a)), the advancing and receding contact angles are measured at $155.9^{\circ} \pm 3.3^{\circ}$ and $148.1^{\circ} \pm 3.0^{\circ}$, respectively. Therefore, contact angle hysteresis at the sliding condition is $7.7^{\circ} \pm 0.8^{\circ}$ which satisfies the condition $< 10^{\circ}$ for the hydrophobic surfaces [48].

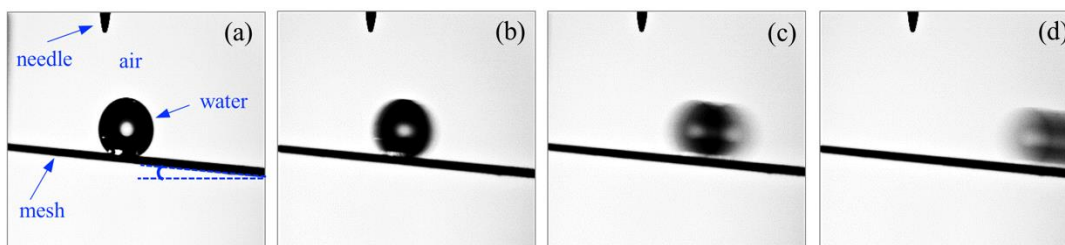


Figure 3.5. Snapshot of the water droplet starting to slide on an SHSO mesh (coated with F12) by increasing the inclination angle. The sliding starts in the frame (b).

3.3.2. Surface characterization analysis

Transmission electron microscopy (TEM): In this subsection, we present the TEM results from the NPs, MPs, and a 3:1 mixture of NPs to MPs (corresponding to 75 wt% NPs and 25 wt% MPs) as shown in Figure 3. 6. A 5 wt% solution of solids in ethanol is prepared, following by 10 mins sonication for sample preparation. The TEM pictures are taken using Secnai™ Spirit TEM (FEI Company), using field emission electron of 80 kV, equipped with 4 Mega pixel AMG digital camera. The pictures demonstrate the morphology of the aggregates in Figure 3. 6 for (a) NPs (alone), (b) MPs (alone), and (c) a 3:1 mixture of NPs and MPs (corresponding to 75% NPs in the solid compartment).

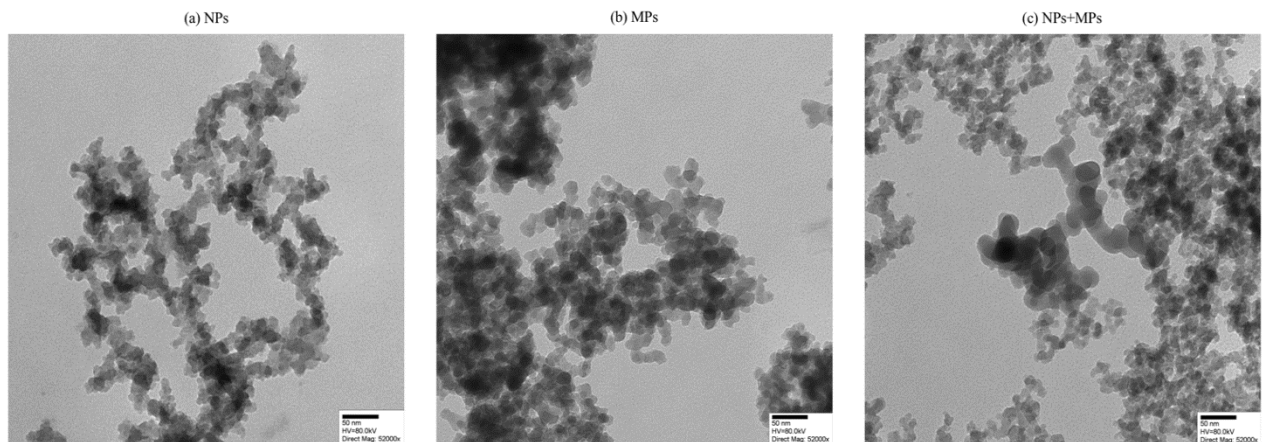


Figure 3. 6. Transmission electron microscopy (TEM) pictures from solids used in the coating solution: (a) NPs (Aerosil® R812), (b) MPs (SIPERNAT® D13), and (c) mixture of NPs+MPs.

Scanning electron microscopy (SEM): We use SEM to visualize the morphology of the SHSO mesh membranes, coated with long-chain silane and a mixture of NPs and MPs. In Figure 3.7, the SEM pictures are shown for four characteristic coating solutions at 1,000X magnification; the bar scale is 100 (μm). The SEM picture in Figure 3.7 (a) is for the SHSO mesh coated with the prime solution F7 (without any solids for roughness). Figure 3.7 (b) depicts the SEM picture for the mesh

with coating solution F8, containing 100% MPs in the solid part. Figure 7(c) includes the SEM picture for the coating solution F11 where the solid mixture contains 75% NPs and 25% MPs. As observed in Figure 3.4, the coating shown in Figure 3.7 (c) gives the maximum WCA. The SEM picture for the mesh coated with solution F12, containing 100% NPs, is given in Figure 7(d). Among the four coating characteristic solutions, the coating solution F12 with 100% NPs provides flower-like hierarchical surface roughness with an extended surface area (see Figure 3.7). Referring to Figure 3.7 (d), the fractures, which are observed within this flower-like surface roughness, have occurred during the drying and curing processes. The fractures provide regions of high capillary pressure for the oil (as the wetting phase), which are suitable for capturing smaller oil droplets from water when they are brought in contact with these high capillary regions. However, such a hierarchical surface roughness may cause membrane vulnerability to the fluids shear and impact by the solid contaminations in the liquid. As clear from Figure 3.7 (b), the coating solution F8 with only MPs in the solid mixture does not uniformly cover the entire surface of the mesh material as some parts of the mesh are not covered with the rough solids. However, with additional surface roughness caused by the MPs, the WCA is increased from $134.2^{\circ} \pm 1.8^{\circ}$ (F7) to $152.9^{\circ} \pm 1.8^{\circ}$ (F8); the difference is statistically significant at a 95% confidence level. This increased contact angle with the added roughness is expected [50]. Moreover, Figure 3.7 (c) reveals that the coating solution F11 with 75% NPs and 25% MPs provides more roughness on the surface, compared to Figure 3.7 (b). According to Figure 3.4, a statistically significant increase in the WCA values are observed because of the hierarchical roughness induced by the mixture of MPs and NPs in the coating. The WCA for the mesh shown in Figure 3.7 (b) increases from $152.9^{\circ} \pm 1.8^{\circ}$ to $165.8^{\circ} \pm 2.0^{\circ}$ for the mesh corresponding to Figure 3.7 (c).

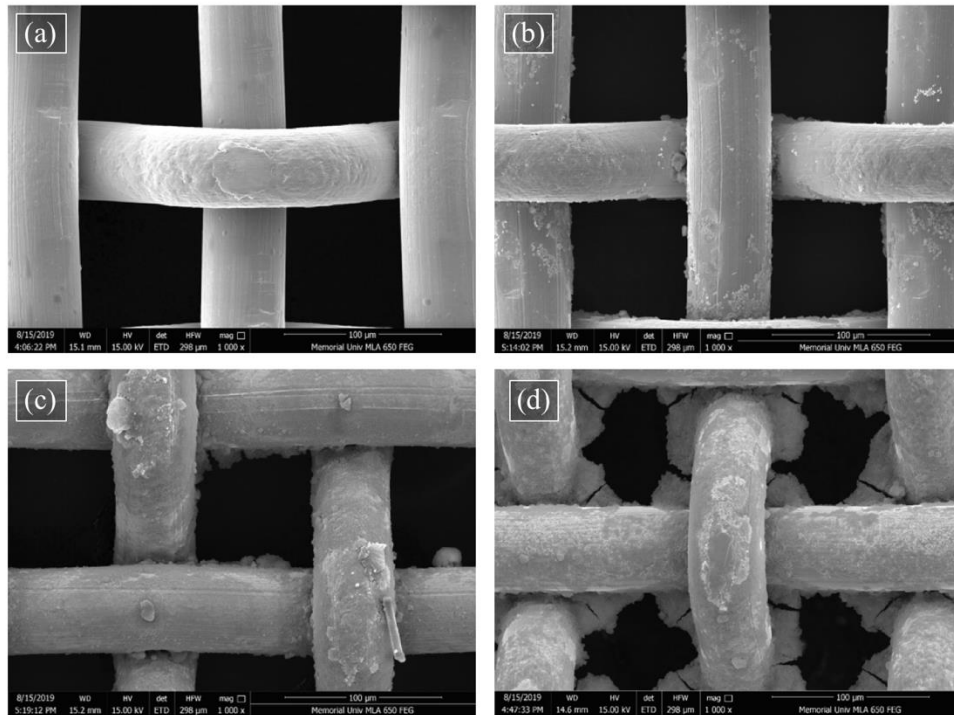


Figure 3.7. Scan electron microscopy of four SHSO mesh samples at 1,000X magnification: (a) silanized (F7), (b) F8 coating with 100% MPs, (c) F11 coating with 75% NPs and 25% MPs, and (d) F12 coating with 100% NPs. The long-chain silane is used in all coatings. The nominal size of the mesh opening is 75 μm .

Comparing Figure 3.7 (c) and 5(d), the flower-like roughness features are only observed for the coating, containing only NPs as solids (see Figure 3.7 (d)). A better mechanical stability (against shear and impact) is expected from the coating solution F11 compared to F12; spray coating is expected to be a better option when coating the activated mesh with F11. Despite the significant differences in the apparent surface roughness features in Figure 3.7 (c) and (d), the difference in the WCA for these two mesh samples is not statistically significant at a 95% confidence level; however, the roughness shown in Figure 3.7 (d) can facilitate the separation of disperse oil-in-water droplets.

In Figure 3.8, we demonstrate approximate size analysis of the flower-like surface roughness for a given part of the mesh sample with eight mesh openings, coated with F12 solution. For

comparison, we also show the 200 μm scale bar. This SEM picture is obtained at the 500X magnification level. We fit a circle to the mesh pore opening without considering the coating, which is shown with dashed yellow circles (see Figure 3.8). For each mesh opening, another circle is also indicated with solid white color that is fitted to the available pore opening at the condition corresponding to the breakthrough of the non-wetting phase. Figure 3.8 depicts (approximate) uncoated mesh opening diameter of 75.4 μm – 77.7 μm with an average of (76.4 \pm 0.6) μm that is reduced to 45.5 μm – 50.5 μm for the coated mesh, with an average diameter of (48.3 \pm 1.7) μm .

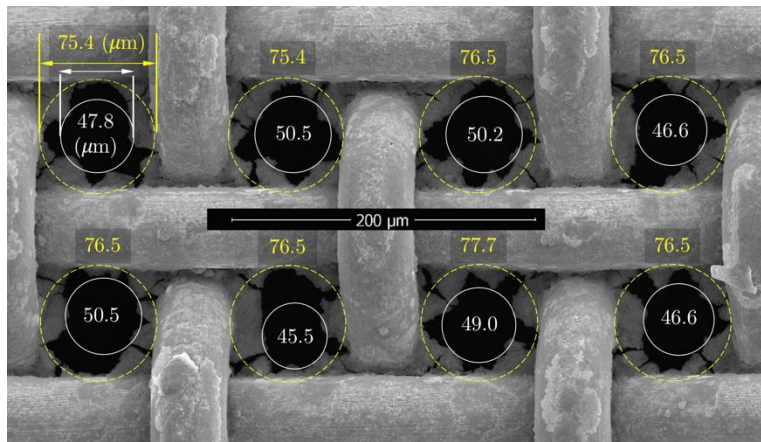


Figure 3.8. A schematic of the flower-like roughness features of the SHSO mesh (coated with F12). The dashed yellow circles are approximately fitted to the mesh opening, and the white circles are fitted to the pore opening, corresponding to the breakthrough condition for the non-wetting phase. The numbers in the figure show diameter in μm .

X-ray diffraction (XRD): Figure 3.9 shows an overlay of the XRD patterns for three cases, including cleaned mesh, silanized mesh (coating solution F7), and coated mesh (coating solution F12). The main diffraction peaks are located at 43.4°, 44.7°, 50.9°, and 74.7° which can be attributed to γ (111), α (110), γ (200), and γ (220), respectively; furthermore, there are two minor peaks at 64.9° and 82.4° that can be attributed to α (200) and α (211) [57]. The location of the diffraction peaks are in agreement with those obtained in XRD spectrum of AISI 316 grade SS plate from Qin et al. [57]. As it is clear in Figure 9, the silane solution F7 and the coating solution

F12 do not shift the position of diffraction peak while there are some minor effects on the intensity of peaks. Hence, these coating solutions do not affect the crystalline structure of the AISI 316 SS. There are not distinct differences between the locations, and intensities of the peaks, especially for the clean and coated mesh samples. These similarities confirm the amorphous structure of the mesh coating. In the coating solution F12, the used silica nanoparticles of Aerosil® R812, which are amorphous, does not affect the crystallinity of the bare mesh.

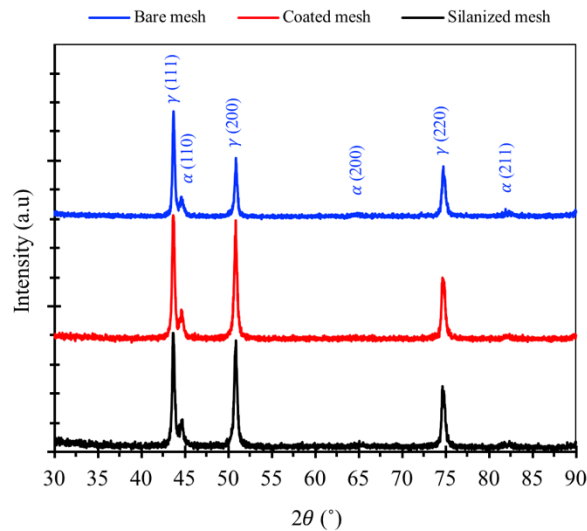


Figure 3.9. Overlay of XRD patterns for the clean mesh (blue), silanized mesh (red), and mesh coated with F12 (black); γ and α are austenite and martensite steel phases, respectively.

Energy-dispersive X-ray spectroscopy (EDX): In Figure 3.10, we show the EDX analysis of the mesh coated with F12 formulation. The weight percent of the elements and standard deviation (σ) are also reported in Figure 10; the highest detected element counts and X-ray energy belongs to Si with 56.11 wt% of the detected sample area at an energy level of 1.74 keV. For the EDX analysis, we choose an area-of-interest on the coated mesh wires and dismiss the mesh empty area that has no coating. The wt% of Si in the long-chain silane is less than 3 wt%. The NPs are fumed silica (SiO_2) for which their surface area is functionalized with hexamethyldisilazane (HMDS). The

ratio of Si/F in the coating is much higher than that in the silane, confirming that the NPs are successfully bonded onto the mesh surface.

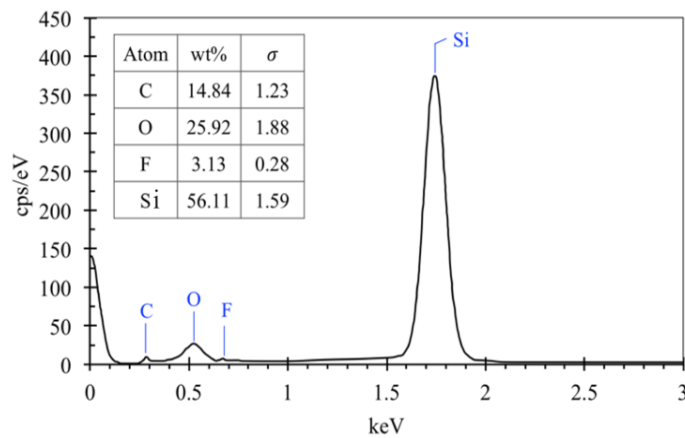


Figure 3.10. EDX analysis of the SHSO mesh coating (F12).

Fourier-transform infrared spectroscopy (FTIR): The FTIR transmittance for the SHSO mesh coated with F12 solution is demonstrated in Figure 3.11 in the wavelength range 400 cm^{-1} to 4000 cm^{-1} . A large band with a strong peak is observed at 452 cm^{-1} , which is due to Si-O-Si rocking [58]. The absorption band at 807 cm^{-1} corresponds to the Si-O-Si bending; the O-Si-O bending gives an IR peak at about 475 cm^{-1} [59]. The strong absorption at 1060 cm^{-1} is due to the stretching of the Si-O-Si bond [60]. These three intense absorption peaks at 452 , 807 , and 1060 cm^{-1} are due to the silica NPs on the coated mesh surface. The peak around 700 cm^{-1} is due to the vibration of the $-\text{CH}_2$ groups for the silane-modified silica NPs, and the absorption peak at 895 corresponds to the deformation of Si-OH bonds [61]. Furthermore, the peaks at 1240 cm^{-1} and 1150 cm^{-1} are attributed to the C-F asymmetric stretching vibrations for the $-\text{CF}_2-$ and $-\text{CF}_3$ groups, respectively [62]. The peak at 1190 cm^{-1} may be assigned to the symmetrical stretching of the CF-F bonds [63]. The absorption peak for the stretching of bond Si- CH_3 (in NPs) is not observed at $\sim 1297\text{ cm}^{-1}$ (detected in the FTIR spectra of the NPs) [60], implying that the NPs are completely hydrolyzed in the final coating. The broad (but weak) absorption band in the range $2890\text{--}3680\text{ cm}^{-1}$ is a

characteristic of the O-H stretching from water vapor [64]; the weak band around 1482 cm^{-1} is also attributed to the adsorbed water [61].

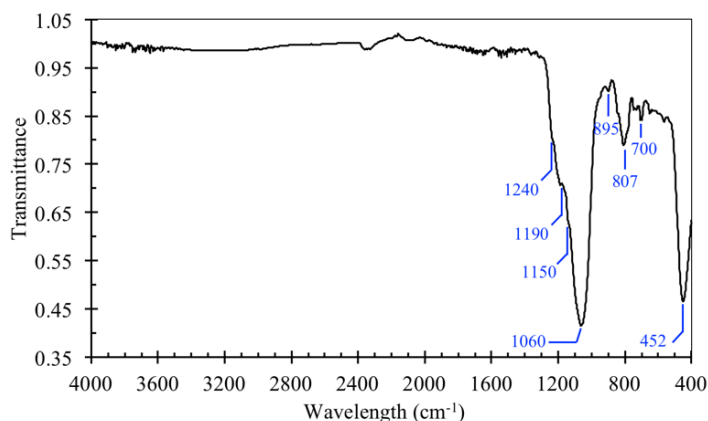


Figure 3.11. FTIR spectra of the SHSO mesh (coated with F12) in wavelength range 400 to 4000 cm^{-1} .

3.3.3. Mesh chemical stability analysis

The stability of the SHSO mesh against chemicals can be assessed by WCA measurements, after aging the coated mesh in harsh environments. The static contact angle results for the SS mesh coated with the solution F12 are provided in Figure 3.12 for which the samples are aged over a 4-week period in 0.1 M acid (H_2SO_4), 0.1 M alkaline (NaOH), and 1 M brine (NaCl) solutions. The contact angle measurements reported in Figure 3.12 are the average of five replicates (mesh samples); onto each mesh sample, we dispense three drops. Prior to aging in acid, alkaline, and brine solutions, the $\text{WCA}=163.8^\circ\pm 1.8^\circ$. After one week, the WCA is not significantly affected for the sample aged in 1 M NaCl solution; however, the WCA is dropped to $153.9^\circ\pm 1.8^\circ$ for 0.1 M H_2SO_4 -aged mesh and to $154.4^\circ\pm 0.8^\circ$ for 0.1 M NaOH -aged mesh sample. There is not an appreciable surface wetness change from the acid after this early effect on the coating. For instance, the WCA after four weeks is marginally reduced to $151.6^\circ\pm 1.2^\circ$, considering the variability in the measurements. The WCA for the mesh samples aged in the brine slightly

decreases over time (e.g., the contact angle for the brine-aged mesh is $159.2^{\circ} \pm 0.8^{\circ}$ after four weeks). The effect of alkaline solution on the mesh coating is the most significant such that $WCA=145.9^{\circ} \pm 1.7^{\circ}$ after four weeks of aging. In agreement with the literature [65], the hydrophobicity of the silica-based surfaces declines in strong alkaline solutions due to its effect on the Si-O-Si bonding.

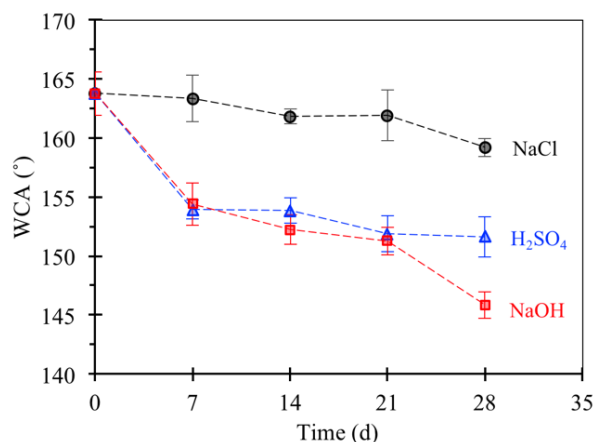


Figure 3.12. Chemical stability analysis through WCA measurements. The SHSO mesh samples are aged at room temperature in H₂SO₄ (0.1 M, shown in blue), NaOH (0.1 M, shown in red), and brine (1 M, shown in black) solutions over four weeks. The markers indicate the average of contact angle values for five replicates.

We also examine the chemical stability analysis in extremely concentrated acid and alkaline solutions where the concentration is 1 M. Similar to the chemical stability tests using 0.1 M chemicals, five replication samples of the mesh are considered where three water droplets are placed on each mesh (on different locations). A significant effect by 1 M NaOH solution on the mesh coating is observed; after one week, the WCA drops to $93.4^{\circ} \pm 6.2^{\circ}$. Not only the contact angle is considerably altered by the 1 M alkaline solution, the variability in the WCA measurements is also drastically increased. If the water-mesh contact is influenced by concentrated NaOH solution, a loss of hydrophobicity is observed, resulting in WCA reduction. We observe a high standard deviation of $S=10.9^{\circ}$ for the mesh samples aged for one week in 1 M NaOH solution, which is

significantly higher than $S < 1^\circ$ attained for the samples aged in 0.1 M NaOH solution (after one week). When the mesh samples are placed in 1 M H_2SO_4 solution, the strong acid does not affect the mesh coating; after 1-week aging, $WCA = 152.5^\circ \pm 1.0^\circ$ is observed. The standard deviation for the mesh samples aged in 1 M acid solution is one order of magnitude lower. Therefore, the mesh coating is not significantly influenced by highly concentrated acid. The difference in the chemical stability of the SHSO mesh against 1 M acid and 1 M alkaline solutions is also confirmed by the SEM pictures, as depicted in Figure 3.13.

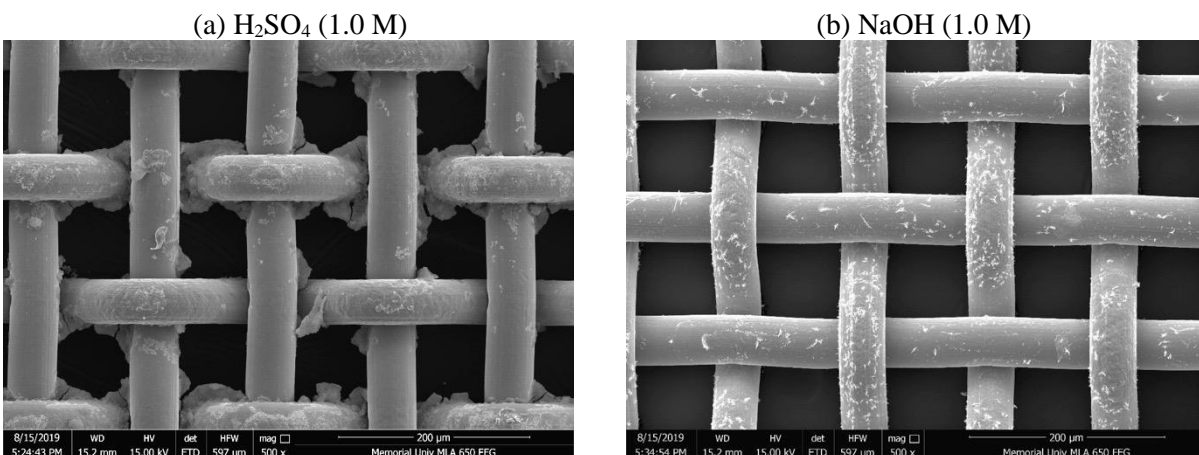


Figure 3.13. Scanning electron microscopy pictures (at 500X magnification) of the SHSO mesh exposed to: (a) 1.0 M H_2SO_4 , and (b) 1.0 M NaOH for one week.

The SEM images shown in Figure 3.13 are obtained at 500X magnification, and the scale bar is 200 μm . There are some differences between the flower-like roughness features (compared to those in Figure 3.7 (d)), due to handling and reaction with concentrated acid solution. Although the change in surface roughness affects the capillary pressure for the retention of the wetting phase (oil), it does not considerably alter the contact angle. On the contrary, the mesh sample aged in 1 M NaOH solution experiences significant dissolution of the coating in strong alkaline solution (see Figure 3.13 (b)), which is in agreement with the WCA measurements.

For strong alkaline solutions ($\text{pH} > 13$), the OH^- ion can react with silica aggregates with poor crystallinity [66]. For our coating, such a potential is possible for the micro-nanoparticle aggregates of amorphous silica. Also the OH^- ions in strong alkaline solution can attack the Si-O-Si bonds that connect adjacent silane groups, weakening the 3D network of silane functional groups. Moreover, the OH^- ions can remove the fluorinated functional groups from mesh surface by breaking the Si-O bonds that are attached to the mesh surface (see Figure 3.2), causing partial de-hydrolysis [66]. As a result of these reactions between silica and a strong alkali, the coated mesh loses its superhydrophobicity strength.

3.3.4. Oil-water separation test

The oil-water separation is conducted according to the process flow diagram shown in Figure 3.3 (a). The actual picture of the set-up is given in Figure 3.3 (b). Kerosene is used to simulate the oil phase that permeates through the fabricated tube mesh. The water phase is expected to be blocked from permeating through the SHSO membrane at pressures lower than the breakthrough capillary pressure of the water phase. As soon as the water wets the mesh tube, it starts draining out of the glass tube through the mesh. The oil is collected in the beaker with an excellent separation efficiency $> 99\%$, whereas the water is blocked around the tube mesh. The permeation of the water into the mesh under gravity drainage is not observed. In the separation tests, we repeat the experiments with kerosene four times, and the separation efficiency is $(99.0 \pm 0.6)\%$ in a period of 1 min. In a follow up study, we are systematically investigating the dynamics of oil-water separation in the same mesh shown in Figure 3.3 (b), where the effects of flow rate, oil-to-water ratio, and oil dispersion are assessed. We also use the effect of vacuum on the permeate phase to accelerate the oil permeation. For the case of kerosene, the gravity-based separation is fast;

however, for more viscose oils (crude oil or vegetable oil), the oil permeation rate through membrane will dictate the size of separation unit.

3.4. Conclusions

We fabricate a superhydrophobic-superoleophilic (SHSO) stainless steel mesh-based membrane through a facile dip-coating technique, and use the membrane for oil-water separation application. The effect of silane alkyl-chain length by using a short-chain silane (Dynasylan[®] Sivo 408), and a long-chain silane (Dynasylan[®] F8261) on the water contact angle (WCA) is studied. We also investigate the influence of solid composition in the coating (1 wt% solid in liquid coating solution) with hydrophobic nanoparticles (NPs, Aerosil[®] R812) and microparticles (MPs, SIPERNAT[®] D13) on the wetness characteristic of the mesh. A total number of 12 coating formulations are tested by varying the silane and solid composition. The following conclusions are drawn based on the research results:

- The WCA results show that at all solid compositions, the long silane generates a more hydrophobic surface than the short silane.
- A maximum in the WCA is observed with both silanes for a solid mixture, containing 75 wt% NPs and 25 wt% MPs. The maximum WCA for the long silane is $165.8^{\circ} \pm 2.0^{\circ}$, which is not statistically different from that for the short silane. By increasing the contribution of the NPs to 100%, the WCA decreases for both silanes; however, this reduction is more significant for the short silane. Therefore, it is possible to achieve a similar hydrophobicity with a shorter silane that contains less F atoms (less harmful) by adjusting the composition of the solid part of the coating.

- According to the SEM images, flower-like hierarchical micro- and nano-roughness with a high capillary pressure for the coating solution that contains only NPs (1 wt% in the coating) is attained.
- The 4-week stability tests exhibit an excellent chemical resistance of the SHSO mesh to H₂SO₄ (0.1 and 1 M), NaCl (1 M), and NaOH (0.1 M), where WCA>145° after four weeks. The alkaline solution affects the coating more; the majority of the changes to the hydrophobicity occurs during the first week in all cases. However, loss of hydrophobicity is observed after 1-week exposure to 1 M NaOH.
- The as-fabricated SHSO mesh separates kerosene from an oil-water mixture with an efficiency of greater than 99%.
- The proposed fabrication of the SHSO mesh is simple, facile, low-cost, and effective that has applications in selective oil-water separation.

Acknowledgements

The financial assistance from the Natural Sciences and Engineering Research Council of Canada (NSERC), InnovateNL, Equinor Canada, Terra Nova Young Innovator Award, and Memorial University are appreciated. The authors thank Evonik Industries AG for providing fumed silica and silane samples. We also acknowledge the help from Dr. Yahui Zhang and Mr. Rene Silva for conducting FTIR tests.

Nomenclatures

Acronyms

DI	Deionized
DMS	Dimethylsiloxane

EDX	Energy-dispersive X-ray spectroscopy
FTIR	Fourier-transform infrared spectroscopy
ID	Inner diameter
MPs	Microparticles
NPs	Nanoparticles
OD	Outer diameter
PDA	Polydopamine
PDMS	Polydimethylsiloxane
PFAS	Perfluoroalkylsilane
PFTOS	Perfluorooctyltriethoxysilane
PTFE	Polytetrafluoroethylene
SEM	Scanning electron microscope
SHSO	Superhydrophobic and superoleophilic
SS	Stainless steel
WCA	Water contact angle
XRD	X-ray diffraction

References

1. Wang, Q.; Cui, Z.; Xiao, Y.; Chen, Q., *Stable highly hydrophobic and oleophilic meshes for oil–water separation*. 2007; Vol. 253, p 9054-9060.
2. Du, Z.; Ding, P.; Tai, X.; Pan, Z.; Yang, H., *Facile Preparation of Ag-Coated Superhydrophobic/Superoleophilic Mesh for Efficient Oil/Water Separation with Excellent Corrosion Resistance*. *Langmuir* 2018, 34 (23), 6922-6929.

3. Varshney, P.; Nanda, D.; Satapathy, M.; Mohapatra, S. S.; Kumar, A., A facile modification of steel mesh for oil–water separation. *New Journal of Chemistry* 2017, 41 (15), 7463-7471.
4. Feng, L.; Zhang, Z.; Mai, Z.; Ma, Y.; Liu, B.; Jiang, L.; Zhu, D., A super-hydrophobic and super-oleophilic coating mesh film for the separation of oil and water. *Angew Chem Int Ed Engl* 2004, 43 (15), 2012-4.
5. Li, H.; Zheng, M.; Ma, L.; Zhu, C.; Lu, S., Two-dimensional ZnO nanoflakes coated mesh for the separation of water and oil. *Materials Research Bulletin* 2013, 48 (1), 25-29.
6. Liu, Y.; Zhang, K.; Yao, W.; Liu, J.; Han, Z.; Ren, L., Bioinspired structured superhydrophobic and superoleophilic stainless steel mesh for efficient oil-water separation. *Colloids and Surfaces A: Physicochemical and Engineering Aspects* 2016, 500, 54-63.
7. Xiang, M.; Jiang, M.; Zhang, Y.; Liu, Y.; Shen, F.; Yang, G.; He, Y.; Wang, L.; Zhang, X.; Deng, S., Fabrication of a novel superhydrophobic and superoleophilic surface by one-step electrodeposition method for continuous oil/water separation. *Applied Surface Science* 2018, 434, 1015-1020.
8. Matin, A.; Baig, U.; Gondal, M. A.; Akhtar, S.; Zubair, S. M., Superhydrophobic and superoleophilic surfaces prepared by spray-coating of facile synthesized Cerium(IV) oxide nanoparticles for efficient oil/water separation. *Applied Surface Science* 2018, 462, 95-104.
9. Cao, W.-T.; Liu, Y.-J.; Ma, M.-G.; Zhu, J.-F., Facile preparation of robust and superhydrophobic materials for self-cleaning and oil/water separation. *Colloids and Surfaces A: Physicochemical and Engineering Aspects* 2017, 529, 18-25.

10. Matin, A.; Baig, U.; Gondal, M. A.; Akhtar, S.; Zubair, S. M., Facile fabrication of superhydrophobic/superoleophilic microporous membranes by spray-coating ytterbium oxide particles for efficient oil-water separation. *Journal of Membrane Science* 2018, *548*, 390-397.
11. Yang, H.; Zhang, X.; Cai, Z.-Q.; Pi, P.; Zheng, D.; Wen, X.; Cheng, J.; Yang, Z.-r., Functional silica film on stainless steel mesh with tunable wettability. *Surface and Coatings Technology* 2011, *205* (23), 5387-5393.
12. Zhang, Y.; Wang, X.; Wang, C.; Liu, J.; Zhai, H.; Liu, B.; Zhao, X.; Fang, D., Facile fabrication of zinc oxide coated superhydrophobic and superoleophilic meshes for efficient oil/water separation. *RSC Advances* 2018, *8* (61), 35150-35156.
13. Yang, J.; Tang, Y.; Xu, J.; Chen, B.; Tang, H.; Li, C., Durable superhydrophobic/superoleophilic epoxy/attapulgite nanocomposite coatings for oil/water separation. *Surface and Coatings Technology* 2015, *272*, 285-290.
14. Qin, F.; Yu, Z.; Fang, X.; Liu, X.; Sun, X., A novel composite coating mesh film for oil-water separation. *Frontiers of Chemical Engineering in China* 2009, *3* (1), 112-118.
15. Wang, C.-F.; Tzeng, F.-S.; Chen, H.-G.; Chang, C.-J., Ultraviolet-Durable Superhydrophobic Zinc Oxide-Coated Mesh Films for Surface and Underwater–Oil Capture and Transportation. *Langmuir* 2012, *28* (26), 10015-10019.
16. Xiao, C.; Si, L.; Liu, Y.; Guan, G.; Wu, D.; Wang, Z.; Hao, X., Ultrastable coaxial cable-like superhydrophobic mesh with self-adaption effect: facile synthesis and oil/water separation application. *Journal of Materials Chemistry A* 2016, *4* (21), 8080-8090.
17. Wu, J.; Chen, J.; Qasim, K.; Xia, J.; Lei, W.; Wang, B.-p., A hierarchical mesh film with superhydrophobic and superoleophilic properties for oil and water separation. *Journal of Chemical Technology & Biotechnology* 2012, *87* (3), 427-430.

18. Lee, C.; Baik, S., Vertically-aligned carbon nano-tube membrane filters with superhydrophobicity and superoleophilicity. *Carbon* 2010, *48* (8), 2192-2197.
19. Lee, C. H.; Johnson, N.; Drelich, J.; Yap, Y. K., The performance of superhydrophobic and superoleophilic carbon nanotube meshes in water–oil filtration. *Carbon* 2011, *49* (2), 669-676.
20. Crick, C. R.; Gibbins, J. A.; Parkin, I. P., Superhydrophobic polymer-coated copper-mesh; membranes for highly efficient oil–water separation. *Journal of Materials Chemistry A* 2013, *1* (19), 5943-5948.
21. Feng, L.; Zhang, Z.; Mai, Z.; Ma, Y.; Liu, B.; Jiang, L.; Zhu, D., A Super-Hydrophobic and Super-Oleophilic Coating Mesh Film for the Separation of Oil and Water. *Angewandte Chemie* 2004, *116* (15), 2046-2048.
22. Ju, J.; Wang, T.; Wang, Q., A facile approach in fabricating superhydrophobic and superoleophilic poly (vinylidene fluoride) membranes for efficient water–oil separation. *Journal of Applied Polymer Science* 2015, *132* (24).
23. La, D.-D.; Nguyen, T. A.; Lee, S.; Kim, J. W.; Kim, Y. S., A stable superhydrophobic and superoleophilic Cu mesh based on copper hydroxide nanoneedle arrays. *Applied Surface Science* 2011, *257* (13), 5705-5710.
24. Pi, P.; Hou, K.; Zhou, C.; Li, G.; Wen, X.; Xu, S.; Cheng, J.; Wang, S., Superhydrophobic Cu₂S@Cu₂O film on copper surface fabricated by a facile chemical bath deposition method and its application in oil-water separation. *Applied Surface Science* 2017, *396*, 566-573.
25. Yu, L.; Zhang, S.; Zhang, M.; Chen, J., Superhydrophobicity construction with dye-sensitised TiO₂ on fabric surface for both oil/water separation and water bulk contaminants purification. *Applied Surface Science* 2017, *425*, 46-55.

26. Xue, C.-H.; Ji, P.-T.; Zhang, P.; Li, Y.-R.; Jia, S.-T., Fabrication of superhydrophobic and superoleophilic textiles for oil–water separation. *Applied Surface Science* 2013, 284, 464-471.
27. Zhang, X.; Geng, T.; Guo, Y.; Zhang, Z.; Zhang, P., Facile fabrication of stable superhydrophobic SiO₂/polystyrene coating and separation of liquids with different surface tension. *Chemical Engineering Journal* 2013, 231, 414-419.
28. Liu, H.; Huang, J.; Chen, Z.; Chen, G.; Zhang, K.-Q.; Al-Deyab, S. S.; Lai, Y., Robust translucent superhydrophobic PDMS/PMMA film by facile one-step spray for self-cleaning and efficient emulsion separation. *Chemical Engineering Journal* 2017, 330, 26-35.
29. Chakradhar, R. P. S.; Kumar, V. D.; Rao, J. L.; Basu, B. J., Fabrication of superhydrophobic surfaces based on ZnO–PDMS nanocomposite coatings and study of its wetting behaviour. *Applied Surface Science* 2011, 257 (20), 8569-8575.
30. Zhang, M.; Wang, C.; Wang, S.; Li, J., Fabrication of superhydrophobic cotton textiles for water–oil separation based on drop-coating route. *Carbohydrate polymers* 2013, 97 (1), 59-64.
31. Cao, M.; Luo, X.; Ren, H.; Feng, J., Hot water-repellent and mechanically durable superhydrophobic mesh for oil/water separation. *Journal of Colloid and Interface Science* 2018, 512, 567-574.
32. Wang, S.; Li, M.; Lu, Q., Filter Paper with Selective Absorption and Separation of Liquids that Differ in Surface Tension. *ACS Applied Materials & Interfaces* 2010, 2 (3), 677-683.
33. Qing, W.; Shi, X.; Deng, Y.; Zhang, W.; Wang, J.; Tang, C. Y., Robust superhydrophobic-superoleophilic polytetrafluoroethylene nanofibrous membrane for oil/water separation. *Journal of Membrane Science* 2017, 540, 354-361.

34. Shang, Y.; Si, Y.; Raza, A.; Yang, L.; Mao, X.; Ding, B.; Yu, J., An in situ polymerization approach for the synthesis of superhydrophobic and superoleophilic nanofibrous membranes for oil–water separation. *Nanoscale* 2012, 4 (24), 7847-7854.
35. Zhang, W.; Lu, X.; Xin, Z.; Zhou, C., A self-cleaning polybenzoxazine/TiO₂ surface with superhydrophobicity and superoleophilicity for oil/water separation. *Nanoscale* 2015, 7 (46), 19476-19483.
36. Yu, T.; Lu, S.; Xu, W.; Boukherroub, R., Preparation of superhydrophobic/superoleophilic copper coated titanium mesh with excellent ice-phobic and water-oil separation performance. *Applied Surface Science* 2019, 476, 353-362.
37. Wei, C.; Dai, F.; Lin, L.; An, Z.; He, Y.; Chen, X.; Chen, L.; Zhao, Y., Simplified and robust adhesive-free superhydrophobic SiO₂-decorated PVDF membranes for efficient oil/water separation. *Journal of Membrane Science* 2018, 555, 220-228.
38. Mi, H.-Y.; Jing, X.; Xie, H.; Huang, H.-X.; Turng, L.-S., Magnetically driven superhydrophobic silica sponge decorated with hierarchical cobalt nanoparticles for selective oil absorption and oil/water separation. *Chemical Engineering Journal* 2018, 337, 541-551.
39. Hou, W.; Mu, B.; Wang, Q., Studies on wettability of polypropylene/methyl-silicone composite film and polypropylene monolithic material. *Journal of Colloid and Interface Science* 2008, 327 (1), 120-124.
40. Darmanin, T.; Nicolas, M.; Guittard, F., Electrodeposited polymer films with both superhydrophobicity and superoleophilicity. *Physical Chemistry Chemical Physics* 2008, 10 (29), 4322-4326.

41. Hsieh, C.-T.; Hsu, J.-P.; Hsu, H.-H.; Lin, W.-H.; Juang, R.-S., *Hierarchical oil–water separation membrane using carbon fabrics decorated with carbon nanotubes*. 2016; Vol. 286, p 148-154.
42. Shi, Z.; Zhang, W.; Zhang, F.; Liu, X.; Wang, D.; Jin, J.; Jiang, L., Ultrafast Separation of Emulsified Oil/Water Mixtures by Ultrathin Free-Standing Single-Walled Carbon Nanotube Network Films. *Advanced Materials* 2013, 25 (17), 2422-2427.
43. Kaur, H.; Bulasara, V. K.; Gupta, R. K., Influence of pH and temperature of dip-coating solution on the properties of cellulose acetate-ceramic composite membrane for ultrafiltration. *Carbohydrate Polymers* 2018, 195, 613-621.
44. Nandi, B. K.; Uppaluri, R.; Purkait, M. K., Effects of dip coating parameters on the morphology and transport properties of cellulose acetate–ceramic composite membranes. *Journal of Membrane Science* 2009, 330 (1), 246-258.
45. Wang, Q.; Cui, Z.; Xiao, Y.; Chen, Q., Stable highly hydrophobic and oleophilic meshes for oil–water separation. *Applied Surface Science* 2007, 253 (23), 9054-9060.
46. Zhang, L.; Chen, H.; Sun, J.; Shen, J., Layer-by-Layer Deposition of Poly(diallyldimethylammonium chloride) and Sodium Silicate Multilayers on Silica-Sphere-Coated Substrate—Facile Method to Prepare a Superhydrophobic Surface. *Chemistry of Materials* 2007, 19 (4), 948-953.
47. Zhang, H.; Zeng, X.; Gao, Y.; Shi, F.; Zhang, P.; Chen, J.-F., A facile method to prepare superhydrophobic coatings by calcium carbonate. *Industrial & engineering chemistry research* 2011, 50 (6), 3089-3094.

48. Barati Darband, G.; Aliofkhazraei, M.; Khorsand, S.; Sokhanvar, S.; Kaboli, A., Science and Engineering of Superhydrophobic Surfaces: Review of Corrosion Resistance, Chemical and Mechanical Stability. *Arabian Journal of Chemistry* 2018.
49. Ng, W. F.; Wong, M. H.; Cheng, F. T., Stearic acid coating on magnesium for enhancing corrosion resistance in Hanks' solution. *Surface and Coatings Technology* 2010, 204 (11), 1823-1830.
50. Wang, C.; Yao, T.; Wu, J.; Ma, C.; Fan, Z.; Wang, Z.; Cheng, Y.; Lin, Q.; Yang, B., Facile approach in fabricating superhydrophobic and superoleophilic surface for water and oil mixture separation. *ACS applied materials & interfaces* 2009, 1 (11), 2613-2617.
51. Pan, Q.; Wang, M.; Wang, H., Separating small amount of water and hydrophobic solvents by novel superhydrophobic copper meshes. *Applied Surface Science* 2008, 254 (18), 6002-6006.
52. Fan, H.; Wright, A.; Gabaldon, J.; Rodriguez, A.; Brinker, C. J.; Jiang, Y. B., Three-Dimensionally Ordered Gold Nanocrystal/Silica Superlattice Thin Films Synthesized via Sol-Gel Self-Assembly. *Advanced Functional Materials* 2006, 16 (7), 891-895.
53. Mostefaï, M.; Auriac, Y.; Shanahan, M.; Bressan, J.; Meslif, A., Fluoroalkylsilanes as non-stick coatings: adhesion of glucose and its thermal byproducts. *International journal of adhesion and adhesives* 1998, 18 (4), 273-281.
54. Sarbada, S.; Shin, Y. C., Superhydrophobic contoured surfaces created on metal and polymer using a femtosecond laser. *Applied Surface Science* 2017, 405, 465-475.
55. Ha, C.-S.; Nagappan, S., *Hydrophobic and Superhydrophobic Organic-Inorganic Nano-Hybrids*. Pan Stanford: 2018.
56. Gao, T.; Meng, G.; Wang, Y.; Sun, S.; Zhang, L., Electrochemical synthesis of copper nanowires. *Journal of Physics: Condensed Matter* 2001, 14 (3), 355-363.

57. Qin, W.; Li, J.; Liu, Y.; Yue, W.; Wang, C.; Mao, Q.; Li, Y., Effect of rolling strain on the mechanical and tribological properties of 316 L stainless steel. *Journal of Tribology* 2019, *141* (2).
58. Brito, J. B.; Costa, T. M. H.; Rodembusch, F. S.; Balzaretto, N. M., Photoluminescence of silica monoliths prepared from cold sintering of nanometric aerosil precursors under high pressure. *Journal of Luminescence* 2017, *187*, 154-159.
59. Wood, D.; Rabinovich, E. M., Study of alkoxide silica gels by infrared spectroscopy. *Applied Spectroscopy* 1989, *43* (2), 263-267.
60. Sanaeepur, H.; Kargari, A.; Nasernejad, B., Aminosilane-functionalization of a nanoporous Y-type zeolite for application in a cellulose acetate based mixed matrix membrane for CO₂ separation. *RSC Advances* 2014, *4* (109), 63966-63976.
61. Ambrożewicz, D.; Ciesielczyk, F.; Nowacka, M.; Karasiewicz, J.; Piasecki, A.; Maciejewski, H.; Jesionowski, T., Fluoroalkylsilane versus alkylsilane as hydrophobic agents for silica and silicates. *Journal of Nanomaterials* 2013, *2013*.
62. Lu, Y.; Sathasivam, S.; Song, J.; Chen, F.; Xu, W.; Carmalt, C. J.; Parkin, I. P., Creating superhydrophobic mild steel surfaces for water proofing and oil–water separation. *Journal of Materials Chemistry A* 2014, *2* (30), 11628-11634.
63. Rajab, F. H.; Liauw, C. M.; Benson, P. S.; Li, L.; Whitehead, K. A., Production of hybrid macro/micro/nano surface structures on Ti6Al4V surfaces by picosecond laser surface texturing and their antifouling characteristics. *Colloids and Surfaces B: Biointerfaces* 2017, *160*, 688-696.
64. Limcharoen, A.; Limsuwan, P.; Pakpum, C.; Siangchaew, K., Characterisation of C₁₈F Polymer Film Formation on the Air-Bearing Surface Etched Sidewall of Fluorine-Based Plasma Interacting with AlO₂/TiC Substrate. *Journal of Nanomaterials* 2013, *2013* (2013).

65. Das, I.; De, G., Zirconia based superhydrophobic coatings on cotton fabrics exhibiting excellent durability for versatile use. *Scientific Reports* 2015, 5, 18503.
66. Murray, C. D., Durability of silane sealer in a highly alkaline environment. 2014.

4. CHAPTER FOUR

Selective and Continuous Oil Removal from Oil-Water Mixture, Using Tubular Superhydrophobic and Superoleophilic Membrane

Abstract

Industrial oily wastewater treatment and oil spills incidents are driving an urgent need for continuous oil-water separation processes. Herein, the performance of a superhydrophobic-superoleophilic (SHSO) membrane for dynamic separation of oil-water mixtures is investigated. The critical affecting factors, including various total flow rates (5, 10, and 15 mL/min) and oil-concentration (10, 30, and 50 vol%), are analyzed using the as-fabricated SHSO mesh tube over 70 minutes. The SHSO membrane is fabricated using dip-coating of tubular stainless-steel mesh into a solution in which its surface energy is reduced with long chain alkyl silane (Dynasylan[®] F8261) and then roughed via functionalized silica nanoparticles (AEROSIL[®] R812). This facile and effective method engenders a uniform coating with flower-like nano roughness on the surface where the pore size decreases from around 80 to 45 μ m. The as-prepared SHSO mesh tube illustrates excellent superhydrophobicity with a water contact angle of 160 $^{\circ}$ and an oil contact angle of zero for hexane. The maximum oil separation efficiency (SE) of 97% is obtained when the oil-water mixture has the lowest flow rate (5 mL/min) with a concentration of 10 vol% oil. While the minimum oil SE (86%) is achieved for the scenario with highest total flow rate and concentration (qt= 15 mL/min, 50 vol% oil). The water SE of around 100% indicates that the water phase is not affected by changing both total flow rate and oil concentration, due to the superhydrophobicity of the fabricated mesh. The effluents of water and oil are crystal clear, indicating the high purity of both phases after dynamic tests. The oil flux increased from 314 to 790 (L/m².h) by increasing the oil permeate flow rate from 0.5 to 7.5 ml/min. The linear behavior of oil and water collection rates by the time demonstrates the high separation performance of a single SHSO mesh without any pore-blocking during dynamic tests. The significant dynamic SE

(97%) of the fabricated SHSO membranes with robust chemical stability shows their promising potential for industrial-scale oil-water separation applications.

Keywords: Superhydrophobic-superoleophilic membrane, Continues oil-water separation, Flow rate, Oil in water concentration.

4.1. Introduction

The globally increasing oily wastewater, related to the development of modern industries and human growth, triggers a concern regarding the potential negative impacts on human health and aquatic ecosystem [1]. For example, a mining operation generates around 140,000 L of oily wastewater every day. Furthermore, the failure to address the recent oil spill disasters, especially the 2010 Deepwater Horizon incident in the Gulf of Mexico, highlighted an urgent need for novel oil-water separation approaches [2]. The available conventional techniques include adsorption [3], air flotation [4], coagulation [5], centrifugation [6], gravity separation [7-9], and electric field [10]. These techniques occupy large space, generate secondary pollutants, and are time-consuming, expensive, and operator-based [2]. Facing these challenges motivated scientists to develop a durable, inexpensive, and super wetting material for high efficient oil-water separation [2]. Among them, the membrane has been acknowledged as the most advanced technology for oil-water separation applications [2]. Super wetting surfaces by selective filtration of oil or water from oil-water mixture have attracted great interest in recent years. Accordingly, four states of wettability, such as superhydrophobic-superoleophilic, superhydrophobic-superoleophobic, superhydrophilic-superoleophilic, and superhydrophilic-superoleophobic can be developed by the modification of surface energy and morphology [11].

Oil contaminants in oily wastewater are classified based on the diameter (d) of the dispersed phase as follows: free oil ($d > 150 \mu\text{m}$), dispersed oil ($150 \mu\text{m} > d > 20 \mu\text{m}$), and emulsified oil ($d < 20$

μm) [12]. For a given oil in water mixture, there are three different phases of oil, oil in water, and water [13, 14]. To obtain an effective separation of these three phases, especially in a gravity-driven process, the membrane is expected to be both superhydrophilic and superoleophobic [15, 16]. However, this strategy has some drawbacks. For instance, passing a huge amount of water through the membrane is not economical because it decreases the membrane lifespan and increases the fouling probability. Moreover, these hydrophilic membranes cannot efficiently separate the free oil-water mixtures or water in oil emulsions [17].

Recently, the stainless steel (SS) mesh-based membranes with superhydrophobic-superoleophilic (SHSO) wettability have gained remarkable attention owing to their higher permeability, lower pressure drops, and higher mechanical stability [18, 19]. However, there are several limitations to the industrial applications of SHSO membranes. For instance, (i) these surfaces can be utilized in a batch scale to separate small volumes of oil-water mixtures; or fabrication of SHSO surfaces relies on both complex surface texture and toxic long-chain perfluorinated compounds [20].

The SHSO surfaces are generally constructed by creating hierarchical roughness on the membrane surface and modifying the surface chemistry by applying low surface energy materials [21]. Many studies have shown the importance of surface modification on the performance of SHSO membranes in oil-water separation applications. The first SHSO mesh was fabricated by Feng et al. [22] in 2004 through spray-coating of polytetrafluoroethylene (PTFE) particles (30 wt%) onto SS mesh, featured a water contact angle (WCA) of 156° and a sliding angle of 4° . Qin et al. [23] modified Feng's experimental method by utilizing polypropylene sulfide (PPS) in the coating process and attained a similar WCA of 156° . Yang et al. [24] also applied the same methodology while coated mesh with epoxy/attapulgite (44.4 wt%). A WCA of 160° and 98% oil-water SE were obtained after 30 cycles. Their prepared mesh showed high stability in harsh conditions (150°C

and 95% relative humidity for 48 h). Liu et al. [21] constructed a SHSO SiO₂/carbon SS mesh through candle soot coating followed by a chemical vapour deposition method. The fabricated membrane with a WCA>150° selectively separated oil-water with a high flux of more than 930 L/m².h and collecting efficiency of 97% after a 15-cycle experiment.

The SHSO stainless steel meshes have been widely implemented in static oil-water separation set up [12, 19, 24-41]. These static separations are mostly operated by a dead-end membranes, while for continuous oily wastewater treatment the membrane is commonly designed as a cross-flow model [42]. In this case, the membrane is exposed to a continuous flow where the liquid turbulence adds more variables to the process and makes the oil-water separation more challenging [43]. To the best of our knowledge, there are only a few studies to evaluate continuous oil-water SE using the super wetting surfaces. For instance, Dunderdale et al. [20] designed an apparatus using two antagonistic SS meshes, including poly(sodium methacrylate) as superoleophobic mesh and poly(stearyl methacrylate) as superhydrophobic mesh. They dynamically separated oil and water with a purity of around 100% from an n-hexadecane/water (50/50% v/v). Ezazi et al. [44] investigated the performance of Fe-TiO₂ spray-coated SS meshes for continuous separation of stabilized oil-in-water emulsion and in-situ photocatalytic degradation of organic matter. The thermally sensitized coated mesh featured in-air superhydrophilic and underwater superoleophobic properties with SE more than 97%. Moreover, the flux recovery around 99% observed upon irradiation of visible light on the membrane surface while continuous separation process.

Herein, we report a successful fabrication SHSO mesh tube to evaluate continuous oil-water SE. In contrast to typical 2D filters, our novel tubular SS mesh with SHSO feature provides more area in a limited space to achieve better oil-water SE. The as-fabricated mesh is integrated into a vertical cross-flow separation set-up that enables continuous oil-water separation. The oil-water mixture

characteristics such as flow rate and oil concentration are also analyzed for effective separation. Finally, the designed set-up continuously purifies both oil and water phases from the mixtures at the same time through one step process. Considering that our separation methodology can be easily scaled up to a larger size, it could be a basis for a rational design and implementation in petroleum refining, wastewater treatment, and oil spills clean-up.

4.2. Experimental Methods

4.2.1. Chemicals used

Stainless steel mesh tubes (316 mesh) are purchased from (McMaster-Carr) with an opening size of 75 μm . Sulfuric acid (98 wt%) is obtained from Caledon Laboratory Ltd. Hydrochloric acid (37 wt%), hydrogen peroxide (30 wt%), and acetone (99.5 wt%) are purchased from ACP Chemicals. Long-chain alkyl silane (Dynasylan[®] F8261 solution) and hydrophobic SiO₂ nanoparticles (NPs) of AEROSIL[®] R812 are provided from Evonik Industries AG. All chemicals are used as received without any purification. Sunflower oil, which is utilized in oil-water separation tests, is purchased from the local market. Deionized water (DI, 18.2 M Ω .cm) is provided through RODI-C-12A, Aqua Solution[®] in the lab.

4.2.2. Fabrication process of SHSO mesh tube

The general procedure of fabricating SHSO mesh includes three main steps, including cleaning, activation, and coating. After cleaning SS mesh tubes with ethanol and acetone for 15 minutes each in the ultrasound system, the activation of cleaned meshes is processed by piranha solution with a volume ratio of 3:1 for a mixture of H₂SO₄ (98 wt%) and H₂O₂ (30 wt%). Then we prepared a prime solution of Dynasylan[®] F8261 (1 wt%) in ethanol (90 wt%), water (8.8 wt%), and hydrochloric acid (0.2 wt%). This prime solution is uniformly mixed via magnetic stirrer under

1000 rpm for two hours. The final coating solution was prepared by mixing the homogenous prime solution with functionalized silica NPs (1 wt% of coating solution). These NPs with an average size of 7 nm are also utilized to create a hierarchical nano surface roughness. Subsequently, the coating solution is mixed under 1000 rpm and then ultrasonically dispersed for 30 min. Finally, the dried activated mesh tubes are immersed in the final coating solution to form a stable layer of SHSO on the mesh tubes. The excess of coating solution on mesh tubes is drained using a tissue. Therefore, the surface energy and morphology of the mesh tubes are modified simultaneously under one-step dip-coating. The coated mesh tubes are cured for 120 minutes on a heater to strengthen the covalent bonding between the coating layer and the SS mesh surface. These hot mesh tubes should reach the ambient temperature before using in the separator.

4.2.3. Characterization methods of the SHSO mesh tube

The surface characterization tests are also performed to assess the mesh performance. The morphologies of the SS mesh and SHSO coated mesh after coating with a gold layer are examined by FEI MLA 650FEG Scanning Electron Microscopy (SEM). The samples are attached to the surface of an aluminum stub using a double-side carbon tape. Functionalized fumed silica NPs are also studied using a Tecnai G2 Spirit Transmission Electron Microscopy (TEM), operated at an accelerating voltage of 80 kV. Samples for TEM analysis are diluted in ethanol (95%), then sonicated for 5 minutes. For each sample, 5 μ L NPs dispersions is applied to a copper grid (300 mesh) coated with carbon, and then drying in room temperature. The surface wettability of as-fabricated SHSO mesh is characterized by equilibrium water and oil contact angle measurements using OCA 15EC, DataPhysics Instruments GmbH, Germany, under ambient temperature in air. A holder is also designed to assure that the mesh has no curvature when measuring happens. For each test, 10 μ L water droplet is dispersed on the surface of cleaned and SHSO meshes and

replicated for three times. The reported contact angles are the average of three points on the mesh surface where each point represents the average of both left and right contact angles.

4.2.4. Separation test set up, procedure, and assessment

The dynamic oil-water separation is conducted according to Figure 4.1. A 1.27 cm SHSO mesh tube (inner diameter = 1/2 inch) is employed to separate oil from an oil-water mixture under gravity. A Swagelok® reducer fitting is used to support the SHSO mesh tube. This mesh is sealed with Teflon® shrink tube and a clamp. Also, a 0.63 cm Teflon tube (outer diameter = 1/4 inch) is attached to the reducer fitting to pass the separated oil to an oil collector. This Teflon tube passed through a rubber stopper that is used to seal the bottom of the glass tube with 3.1 cm outer diameter. A sponge cap is used to almost cover the top part of the glass tube while provides atmospheric pressure inside of the glass tube.

Sunflower and DI water are used as the wetting and non-wetting phases, respectively. To avoid the air bubbles, the outlet of pumps is vacuumed using a 10 ml disposable syringe before each run. The sources of oil and water are also de-aerated using a vacuum pump under the vacuum pressure of 22 mm Hg for 5 min. The inlet and outlet of the pumps are connected to the 1/8- and 1/4-inches Teflon tubes, respectively. These tubes are connected to the pumps using PTFE ferrules and nuts. After de-aeration, to assure there is no air trapped into the tubes, oil and water are injected into the system under a high flow rate of 20 mL/min.

After installation and sealing the separator parts, the glass column is filled with DI water. It is found that the breakthrough capillary pressure through as-fabricated SHSO mesh tube occurs at a pressure of $> 3 \text{ cm H}_2\text{O}$. We kept the water level below the breakthrough pressure of the SHSO mesh tube by adjusting the height of the water effluent valve. Using these adjustments, the pressure of oil-water mixture is maintained within a safe margin to avoid the water breakthrough.

The injected oil and water are mixed using a T-shape connector to create an oil-water mixture. To avoid the turbulence around the SHSO mesh tube, the mixture of oil in water is poured from a level attached to the interface. Almost 5 mm round glass beads are used to trap the oil droplets at the point where water leaves the glass tube to enhance the purity of the collected water (Figure 4.1). To minimize the water splashing, we attached a Teflon tube between the outlet valve and inside of the water collector.

Oil-water mixture with total flow rates (qt) of 5, 10 and 15 mL/min and oil concentrations of 10, 30, and 50 vol% are generated using the Eldex pumps. During the dynamic oil-water separation process, pictures are captured at scheduled timeframes using a digital camera. The whole process lasted for 70 minutes. We used a two-and five-minute intervals for the first 10 min and between 10 to 70 min, respectively. Using a ruler attached to the outside of the glass tube, the height of oil above the water column is measured. By comparing the volume of original and collected oil and water samples, the SE is determined with the following equation [21]:

$$SE = \frac{V_c}{V_i} \quad (4.1)$$

where SE is separation efficiency; V_c and V_i represent the volume of collected water/oil after filtration and initial water/oil volume (L), respectively.

Later, we also use these results for measuring permeate flux according to the following equation:

$$Flux = \frac{V}{S \cdot t} \quad (4.2)$$

where V is the volume of water/oil collected (L); S is the projected area of the SHSO mesh in contact with the oil-water mixture (m^2); and t represents the separation time (h). The lateral surface area/projected area is calculated as follows:

$$S = 2\pi rh \quad (4.3)$$

where h is the height of oil around the mesh tube (m), and r is the radius of the circle (m).

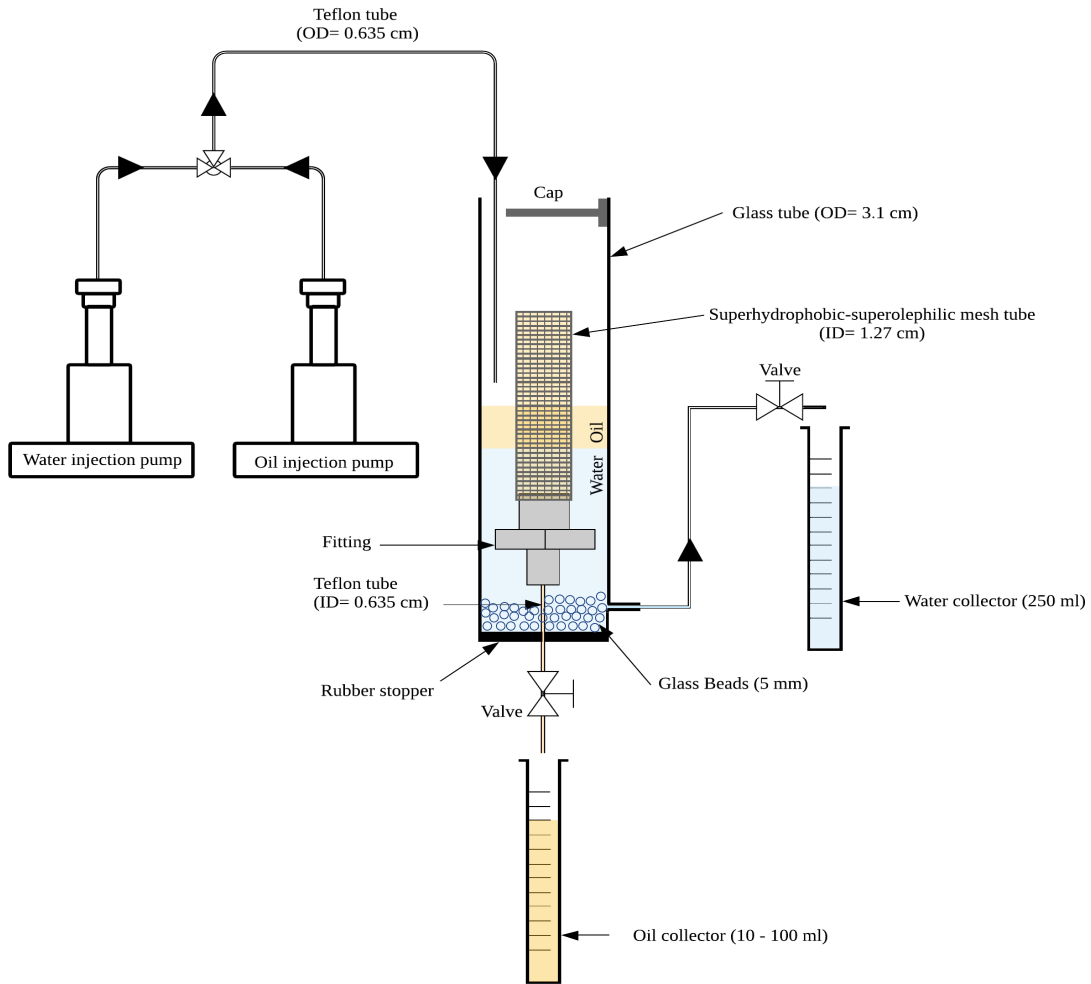


Figure 4.1. Schematic of dynamic oil-water separation setup

For cleaning after each run, a three inches Teflon tube connected to the vacuum is used to remove the oil accumulated/dispersed in the oil-water interface. This tube suctions out the sludge until it meets the interface. The separator refill with DI water and suction is repeated for a couple of times. We replicated the dynamic oil-water separation three times and utilized a new coated mesh for each replication.

4.3. Results and Discussion

4.3.1. Morphological evaluation of the SHSO stainless-steel mesh

The SEM image of the cleaned SS mesh and the shape of the water droplet on the mesh surface is shown in Figure 4.2a. The results show that the cleaned SS mesh has an average pore diameter of around 80 μm with a contact angle above 90° which shows hydrophobic property. It is totally accepted that the pore diameter has a significant impact on the performance of the final coated mesh [22, 45].

Wettability aside, the separation mechanism of all membrane filtration systems can be justified based on the “size-sieving” effect. The pore size of our fabricated membrane, as a superoleophilic surface, should be reduced during functionalization by creating roughness on its surface, to become smaller than oil droplets (dispersed and emulsified). On the other hand, smaller pore size leads to increasing the breakthrough pressure, the pressure required for a non-wetting phase (water phase) to enter the membrane largest pore. In addition, pore size reduction can enhance the probability of fouling, resulting in a rapid depletion of permeability. Hence, achieving an optimum pore opening after coating process is always challenging. Cai et al. [45] concluded that a WCA of above 150° is obtained if the original mesh pore diameter is between 50-200 μm . That is why, in our study, the original mesh with an average around 80 μm pore size is chosen to be utilized for fabrication of SHSO membranes.

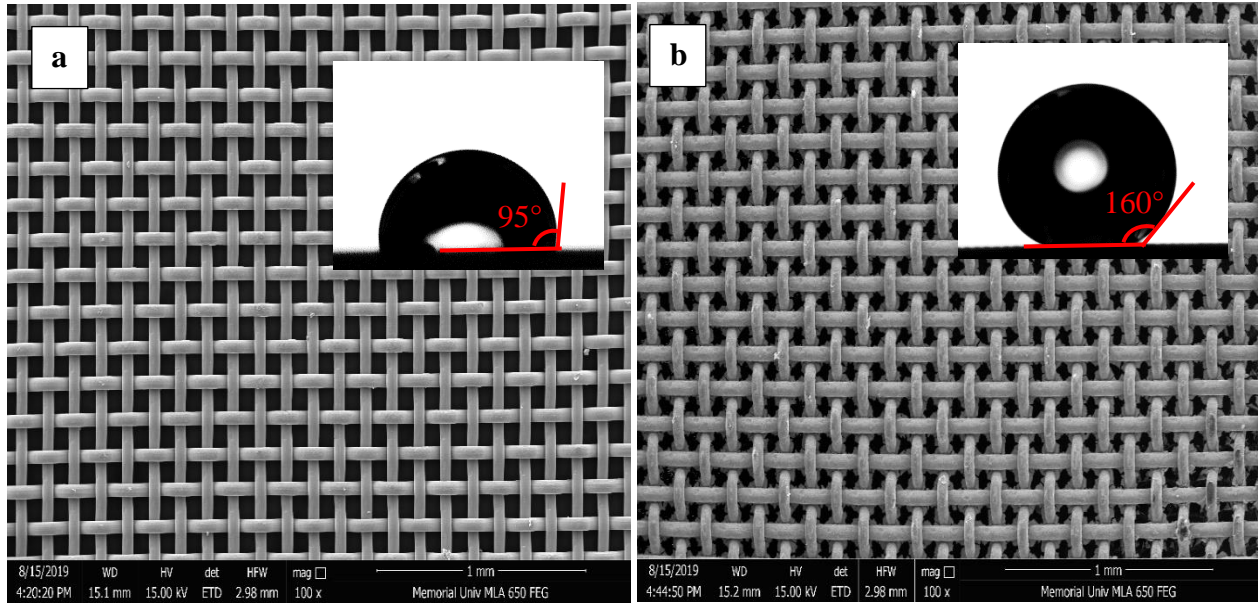


Figure 4.2. SEM images with magnification of 100X and the shape of water droplet on the mesh (a) cleaned and (b) SHSO coated mesh.

Figure 4.2b illustrates the SEM image of as-fabricated SHSO mesh and its surface morphology after coating. The flower-like nanoscale structures are obvious on the surface of the coated mesh. The coated mesh resulted in a WCA of 160°. Further, these roughness structures with visible fractures on the surface (Figure 4.3a) provide high capillary pressure regions that can imbibe the oil droplets. The shape of the water droplet on the surface of the coated mesh confirms that the coated mesh repels the water.

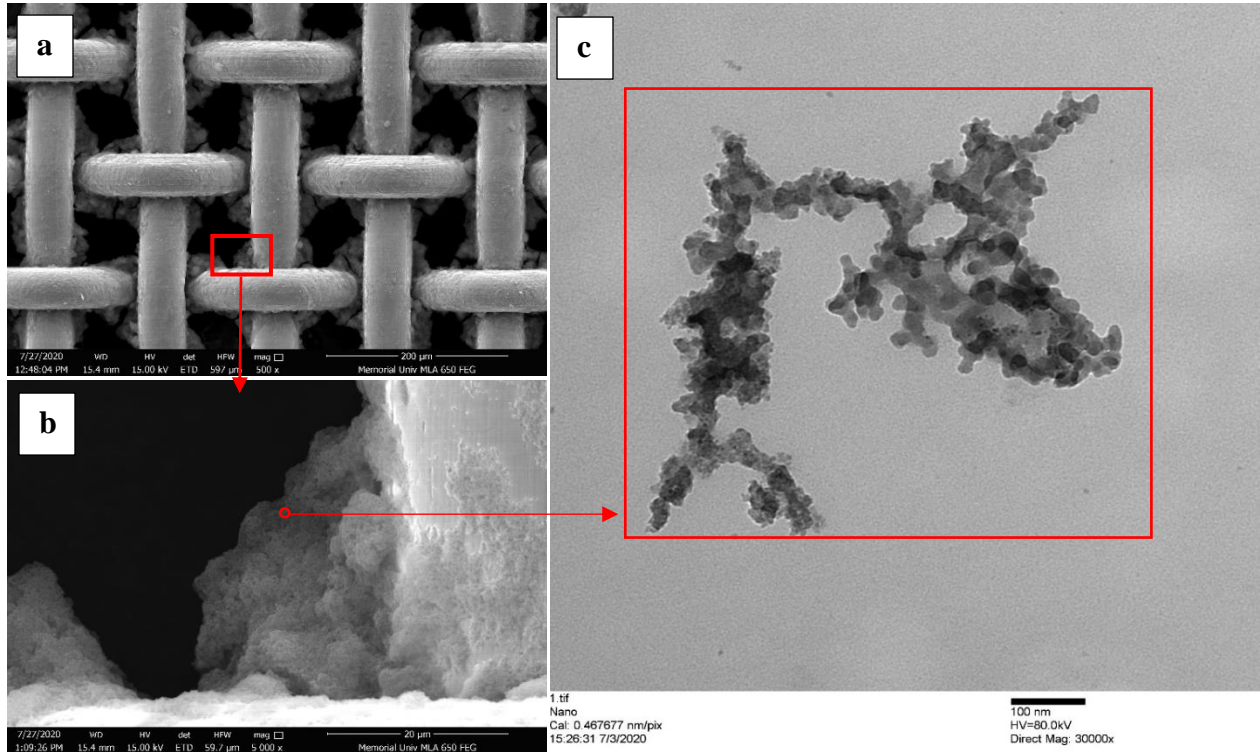


Figure 4.3. SEM and TEM images of the SHSO mesh; (a) SHSO mesh with 500X magnification and (b) with 5,000X magnification. (c) The TEM image of functionalized silica NPs as roughness on the surface of mesh with 30,000X magnification.

4.3.2. Dynamic oil-water separation tests

4.3.2.1. Oil and water collection

Cumulative produced volumes of oil and water are plotted with time as shown in Figure 4.4.a and b, respectively. The production rates ($q = dV/dt$) for both oil and water are constant during the entire experiment. The high coefficient of determination ($R^2 \sim 1$) confirms that the cumulative produced volumes are a linear function of separation time (Table 4.1). This observation confirms that there is no blockage or fouling to reduce the rate of oil-water collection throughout the experiment. This is a pure filtration in which the flux is limited with membrane resistance/permeability [46] according to Darcy's law as follows:

$$k = (q \cdot \mu \cdot L) / (S \cdot \Delta P) \quad (4.4)$$

where k represents the SHSO mesh permeability (m^2), q is the flow rate through mesh pores (m^3/s), μ is the viscosity of the permeated oil ($\text{Pa}\cdot\text{s}$), L represents the thickness of the mesh (m), S is the projected area (m^2), and ΔP is the applied pressure difference (Pa). The pressure gradient is also calculated based on following formula:

$$\Delta P = \Delta\rho \cdot g \cdot h \quad (4.5)$$

where $\Delta\rho$ is the difference between the density of oil and air (kg/m^3), g is the gravitational acceleration (m/s^2), and h is the height of oil around the mesh tube (m). The height is related to the different between the amount of oil fed to system and that drained from the system, which is dictated by the resistance of membrane as well.

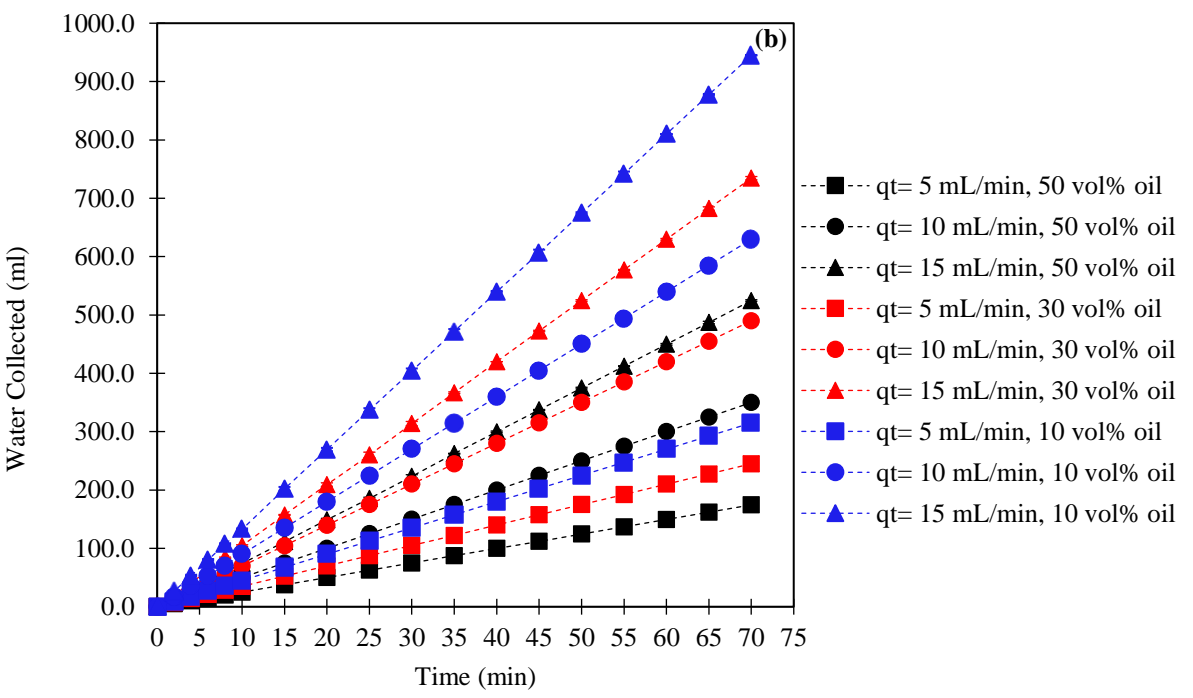
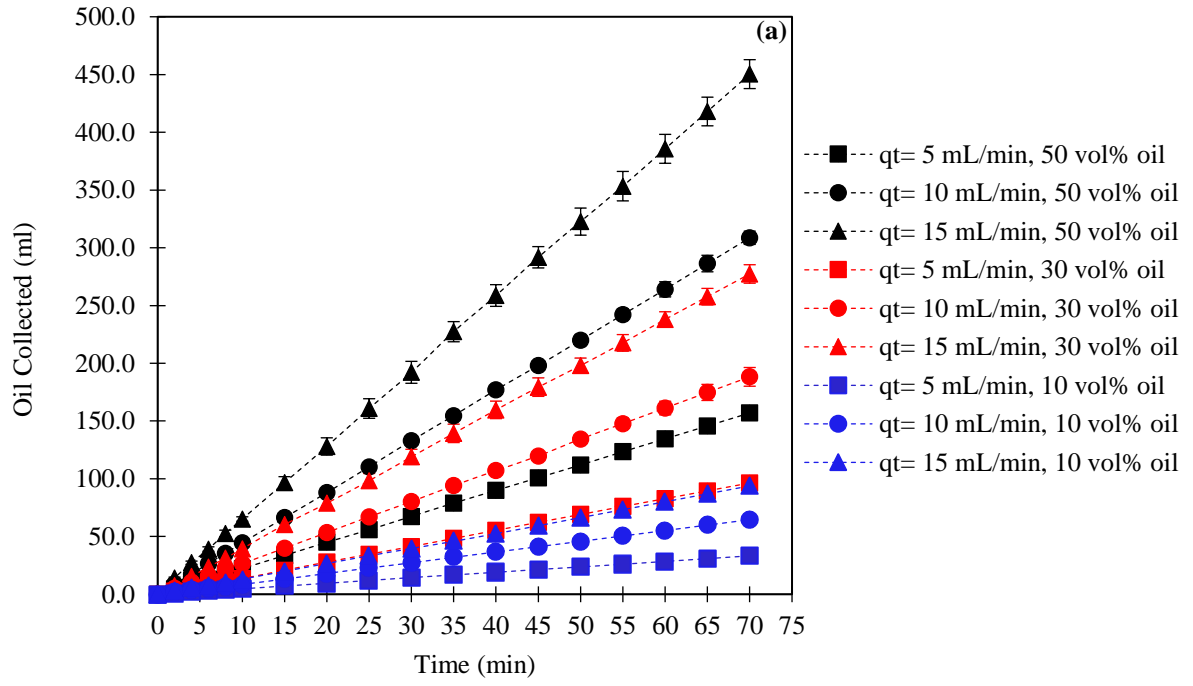


Figure 4.4. Oil (a) and water (b) collection vs time in dynamic oil-water separation test for oil-water mixtures under different flow rates and concentrations (% vol oil)

Table 4.1. The rate of oil and water collection for different scenarios of oil-water mixture

Total Flow Rate (mL/min)	Concentration (% vol oil)	Oil Collection (mL)		Water Collection (mL)	
		$q = dV/dt$	R^2	$q = dV/dt$	R^2
5	10	0.4	1	2.4	1
	30	0.9	1	3.4	1
	50	1.3	1	4.5	1
10	10	1.3	1	5	1
	30	2.2	1	6.9	1
	50	2.6	1	7.4	1
15	10	3.9	0.9	8.9	1
	30	4.4	0.9	10.4	1
	50	6.4	0.9	13.5	1

4.3.2.2. SHSO filtration performance

The oil permeation flux evolution during continuous oil-water separation using the SHSO mesh tube are illustrated in Figure 4.5. The flux mentioned here particularly refers to a gravity-driven separation flux that does not need an additional energy driving source (such as pressure), which is an advantage of our system design. By considering three levels for both total flow rates ($q_t= 5, 10, 15$ mL/min) and concentration (10, 30, 50 vol% oil), nine scenarios are created for the oil-water separation analysis over 70 minutes. Higher permeate flux are achieved when increasing the oil flow rate at different scenarios. One point is that at higher injection flow rates, the wetted area (used in the flux calculations) also increases. A high separation flux enables the membranes to process large volumes of oil-water mixture in a shorter period of time [47]. By increasing the rate of injected oil from 0.5 mL/min ($q_t = 5$ mL/min, 10 vol% oil) to 7.5 mL/min ($q_t = 15$ mL/min, 50% oil), the flux is increased from around 314 to 790 (L/m².h), in the range of flow rates used. More importantly, the flux for each individual scenario remained constant without any noticeable decline, which means the SHSO stainless-steel mesh tube is durable and stable over a 70-minute

experiment. Though, further evaluation is needed especially in a longer time-scale to assure the mesh reusability [21].

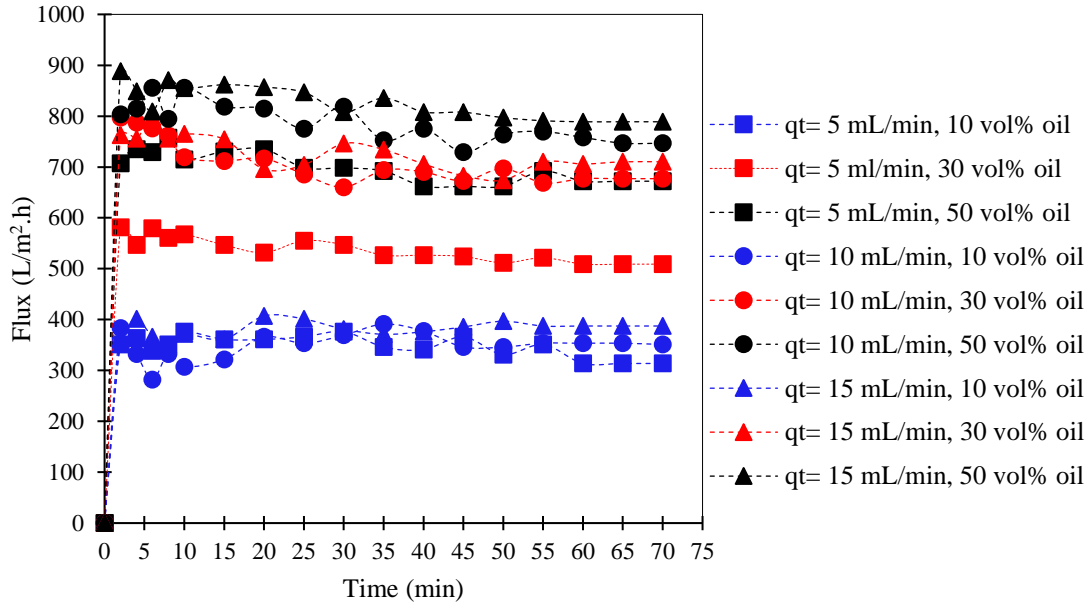


Figure 4.5. The oil permeates flux vs time in dynamic oil-water separation for different oil concentrations and total flow rate of the oil-water mixture.

Moreover, flux is directly and inversely proportional to the flow rate and the height of oil around the mesh tube, respectively. Based on the flux equation (Equation 4.2), higher oil flow rate leaves a positive impact on flux by an increase in feed-oil flow rate (q); and a negative impact on flux by increasing the height of oil around the SHSO mesh tube (h), which directly increases the projected area (S). Therefore, both factors of oil flow rate (q) and oil height around SHSO mesh tube (h) simultaneously interact with each other to change the flux for a given scenario. The measured values for the flux are comparable to those reported for cross-flow filtration [48-51] where separation process was accelerated by an energy intensive, externally applied pressure difference, compared to our gravity-based separation. Further, no flux reductions over 70 mins test strength this assumption that the SHSO membrane can also be resistant to fouling by oil, which is an interesting topic for future investigation. This finding contrasts with the flux reduction reported

for most hydrophobic membranes [50, 51]. As discussed in Darcy's equation (Equation 4.4), the SHSO coated mesh can pass a certain amount of oil due to the permeability effect; a higher oil flow rate can cause a higher dead volume around the mesh tube (h) (Figure 4.7). The height of oil around the SHSO mesh tube is plotted for all nine scenarios (Figure 4.6). The oil layer height remains relatively constant around the mesh tube for each individual scenario. As the total flow rate increases, the height of the oil column increases, leads to enhance the pressure on the membrane, which eventually causes the water to penetrate the membrane when it reaches the breakthrough pressure of the membrane. The water first penetrates the pores with larger size owing to the lowest resistance against the non-wetting phase. This is followed with the pores with smaller size [52]. To continue the separation process, the oil must be drained off before the oil-water mixture reaches this critical height. Thus, having higher breakthrough pressure enable the as-fabricated SHSO mesh tube to separate larger amount of oil-water mixtures.

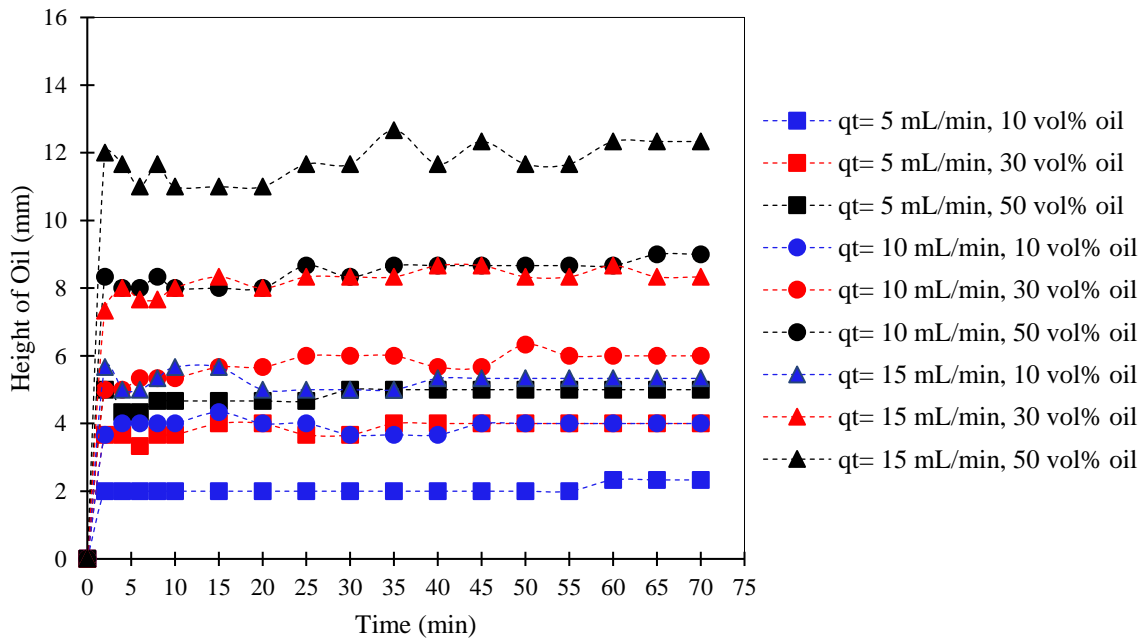


Figure 4.6. The height of oil around SHSO mesh tube vs time in dynamic oil-water separation for different O:W concentrations and total flow rate of the oil-water mixture.

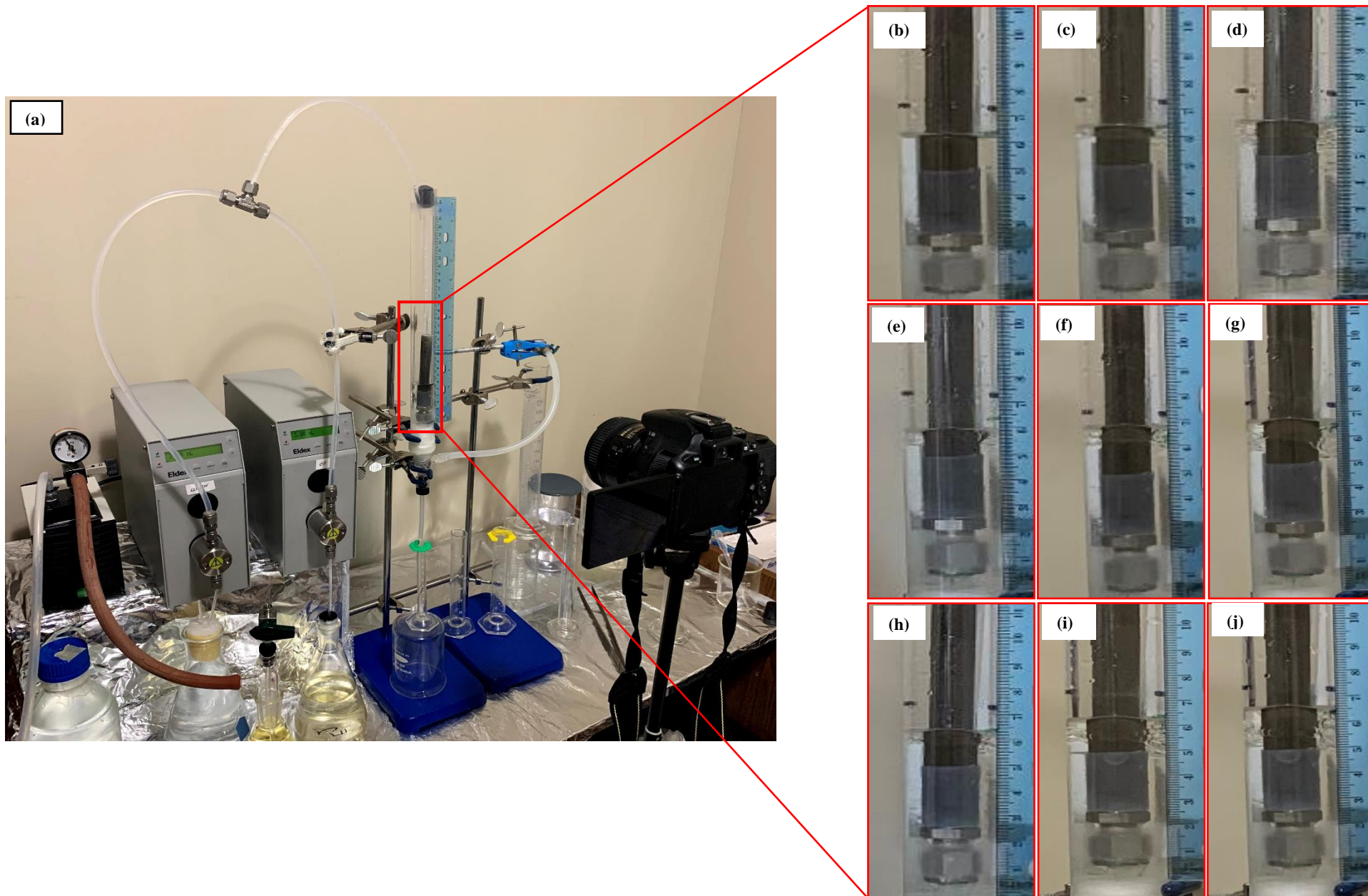


Figure 4.7. Dynamic oil-water separation set up (a) and the height of oil around mesh tube at (b) $q_t=5$ mL/min, 10 vol% oil, (c) $q_t=5$ mL/min, 30 vol% oil, (d) $q_t=5$ mL/min, 50 vol% oil, (e) $q_t=10$ mL/min, 10 vol% oil, (f) $q_t=10$ mL/min, 30 vol% oil, (g) $q_t=10$ mL/min, 50 vol% oil, (h) $q_t=15$ mL/min, 10 vol% oil, (i) $q_t=15$ mL/min, 30 vol% oil, (j) $q_t=15$ mL/min, 50 vol% oil.

4.3.2.3. Effect of oil concentration on SE

To characterize the SE of the fabricated SHSO mesh for a dynamic/continuous oil-water separation, the influence of oil concentration on SE is evaluated. We measure the effect of three different oil concentrations (10, 30, and 50 vol%), by considering total flow rate constant, on both oil SE and water SE are analyzed over a 70-minute time-scale. All the experiments are replicated three times, and the reported values are average of the replicates.

The oil SE versus time at various oil concentrations are presented in Figure 4.8a, b, and c. All the graphs reach a plateau in the last ten minutes. The varying oil SE from 86 to 97% shows a better SE at a lower oil concentration. At a total flow rate of 5 mL/min (Figure 4.8a), the SE reaches its maximum of 97% for 10% oil concentration. While it reduced to around 90% for both 30 and 50% oil concentration. As shown in Figure 4.8b, although the SE for the flow rate of 10 mL/min with 10% oil concentration has some fluctuations in the first 40 minutes, but at the end of the separation process, it reaches approximately 93% which is higher than two other oil concentrations with SE around 89% at total flow rate of 10 mL/min. Once total flow rate increases to the highest level at 15 mL/min (Figure 4.8c), the SE values of 92, 87, and 86% are observed for 10, 30, and 50% oil concentrations, respectively. It confirms that the performance of fabricated SHSO mesh for continuous oil-water separation slightly decreases when the concentration of oil increases; although the mean values for SE decrease with increasing the oil concentration, the differences are not statistically significant for most cases.

The effect of changing oil concentrations on the water SE is illustrated in Figure 4.8d, e, and f, at three different total flow rates of 5, 10, and 15 mL/min. As indicated in all the plots, the water SE values fluctuate around 100%. However, for the highest total flow rate of 15 ml/min (Figure 4.8f), there are more fluctuations in three different concentrations compared to the two other flow rates

(Figure 4.8d and e) that can be due to changes in flow regime and shear forces, which is stronger for higher flow rates. Consequently, there is no significant effect on water SE when oil concentrations are changed at three different total flow rates of the oil-water mixtures.

4.3.2.4. Effect of total flow rate on SE

The total flow rate of the oil-water mixture is a critical parameter to be analyzed to obtain a better performance analysis of the SHSO mesh tube for continuous oil-water separation. Thereby the influence of three total flow rates of 5, 10, and 15 mL/min, at constant oil concentrations, on both oil SE and water SE are evaluated over 70 minutes. The error bars indicate the 95% confidence interval for three replications.

The effect of changing total flow rate on the oil SE is shown in Figure 4.9a, b, and c. All the plots approach a plateau after 60 minutes of pumping, which indicates that 70 minutes time-scale is adequate for the separation test. As illustrated in Figure 4.9a, at oil concentration of 10 vol%, by increasing the total flow rate of the oil-water mixture from 5 to 15 mL/min, the SE is reduced from 97 to 91%. The total flow rate of 10 mL/min shows a SE around 93%. The trend is slightly different at higher oil concentrations. At 30 vol% oil concentration, (Figure 4.9b), both total flow rates of 5 and 10 mL/min illustrate a SE value of 90%, while this value decreases to 87% at 15 mL/min. By increasing the oil concentration up to 50%, the oil SE reduces around 1% for all three total flow rates (Figure 4.9c). Thus, there is a slight decrease in the performance of fabricated SHSO mesh for continuous oil-water separation by increasing total flow rates and oil concentrations. The decrease in the efficiency of oil separation is that for steady-state operation. If the process is shut down, the additional oil can still be separated completely. The decrease in the amount of oil separation is justified by the increase in the column of oil accumulation in the column. If it is required to get the same SE, the ratio of processing flow rate/mesh area is required to decrease.

This ratio can be decreased by two ways: 1) decreasing the flow rate, and 2) increasing the area of mesh. Therefore, at a given flow rate, the area of mesh should increase to obtain the same target SE value. In our tests, such an increase in mesh area (to maintain a similar SE) is only required for the highest flow rate of 15 mL/min as the SE is nearly constant in the range 5-10 mL/min.

A comparison between the water SE for total flow rates of 5, 10, and 15 mL/min under constant oil concentrations, are shown in Figure 4.9d, e, and f. As illustrated in Figure 4.9d, the water SE for 10% oil concentration, show the same pattern as reaching the plateau state at around 100% at all flow rates after 20 minutes. Whereas at two other oil concentrations the water SE values have not reached a plateau level after 70-minute separation process.

As can be seen, the SE of fabricated SHSO tube mesh for continuous oil-water separation is reduced at higher flow rates (15 mL/min) and oil concentrations (50 vol%). Moreover, the improved SE at lower oil concentrations (10 vol%) and total flow rates (5 mL/min) is due to the fact that less oil is required to permeate through the membrane and is also related to the membrane resistance. For instance, if flow rate and oil concentration are fixed, the SE is expected to decrease if the mesh becomes finer, as it will increase the mesh resistance. If the oil flow rate injected into the system is much less than the mesh capacity to permeate it across the membrane, the SE for oil will not be much affected by the flow rate of oil entering the system (similar to the effect of water in Figure 4.8 and Figure 4.9). Besides, at the higher flow rate (15 mL/min), the retention time is not adequate for effective oil-water separation [53].

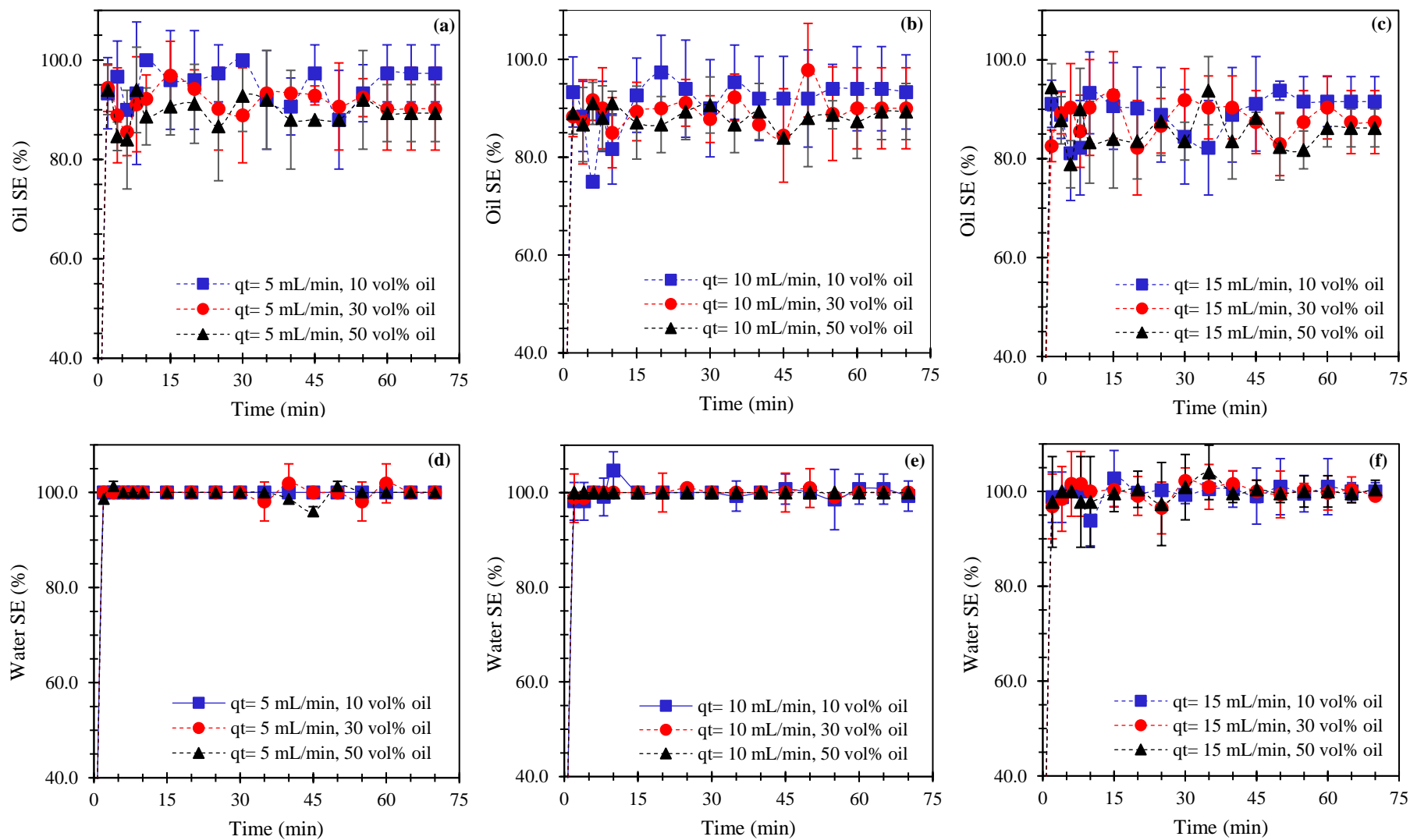


Figure 4.8. Separation efficiency tests for oil (a, b, c) and water (d, e, f) vs time at different oil concentrations under constant total flow rate (qt).

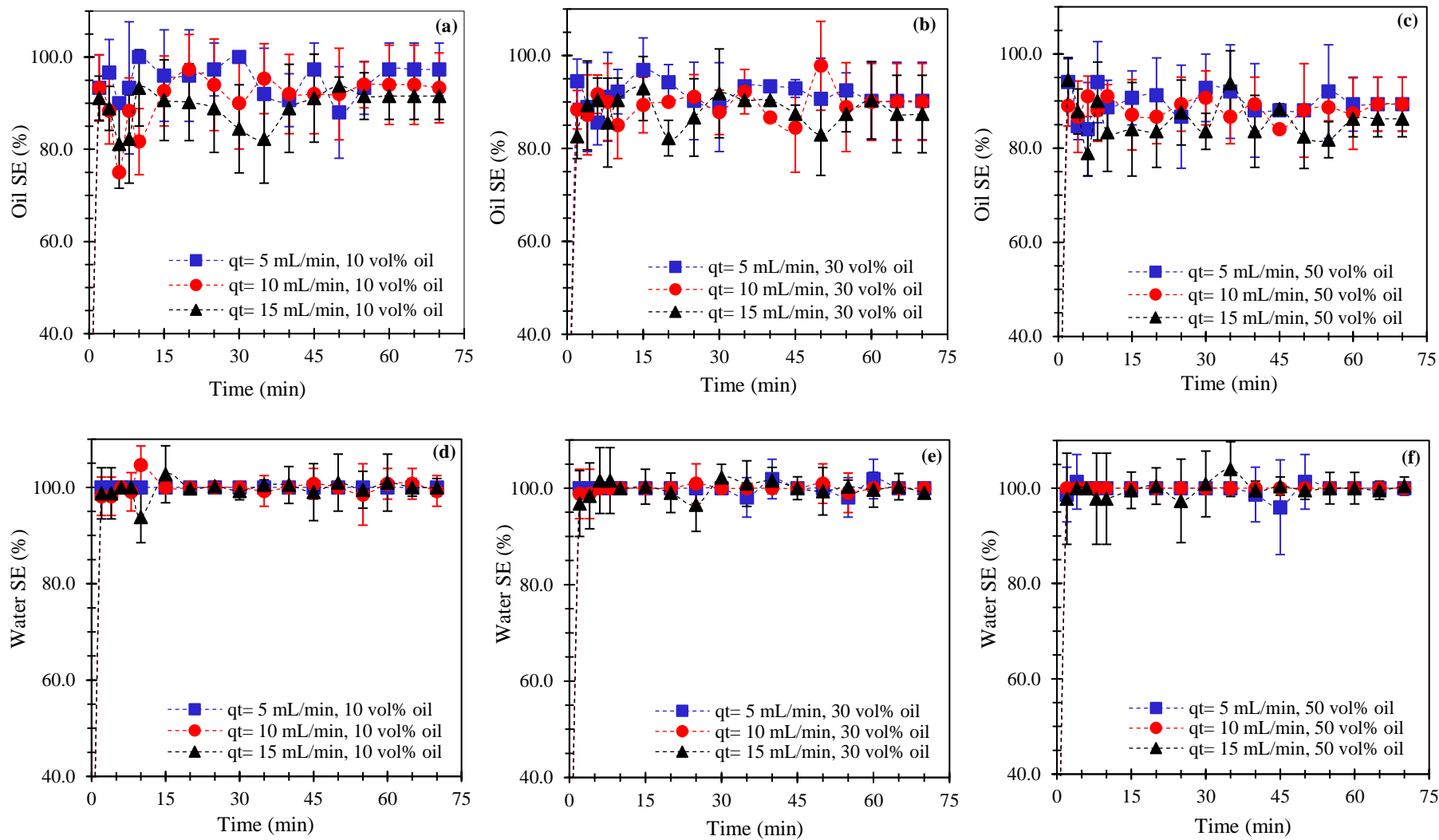


Figure 4.9. Separation efficiency tests for oil (a, b, c) and water (d, e, f) vs time at different total flow rates (qt) under constant oil concentration.

4.3.2.5. Practical implications and challenges

To establish the level of confidence in our study, the tests are replicated three times. Moreover, several flow readings at different locations (i.e., inlet and outlet of the pumps and after T-shape connection) are measured and recorded to determine the data quality. Although, except for oil and water SE tests, the degree of variation for some tests are small and not adequate to create visible error bars.

Sealing the welding joint on the mesh tube via hydrophobic glues is recommended. As these spots are vulnerable to lack of enough coating and subsequently leakage problem which reduces the breakthrough pressure of the coated membrane.

As mentioned before, the continuous separation experiments are performed at ambient conditions. Temperature significantly affects oil viscosity which directly influences the SE/flux. To do so, it is better to control the temperature in a batch/controlled system.

As SHSO membranes with micro-sized pores have limitations for separating emulsified oil from water, using demulsifiers to convert emulsion to stratified oil-water mixture before separation process can be an effective method.

In general, our proposed method is of great importance in treating oily wastewater continuously with functionalized membranes that exhibit no fouling and high permeation flux. The drawback of our SHSO membranes is using long-chain silane to create hydrophobicity features on the surface of mesh tube; they carry fluorine atoms which is not eco-friendly. An alternative for this material is using short-chain silanes with less fluorine content and a high superhydrophobicity as high as long chain silanes. However, applying non-chemical strategies, such as 3D printers and lasers can also be considered as novel strategies, where small scale SHSO fabrication is required.

The outcome from this research study seems promising since the proposed separation method can be applicable for any nonpolar organic contaminant in the water phase. There are still technical challenges left to be studied on the construction of high breakthrough pressure SHSO membranes, dynamic/continuous oil-water separation set up, and addressing inevitable membrane fouling. The effects of operating parameters such as temperature, pH, trans-membrane pressure, cross-flow velocity, and the oil droplet size in separation mechanism should not be underestimated, particularly when fouling is occurred in the system. However, our novel design accompanied with SHSO mesh tube will enable us to repel the solid particles that is carried with water phase. Hence, we expect that this methodology can be successfully employed in industrial oily wastewater treatment where an effective separation is required.

4.4. Conclusions

In this study, the SHSO mesh tube is employed in a vertical cross-flow filtration set up to continuously separate oil-water mixtures with different oil concentrations (10, 30, 50 vol%) and total flow rates (5, 10, 15mL/min). A stainless-steel mesh tube is activated with a piranha solution; the surface chemistry and morphology of the mesh are then modified to SHSO by dip-coating into a solution containing different percentages of DYNASYLAN[®] F8261, ethanol, water, hydrochloric acid, and functionalized NPs. We use hexamethyldisilazane (HMDS) modified fumed silica with average sizes of 10 nm to create a hierarchical nano roughness. To study the performance and mechanism of our novel dynamic set up, a tubular SHSO membrane with 10.5 cm height and an effective surface area of 0.3-1.8 cm² is used. The following conclusions are made from this study:

- According to the SEM images, the flower-like nano roughness not only provides an extended surface area with an effective water repellency feature, but the visible fractures on the extended surface create regions with high capillary pressure that favorably pass through the oil phase. The mesh pore opening of 80 and 45 μm were obtained for the original and coated mesh, respectively.
- Compared to the cleaned mesh with a WCA of $> 90^\circ$, the as-fabricated SHSO mesh demonstrated a WCA of 160° , which was above the value of 150° defined for the superhydrophobic surfaces. Further, the sunflower oil completely wetted the surface of coated mesh, indicated the SHSO property of as-fabricated mesh.
- By the time, the rates of oil and water collection showed a linear behavior which meant there is no blockage in the pores of membrane for the oil-water mixture under different oil concentrations and total flow rates.
- Reduced oil SE is observed with an increase in total flow rate (5 to 15 mL/min) and oil concentration (10 to 50 vol%). An oil-water mixture with 5 mL/min total flow rate and 10 vol% oil concentration led to a maximum SE of 97%. In contrary, a minimum 86% SE is obtained when the oil-water mixture is injected with a total flow rate of 15 mL/min and 50 vol% oil concentration.
- The water SE reached a 100% shortly, indicated that the water phase is not affected by changing total flow rates and oil concentrations.
- The SHSO membrane showed high permeation flux for oil phase (314-790 (L/m².h)) when the oil flow rate is increased from 0.5 to 7.5 mL/min. This permeation flux is limited with membrane permeability; higher than this value resulted in accumulation of the oil phase around the mesh.

- Given that, the oil-water separation via SHSO membranes can be readily scaled up to a larger size, we can parallelly extend the surface area by adding more SHSO mesh tubes. Besides, reusing these non-fouling SHSO membranes cut the cost of oily wastewater treatment. Thus, there is clearly great potential in petroleum refining, wastewater treatment, and oil spills clean-up.

Acknowledgements

The authors would like to thank Natural Sciences and Energy Research Council of Canada (NSERC), InnovateNL, Suncore, and Memorial University of Newfoundland for the financial support for this project.

Nomenclatures

Acronyms

DI	-	Deionized
HDMS	-	Hexamethyldisilazine
NPs	-	Nanoparticles
PPS	-	Polypropylene sulfide
PTFE	-	Polytetrafluoroethylene
SE	-	Separation efficiency
SEM	-	Scanning electron microscopy
SHSO	-	Superhydrophobic-Superoleophilic
SS	-	Stainless steel
TEM	-	Transmission Electron Microscopy
WCA	-	Water contact angle

Variables/Symbols

R^2	- coefficient of determination	-
V_c	- The volume of collected water/oil after filtration	(mL)
V_i	- The initial volume of collected water/oil	(mL)
g	- The gravitational acceleration	(m/s ²)
h	- The height of oil above the water column	(m)
k	- The SHSO mesh permeability	(m ²)
L	- The thickness of the mesh	(m)
q	- The flow rate through mesh pores	(m ³ /s)
r	- The radius of the circle	(m)
S	- The projected area of SHSO mesh in contact with the oil-water mixture	(m ²)
t	- The separation time	(h)
V	- The volume of collected water/oil	(mL)

Greek Letters

ΔP	- The applied pressure difference	(Pa)
$\Delta\rho$	- The difference between the density of oil and air	(kg/m ³)
μ	- The viscosity of the permeated oil	(Pa.s)

References

- [1] Liu N, Zhang Q, Qu R, Zhang W, Li H, Wei Y, et al. Nanocomposite Deposited Membrane for Oil-in-Water Emulsion Separation with in Situ Removal of Anionic Dyes and Surfactants. *Langmuir*. 2017;33:7380-8.
- [2] Deng D, Prendergast DP, Macfarlane J, Bagatin R, Stellacci F, Gschwend PM. Hydrophobic meshes for oil spill recovery devices. *ACS applied materials & interfaces*. 2013;5:774-81.

- [3] Diaz de Tuesta JL, Silva AMT, Faria JL, Gomes HT. Removal of Sudan IV from a simulated biphasic oily wastewater by using lipophilic carbon adsorbents. *Chemical Engineering Journal*. 2018;347:963-71.
- [4] Rocha e Silva FCP, Rocha e Silva NMP, da Silva IA, Ferreira Brasileiro PP, Luna JM, Rufino RD, et al. Oil removal efficiency forecast of a Dissolved Air Flotation (DAF) reduced scale prototype using the dimensionless number of Damköhler. *Journal of Water Process Engineering*. 2018;23:45-9.
- [5] Teh CY, Budiman PM, Shak KPY, Wu TY. Recent Advancement of Coagulation–Flocculation and Its Application in Wastewater Treatment. *Industrial & Engineering Chemistry Research*. 2016;55:4363-89.
- [6] Liu M, Chen J, Cai X, Han Y, Xiong S. Oil–water pre-separation with a novel axial hydrocyclone. *Chinese Journal of Chemical Engineering*. 2018;26:60-6.
- [7] Panchanathan D. Photoinduced Wetting Kinetics of Water on Immersed Nanoporous Titania Surfaces with Application to Oil-Water Separation: Massachusetts Institute of Technology; 2015.
- [8] Abdurahman H. Nour FSM, Rosli M. Yunus and A. Arman, . Demulsification of Virgin Coconut Oil by Centrifugation Method: A Feasibility Study. *International Journal of Chemical Technology*. 2009;1:59-64.
- [9] Saththasivam J, Loganathan K, Sarp S. An overview of oil–water separation using gas flotation systems. *Chemosphere*. 2016;144:671-80.
- [10] Kwon W-T, Park K, Han SD, Yoon SM, Kim JY, Bae W, et al. Investigation of water separation from water-in-oil emulsion using electric field. *Journal of Industrial and Engineering Chemistry*. 2010;16:684-7.

- [11] Brown PS, Bhushan B. Bioinspired, roughness-induced, water and oil super-philic and super-phobic coatings prepared by adaptable layer-by-layer technique. *Scientific reports*. 2015;5:14030.
- [12] Feng L, Zhang Z, Mai Z, Ma Y, Liu B, Jiang L, et al. A Super-Hydrophobic and Super-Oleophilic Coating Mesh Film for the Separation of Oil and Water. *Angewandte Chemie*. 2004;116:2046-8.
- [13] Tadros T, Izquierdo P, Esquena J, Solans C. Formation and stability of nano-emulsions. *Advances in Colloid and Interface Science*. 2004;108-109:303-18.
- [14] Jung YC, Bhushan B. Wetting Behavior of Water and Oil Droplets in Three-Phase Interfaces for Hydrophobicity/philicity and Oleophobicity/philicity. *Langmuir*. 2009;25:14165-73.
- [15] Lin L, Liu M, Chen L, Chen P, Ma J, Han D, et al. Bio-Inspired Hierarchical Macromolecule–Nanoclay Hydrogels for Robust Underwater Superoleophobicity. *Advanced materials (Weinheim)*. 2010;22:4826-30.
- [16] Sun T, Feng L, Gao X, Jiang L. Bioinspired Surfaces with Special Wettability. *Accounts of chemical research*. 2005;38:644-52.
- [17] Tuteja A. Superoleophobic yet Superhydrophilic surfaces for Continuous Liquid-Liquid Separation. 2011.
- [18] Liu Y, Liu F, Ni L, Meng M, Meng X, Zhong G, et al. A modeling study by response surface methodology (RSM) on Sr(ii) ion dynamic adsorption optimization using a novel magnetic ion imprinted polymer. *RSC Advances*. 2016;6:54679-92.
- [19] Zhang Y, Wang X, Wang C, Liu J, Zhai H, Liu B, et al. Facile fabrication of zinc oxide coated superhydrophobic and superoleophilic meshes for efficient oil/water separation. *RSC Advances*. 2018;8:35150-6.

- [20] Dunderdale GJ, Urata C, Sato T, England MW, Hozumi A. Continuous, High-Speed, and Efficient Oil/Water Separation using Meshes with Antagonistic Wetting Properties. *ACS applied materials & interfaces*. 2015;7:18915-9.
- [21] Liu D, Yu Y, Chen X, Zheng Y. Selective separation of oil and water with special wettability mesh membranes. *RSC Advances*. 2017;7:12908-15.
- [22] Feng L, Zhang Z, Mai Z, Ma Y, Liu B, Jiang L, et al. A Super-Hydrophobic and Super-Oleophilic Coating Mesh Film for the Separation of Oil and Water. *Angewandte Chemie International Edition*. 2004;43:2012-4.
- [23] Qin F, Yu Z, Fang X, Liu X, Sun X. A novel composite coating mesh film for oil-water separation. *Frontiers of Chemical Engineering in China*. 2009;3:112-8.
- [24] Yang J, Tang Y, Xu J, Chen B, Tang H, Li C. Durable superhydrophobic/superoleophilic epoxy/attapulgite nanocomposite coatings for oil/water separation. *Surface and Coatings Technology*. 2015;272:285-90.
- [25] Xiang M, Jiang M, Zhang Y, Liu Y, Shen F, Yang G, et al. Fabrication of a novel superhydrophobic and superoleophilic surface by one-step electrodeposition method for continuous oil/water separation. *Applied Surface Science*. 2018;434:1015-20.
- [26] Wang Q, Cui Z, Xiao Y, Chen Q. Stable highly hydrophobic and oleophilic meshes for oil-water separation. *2007*.
- [27] Lee C, Baik S. Vertically-aligned carbon nano-tube membrane filters with superhydrophobicity and superoleophilicity. *Carbon*. 2010;48:2192-7.
- [28] Wang C-F, Tzeng F-S, Chen H-G, Chang C-J. Ultraviolet-Durable Superhydrophobic Zinc Oxide-Coated Mesh Films for Surface and Underwater-Oil Capture and Transportation. *Langmuir*. 2012;28:10015-9.

- [29] Wang S, Li M, Lu Q. Filter Paper with Selective Absorption and Separation of Liquids that Differ in Surface Tension. *ACS Applied Materials & Interfaces*. 2010;2:677-83.
- [30] Yang H, Pi P, Cai Z-Q, Wen X, Wang X, Cheng J, et al. Facile preparation of superhydrophobic and super-oleophilic silica film on stainless steel mesh via sol-gel process. *Applied Surface Science*. 2010;256:4095-102.
- [31] Hsieh C-T, Hsu J-P, Hsu H-H, Lin W-H, Juang R-S. Hierarchical oil-water separation membrane using carbon fabrics decorated with carbon nanotubes 2016.
- [32] Yang H, Zhang X, Cai Z-Q, Pi P, Zheng D, Wen X, et al. Functional silica film on stainless steel mesh with tunable wettability. *Surface and Coatings Technology*. 2011;205:5387-93.
- [33] Li H, Zheng M, Ma L, Zhu C, Lu S. Two-dimensional ZnO nanoflakes coated mesh for the separation of water and oil. *Materials Research Bulletin*. 2013;48:25-9.
- [34] Liu Y, Zhang K, Yao W, Liu J, Han Z, Ren L. Bioinspired structured superhydrophobic and superoleophilic stainless steel mesh for efficient oil-water separation. *Colloids and Surfaces A: Physicochemical and Engineering Aspects*. 2016;500:54-63.
- [35] Matin A, Baig U, Gondal MA, Akhtar S, Zubair SM. Superhydrophobic and superoleophilic surfaces prepared by spray-coating of facile synthesized Cerium(IV) oxide nanoparticles for efficient oil/water separation. *Applied Surface Science*. 2018;462:95-104.
- [36] Baig U, Matin A, Gondal MA, Zubair SM. Facile fabrication of superhydrophobic, superoleophilic photocatalytic membrane for efficient oil-water separation and removal of hazardous organic pollutants. *Journal of Cleaner Production*. 2019;208:904-15.
- [37] Li J, Guan P, Zhang Y, Xiang B, Tang X, She H. A diatomite coated mesh with switchable wettability for on-demand oil/water separation and methylene blue adsorption. *Separation and Purification Technology*. 2017;174:275-81.

- [38] Cao W-T, Liu Y-J, Ma M-G, Zhu J-F. Facile preparation of robust and superhydrophobic materials for self-cleaning and oil/water separation. *Colloids and Surfaces A: Physicochemical and Engineering Aspects*. 2017;529:18-25.
- [39] Xiao C, Si L, Liu Y, Guan G, Wu D, Wang Z, et al. Ultrastable coaxial cable-like superhydrophobic mesh with self-adaption effect: facile synthesis and oil/water separation application. *Journal of Materials Chemistry A*. 2016;4:8080-90.
- [40] Matin A, Baig U, Gondal MA, Akhtar S, Zubair SM. Facile fabrication of superhydrophobic/superoleophilic microporous membranes by spray-coating ytterbium oxide particles for efficient oil-water separation. *Journal of Membrane Science*. 2018;548:390-7.
- [41] Du Z, Ding P, Tai X, Pan Z, Yang H. Facile Preparation of Ag-Coated Superhydrophobic/Superoleophilic Mesh for Efficient Oil/Water Separation with Excellent Corrosion Resistance. *Langmuir*. 2018;34:6922-9.
- [42] Xiong Z, Lin H, Liu F, Xiao P, Wu Z, Li T, et al. Flexible PVDF membranes with exceptional robust superwetting surface for continuous separation of oil/water emulsions. *Scientific reports*. 2017;7:14099-12.
- [43] Binner ER, Robinson JP, Kingman SW, Lester EH, Azzopardi BJ, Dimitrakakis G, et al. Separation of Oil/Water Emulsions in Continuous Flow Using Microwave Heating. *Energy & Fuels*. 2013;27:3173-8.
- [44] Ezazi M, Shrestha B, Kim SI, Jeong B, Gorney J, Hutchison K, et al. Selective Wettability Membrane for Continuous Oil–Water Separation and In Situ Visible Light-Driven Photocatalytic Purification of Water. *Global challenges*. 2020;4:2000009-n/a.

- [45] Cai Y, Li S, Cheng Z, Xu G, Quan X, Zhou Y. Facile fabrication of super-hydrophobic FAS modified electroless Ni-P coating meshes for rapid water-oil separation. *Colloids and Surfaces A: Physicochemical and Engineering Aspects*. 2018;540:224-32.
- [46] Patel SU, Manzo GM, Patel SU, Kulkarni PS, Chase GG. Permeability of Electrospun Superhydrophobic Nanofiber Mats. *Journal of Nanotechnology*. 2012;2012.
- [47] He S, Zhan Y, Bai Y, Hu J, Li Y, Zhang G, et al. Gravity-driven and high flux super-hydrophobic/super-oleophilic poly(arylene ether nitrile) nanofibrous composite membranes for efficient water-in-oil emulsions separation in harsh environments. *Composites Part B: Engineering*. 2019;177:107439.
- [48] Hlavacek M. Break-up of oil-in-water emulsions induced by permeation through a microfiltration membrane. *Journal of Membrane Science*. 1995;102:1-7.
- [49] Sun D, Duan X, Li W, Zhou D. Demulsification of water-in-oil emulsion by using porous glass membrane. *Journal of Membrane Science*. 1998;146:65-72.
- [50] Hu B, Scott K. Influence of membrane material and corrugation and process conditions on emulsion microfiltration. *Journal of Membrane Science*. 2007;294:30-9.
- [51] Maartens A, Jacobs EP, Swart P. UF of pulp and paper effluent: membrane fouling-prevention and cleaning. *Journal of Membrane Science*. 2002;209:81-92.
- [52] Lv Y, Yu X, Tu S-T, Yan J, Dahlquist E. Wetting of polypropylene hollow fiber membrane contactors. *Journal of membrane science*. 2010;362:444-52.
- [53] Oshinowo LM, Vilagines RD. Modeling of oil–water SE in three-phase separators: Effect of emulsion rheology and droplet size distribution. *Chemical Engineering Research and Design*. 2020;159:278-90.

5. CHAPTER FIVE

Summary and Recommendations for Future Work

This study focuses on the fabrication of SHSO membranes and their application for oil-water separation purposes. A cross-flow dynamic setup is used to evaluate the potential of the as-fabricated SHSO mesh tube for the separation of oil/water from an oil-water mixture under various oil concentration and total flow rate conditions. In addition, characterization tests are performed to show how the surface is modified after coating. This thesis includes three main sections: literature review (Chapter Two), fabrication and characterization of SHSO membranes (Chapter Three), and dynamic oil-water separation via SHSO mesh tube (Chapter Four).

5.1. Literature Review (Chapter 2)

Superhydrophobic and superoleophilic surfaces are important in oil-water separation applications, including the treatment of oily wastewater, and oil spill removal. Despite the extensive efforts in the last decade for the fabrication of the superhydrophobic and superoleophilic surfaces, there is no comprehensive review report/work on the subject. In this paper, we review the fabrication and characterization of the SHSO surfaces that are used in the oil-water separation processes. It also further highlights the pros and cons of the fabrication and characterization techniques, current status and prospects of SHSO membranes, and potential future research directions.

- The metallic mesh-based membranes feature higher mechanical strength, lower pressure drop, and higher porosity and permeability, compared to porous membranes.
- Efficient SHSO surface pretreatment techniques are in the following order: air plasma > oxygen plasma > piranha solution > UV irradiation.
- To create hierarchical micro- and nano-roughness structures, a variety of processes are examined. Although advanced methods such as femtosecond laser ablation, replication, templating, 3D printing, and lithography are capable of creating complex and precise

hierarchical structures, these techniques are expensive and still limited to small-scale applications. Alternatively, methods based on electrochemistry and crystal growth techniques are used to create complicated hierarchical structures.

- Using facile methods (based on colloidal assembly) and applying a rough polymer film are found to be cheaper alternatives for creating surface roughness in order to achieve the superhydrophobic and superoleophilic conditions.
- To modify the surface energy for such wetness conditions, a majority of the studies in the literature have used stearic acid, and different silanes and thiols.
- The water contact angle (WCA) $>150^\circ$ and oil contact angle (OCA) $<5^\circ$ are observed for most of the superhydrophobic and superoleophilic membranes, for which an oil-water separation efficiency $>99\%$ is attained.
- Techniques such as scanning electron microscopy (SEM), X-ray powder diffraction (XRD), Fourier transform infrared spectroscopy (FTIR), X-ray photoelectron spectroscopy (XPS), atomic force microscopy (AFM), and permeation tests are also used to quantify the membrane performance, while limited studies have performed short-term stability analysis, using contact angle measurements.
- One of the aspects overlooked in the literature is the influence of fouling on the performance of the superhydrophobic and superoleophilic membranes that can be covered in future research.

5.2. Fabrication and Characterization of SHSO Membranes (Chapter 3)

In this phase of the study, a superhydrophobic-superoleophilic stainless steel mesh-based membrane is fabricated to evaluate the effectiveness of the membrane surface modification on static oil-water separation efficiency. To construct a superhydrophobic-superoleophilic membrane,

the cleaned meshes are activated by piranha solution, then immersed into 12 colloidal solutions that contain silane compounds and a mixture of micro- and nanoparticles of hydrophobized silica. We study the effect of silane alkyl-chain size by including a long chain silane (Dynasylan[®] F8261) and a short-chain silane (Dynasylan[®] Sivo 408) in the coating solution. The impact of roughness by varying the ratio of nano- to microparticles in the solid part of the coating solution is also examined. To create hierarchical morphology, Aerosil[®] R812 and SIPERNAT[®] D13 are used as the nano and microparticles, respectively. Under this one-step dip-coating process, the surface energy and morphology of the membranes are modified simultaneously. The fabricated mesh is characterized by SEM, EDS, ATR-FTIR, equilibrium water and oil contact angle measurements, stability tests, and static oil-water separation analysis. The main outcomes of this experimental research are as follows:

- With both silanes, the maximum contact angle for water is obtained when the solid part of the coating solutions contains 75% nanoparticles and 25% microparticles.
- Increasing the concentration of nanoparticles to 100% reduces the hydrophobicity; however, this decrease is only statistically significant for the short-chain silane. Moreover, the long-chain alkyl silane features a better hydrophobicity at all levels of the solid composition.
- It is possible to compensate for the lower hydrophobicity of the shorter-chain silane by adjusting the size distribution of the solids in the coating suspension by changing the ratio of micro to nanoparticles. Because the shorter silane has less fluorine (F), it will have less environmental impact.
- The characterization tests confirm the superhydrophobicity and superoleophilicity of the coated mesh.

- The fabricated membranes show excellent stability over a four-week immersion into solutions of 0.1 M NaOH, 1 M H₂SO₄, 1 M NaCl.
- The fabricated mesh also separates around 97% canola oil and around 99% hexane from oil-water mixtures.

5.3. Oil-water Separation Tests (Chapter 4)

In the last phase of this research, the effectiveness of as-fabricated SHSO stainless-steel mesh under continuous mode is investigated for an oil-water mixture with different total flow rates and oil concentrations. A tubular mesh is employed in this phase to provide more surface area and improve the permeation flux as a vital factor in treatment of industrial oily wastewater systems. The tubular stainless-steel meshes is dip-coated into the optimum solution, confirmed in the previous chapter, including (100% silica NPs + DYNASYLAN[®] F8261). A vertical cross-flow gravity based set up is designed to dynamically separate both phases, simultaneously. The main outcomes of this research phase are summarized below:

- Compared to the original mesh with a pore opening of around 80 μm , the as-fabricated SHSO mesh tube exhibits a 45 μm pore opening, based on SEM images.
- The cleaned and coated meshes show the WCA of around 90 and 160°, respectively. It is thus found that the oil completely wets the coated mesh; the results confirm the superhydrophobicity and superoleophilicity of the fabricated mesh.
- According to the TEM test, the silica NPs with spherical shapes can create a uniform and stable roughness on the surface. The flower-like nano-roughness shown in SEM images further highlights the potential of SiO₂ NPs for fabricating SHSO membranes.

- Given the linear relationship between cumulative volumes of oil and water with time, it can be concluded that no fouling or blockage in the pores of the as-fabricated SHSO mesh tube occurs during the dynamic experiment.
- The maximum oil SE of 97% is obtained when the oil-water mixture has the minimum oil concentration (10 vol%) and total flow rate (5 mL/min). Conversely, the minimum oil SE (86%) corresponds to the oil-water mixture with an oil concentration of 50 vol% and 15 mL/min total flow rate.
- The water phase reaches a 100% SE shortly, indicating that the water separation is not influenced by the magnitude of total flow rate and oil concentration. This again confirms the superhydrophobicity of the as-prepared SHSO mesh tube.
- By increasing the oil flow rate from 0.5 to 7.5 m/l/min, the oil permeation flux is changed from 314 to 790 (L/m².h). The membrane permeability is a controlling factor in the permeation flux; beyond this threshold, oil accumulation happens around the mesh tube. The height of oil around the mesh tube varies between 2 mm (for the case of 10 vol% oil and 5 m/l/min total flow rate) and 12 mm corresponded to the case of 50 vol% oil and 15 m/l/min total flow rate.

5.4. Recommendations for Future Work

Employing the crossflow gravity-based setup for the dynamic oil-water separation via SHSO mesh tubes, the following recommendations for future work are given:

- One of the aspects overlooked in this research is the influence of fouling on the performance of the SHSO membranes, which can be covered in future research.

- In further work, the oil droplet size and vacuum effects can also be studied in the dynamic oil-water separation process. Accordingly, an oil-water mixture can be created by a static mixer, which is sent into the tube side, with a controlled vacuum connected to the tube.
- It is recommended to assess the impact of different coating materials, especially those with low environmental impacts.
- The momentum and mass transfer in our system can be modeled later using mathematical and simulation approaches such as computational flow dynamics (CFD) and artificial neural networks. A systematic parametric sensitivity analysis would be possible with the aid of effective modeling/simulation strategies to better design and operate the membrane toward optimal condition
- Effects of membrane alignment, turbulence, surface tension, and mesh opening size can be studied in future work through both experimental and modeling phases